Underwater Acoustic Localization with Applications to Multiuser Communications

Li Liao

Doctor of Philosophy

University of York
Electronic Engineering

August 2018

Abstract

Multiuser underwater acoustic communications (UACs) have gained attention because of a number of applications. To assess the performance of multiuser UACs and reduce the cost of experiments, simulations of the signal transmission are used. However, the existing underwater signal transmission simulators suffer from complexity and signal length limitation when investigating multiuser UACs. Therefore, it is useful to develop a signal transmission simulator for UACs. To improve the performance and bandwidth efficiency of multi-user systems, arrays can be used at the transmitter with transmit beamforming, which require the channel state information (CSI) available at the receiver to be sent as a feedback message to the transmitter. A long feedback message in UAC is a waste of the throughput and sometimes impractical. Therefore, it is important to develop an advanced transmit beamforming method for the multiple transmit sensor array systems.

In this thesis, an underwater channel simulator based on acoustic field computation is proposed. We pre-compute and store the acoustic field in the investigation area, thus speeding up the computation whilst maintaining the performance. Based on this, an underwater receiver localization method is then proposed. In the localization, the CSIs at specific points in the investigation area are pre-computed and compared with the CSI measured at the receiver, thus the position of the receiver is estimated as the point with the best match. It offers a more practical solution to the underwater localization problem. A receiver trajectory estimation technique combining the proposed localization and smoothing approach is also proposed to reduce the cost of infrastructure, and it can be applied in a two-dimensional plane and a three-dimensional space. An advanced beamforming technique is introduced in the transmitter design based on the proposed localization technique. It offers accurate detection performance and the length of the feedback message is reduced significantly.

Table of contents

List of tables

List of figures

Acknowledgements

I would like to thank my supervisors, Dr. Yuriy Zakharov and Dr. Paul Mitchell, for all their advice, support and encouragement during the course of my Ph.D. study.

I am very grateful to Prof. David Grace, who is my thesis advisor. David provided a lot of ideas and helped me a lot especially during the beginning of my Ph.D. career.

I would also like to thank all my colleagues in the Communications Research Group, University of York.

This thesis is dedicated to my families who always support and encourage me during my Ph.D. study in York.

I would like to dedicate this thesis to my wife Qian, for all of her love and support.

Declaration

I hereby declare that except where specific reference is made to the work of others, the contents of this dissertation are original and have not been submitted in whole or in part for consideration for any other degree or qualification in this, or any other university. All sources are acknowledged as References.

Publications

Publications directly associated with thesis work

- L. Liao, B. Henson, and Y. Zakharov, "Grid Waymark baseband underwater acoustic transmission model," in *Underwater Acoustics Conference and Exhibition*, Skiathos, Greece, September 2017, pp. 343–350
- L. Liao, Y. V. Zakharov, and P. D. Mitchell, "Underwater localization based on grid computation and its application to transmit beamforming in multiuser UWA communications," *IEEE Access*, vol. 6, pp. 4297–4307, 2018
- L. Liao, B. Henson, and Y. Zakharov, "Underwater trajectory estimation based on grid localization and smoothing," in *the Tenth IEEE Sensor Array and Multichannel Signal Processing Workshop*, Sheffield, UK, July 2018

Other publications

- J. Li, L. Liao, and Y. V. Zakharov, "Space-time cluster combining for UWA communications," in *IEEE OCEANS*, Shanghai, China, 2016, pp. 1–6

Li Liao
August 2018

Acronyms

AUV Autonomous Underwater Vehicle

BER Bit Error Rate

BPSK Binary Phase-Shift Leying

CCI Cochannel Interference

CDF Cumulative Distribution Function

CDMA Code Division Multiple Access

CIR Channel Impulse Response

CSI Channel State Information

DBF Digital Beamforming

DFT Discrete Fourier Transform

FDMA Frequency Division Multiple Access

FFT Fast Fourier Transform

GPS Global Positioning System

IFFT Inverse Fast Fourier Transform

ISI Inter-Symbol Interference

LBL Long Baseline

LMS Least Mean Squares

LS Least Squares

MAC Media Access Control

MIMO Multiple-Input Multiple-Output

NRMSE Normalized Root-Mean-Square Error

OFDM Orthogonal Frequency Division Multiplexing

PDF Probability Density Function

RF Radio-Frequency

SBL Short Baseline

SNR Signal to Noise Ratio

SSP Sound Speed Profile

TDMA Time Division Multiple Access

UAC Underwater Acoustic Communications

USBL Ultra-Short Baseline

UUVs Unmanned Underwater Vehicles

UWA Underwater Acoustic

UW-ASNs Underwater Acoustic Sensor Networks

ZF Zero-forcing

Chapter 1

Introduction

In recent years, demands for underwater communication systems are increasing due to the on-going expansion of human activities in underwater environments such as environmental monitoring, pollution control and tracking, underwater exploration, scientific data collection, maritime archaeology, offshore oil field exploration, port security, tactical surveillance [11–14], etc. Wired systems, particularly fiber optical systems, can be deployed to provide real time communication in underwater applications. However, their high cost and operational disadvantages due to the lack of flexibility become restrictive for most practical cases. This triggers the growing demand for underwater wireless links.

For wireless underwater transmission, radio, optical, or acoustic waves can be used. The transmission ranges of radio and optical underwater systems are usually limited to short distances. In fact, radio waves propagate at long distances through conductive salty water only at extra low frequencies (30-300 Hz), which require large antennae and high transmission power [15]. Optical waves do not suffer from such high attenuation but are affected by scattering. Furthermore, transmitting optical signals requires high precision in pointing the narrow laser beams [16]. With relatively favorable propagation characteristics of acoustic waves, acoustic systems achieve longer transmission ranges underwater and are widely deployed in practice. Meanwhile, acoustic systems offer the best solution for communicating underwater where tethering is unacceptable because it physically limits the moving system [17, 18]. Thus underwater acoustic communications (UACs) have received much attention. Their applications, which were mostly military, are beginning to shift towards various commercial areas. Examples of non-military applications include pollution monitoring, seabed observation, seabed mining, marine biological observation and applications in offshore oil industry [19].

Underwater acoustic propagation is characterized by three major factors: attenuation that increases with signal frequency, time-varying multipath propagation, and low speed of

sound (1500 m/s) [3]. Because acoustic propagation is best supported at low frequencies, the channel capacity can be extremely limited. For example, an acoustic system may operate in a frequency range between 10 and 15 kHz. Although the total available bandwidth is usually low, an acoustic communication system is inherently wideband in the sense that the bandwidth is not negligible with respect to its center frequency. The channel can have a sparse impulse response, where each physical path acts as a time-varying low pass filter, and motion creates additional Doppler spreading and shifting. Surface waves, internal turbulence, fluctuations in the sound speed, and other small-scale phenomena contribute to random signal variations. At this time, there are no standardized models for the acoustic channel fading, and experimental measurements are often made to assess the statistical properties of the channel in particular deployment sites [3].

As the interest in UACs is increasing nowadays, some disadvantages in UACs are also discussed. UACs suffer from a very small available bandwidth and data rates are limited to a few tens of kilobits/sec (kb/s) [11]. To address these new challenges, innovative physical layer designs such as multiple-input multiple-output (MIMO) communication and orthogonal frequency division multiplexing (OFDM) have been used in UWA systems to exploit spatial and multipath diversities.

The underwater acoustic channel also introduces dispersion to signals in both time and frequency domains. The time-domain dispersion due to large delay spread results in severe inter-symbol interference (ISI). The frequency-domain dispersion caused by the motion of the transmitter and receiver and the motion of the sea surface leads to a rapidly time-varying channel [20, 21].

As a result, the benefits and challenges brought by UACs have attracted the attention of researchers from all over the world, and applications have been delivered in this area. In this thesis, we mainly focus on the applications in UACs and propose some advanced techniques with the aim to further improve the UAC performance.

In this chapter, some existing techniques and research related to our work are described:

- Multiple access. The multiple access in UAC is investigated, which enables multiple devices to share a common wireless medium, thus enhancing the throughput of the communication channel.

- Sea surface. In shallow water acoustic communication, most of the sources of ambient noise are at or near the sea surface [22]. The analysis of the effects of reflecting boundaries are also related to the parameters of waves. Therefore, with the understanding of sea surface, we can achieve accuracy in the set up of underwater simulations and the prediction of noise.

- Noise distribution. The investigation in the noise distribution in UAC can contribute to underwater channel modelling, and help us to set up an accurate environment for underwater simulations. Understanding of the directionality of noise in underwater also relates to the noise reduction in the design of receivers.

- Underwater acoustic propagation models. The most common underwater acoustic propagation models, the Kraken [23], the Bellhop [24] and the range-dependent acoustic model (RAM) are investigated. They are based on accurate definition of the velocity profile, range, depth, as well as a characterization of the seabed properties such as roughness.

- Acoustic channel simulators for underwater communications. To assess the communication performance and to reduce the cost of setting up the infrastructure of sea experiments, acoustic channel simulators are applied to simulate UACs. The existing UWA channel simulators, VirTEX, Waymark and Baseband Waymark are discussed.

- Underwater sensor networks. To enable unexplored applications and to enhance the ability to observe and predict the ocean, underwater networks of sensors have been considered [25]. Underwater Acoustic Sensor Networks (UW-ASNs) consist of sensors and vehicles deployed underwater and networked via acoustic links to perform collaborative monitoring tasks [15]. Some problems in UW-ASNs, such as localization and trajectory estimation, are investigated. The investigation in this thesis can contribute to solving these problems, thus enhance the performance of UW-ASNs.

- Underwater localization and trajectory estimation. Underwater localization and trajectory estimation are highly needed in underwater communications such as underwater sensor networks. The monitoring information collected from a sensor node would be meaningless if the locations of the node is unknown to the user. This also introduces the requirement of trajectory estimation in some applications related to underwater mobile nodes or AUV sensors.

- Transmit beamforming in UACs. In radio communications, adaptive beamforming has been widely used at the receiver to reduce both co-channel interference (CCI) and intersymbol interference (ISI) and to improve the capacity by adjusting the beam pattern such that the effective signal-to-interference-plus-noise ratio (SINR) at the output of the beamformer is increased [26]. Since the beamforming in the receiver is often impractical in UACs, the transmit beamforming in UACs is investigated with SDMA.

1.1 Multiple Access in Underwater Communications

Media Access Control (MAC) enables multiple devices to share a common wireless medium [27]. However, challenges have been introduced for MAC in underwater communications by the characteristics of the underwater acoustic channel, especially limited bandwidth and high propagation delays. MAC protocols can be roughly divided into two main categories [28]:

- Scheduled protocols that avoid collision among transmission nodes;
- Contention-based protocols where nodes compete for a shared channel, resulting in probabilistic coordination.

To enhance the throughput of the communication channel, higher system capacities are demanded. The capacity of a radio communication system can be increased directly by enlarging the channel bandwidth. However, the spectrum in UACs is limited. To provide high system capacity and overcome the spectrum limitation, multiple access techniques are often applied in UACs.

Multiple access is a synonym for the channel access method - a scheme that allows several terminals connected to the same physical medium to transmit over it. There are four domains in which capacity sharing can take place [25]: frequency; time; code; space. These techniques are respectively referred to frequency division multiple access (FDMA), time division multiple access (TDMA), code division multiple access (CDMA), and space division multiple access (SDMA) [25].

FDMA divides the frequency spectrum into segments for different users and it was used to deploy first generation cellular systems [29]. With the arrival of digital techniques in the 90s, the techniques of TDMA and CDMA were widely used for the second generation digital cellular system [29, 30]. For TDMA systems, each user apportions the entire transmission resource periodically for a brief period of time, while for CDMA systems, each transmitted signal is modulated with a unique code that identifies the user. SDMA is another widely used multiple access technique in wireless communications [31]. It optimizes the use of radio spectrum and minimizes system cost by taking advantage of the directional properties of dish antennas. The antennas are highly directional, allowing duplicate frequencies to be used for multiple communication zones. For UACs focused in this thesis, FDMA is restrictive due to the narrow bandwidth of the underwater acoustic channel and TDMA is not efficient due to the propagation delay. To achieve high data rates on the severely band-limited UWA channels, array processing for exploitation of SDMA is considered. The ultimate form of SDMA in UACs is to use steered beams at the same carrier frequency to provide service to an individual user, which refers to the techniques of conventional beamforming and adaptive beamforming, respectively. These techniques have drawn considerable interest from the communications community in the recent 15 years [32–35]. As a result, SDMA has been

highlighted as a promising multiple access technique for UACs [36, 25]. In this thesis, the beamforming in SDMA is investigated and an advanced transmit beamforming technique is proposed to improve the detection performance.

1.2 Sea Surface

The study of underwater communications with acoustic signals often includes an analysis of the effects of reflecting boundaries. This is particularly true for signals propagating in the vicinity of the sea's surface, which almost always has a time-varying, random structure. Reflection from the sea surface poses time delay problem which causes the receiver to have more than one arrival of the transmitted signal [37], thus introducing the multipath effect. This problem is further complicated by the time-varying nature of the sea surface.

To investigate the effect introduced by sea surface, we start with the study of wind wave. The distribution of the heights of wind waves is a question of some practical and theoretical interest. If the sea surface is assumed to be the sum of many sine waves in random phase then the wave amplitudes are distributed according to a Rayleigh distribution [38, 39]. The density function of Rayleigh distribution is given by

$$p(H) = \frac{2H}{H_{rms}^2} \exp\left(\frac{-H^2}{H_{rms}^2}\right), \tag{1.1}$$

where H is the wave height and H_{rms} is root mean square wave height.

Subjected to a large number of observational tests, a well-known formula relating the most probable maximum wave height in a record to the significant wave height in that record comes out after the distribution of wave amplitude [38, 39],

$$H_m = H_s \sqrt{\frac{1}{2} \ln N}, \tag{1.2}$$

where H_m is the most probable wave height in the record, N is the total number of waves in a record, and H_s is the significant wave height which is defined traditionally as the average height of the highest one-third waves in a wave spectrum [40]. As shown in Fig 1.1 [2], each dot represents a wave in the spectrum with a height of H, the greatest number of waves in this spectrum is in the mid range of heights (centered under H_m). The highest one-third (33.3%) number of waves in this spectrum is shaded on the figure. The average height of waves in this shaded group is the significant wave height, H_s.

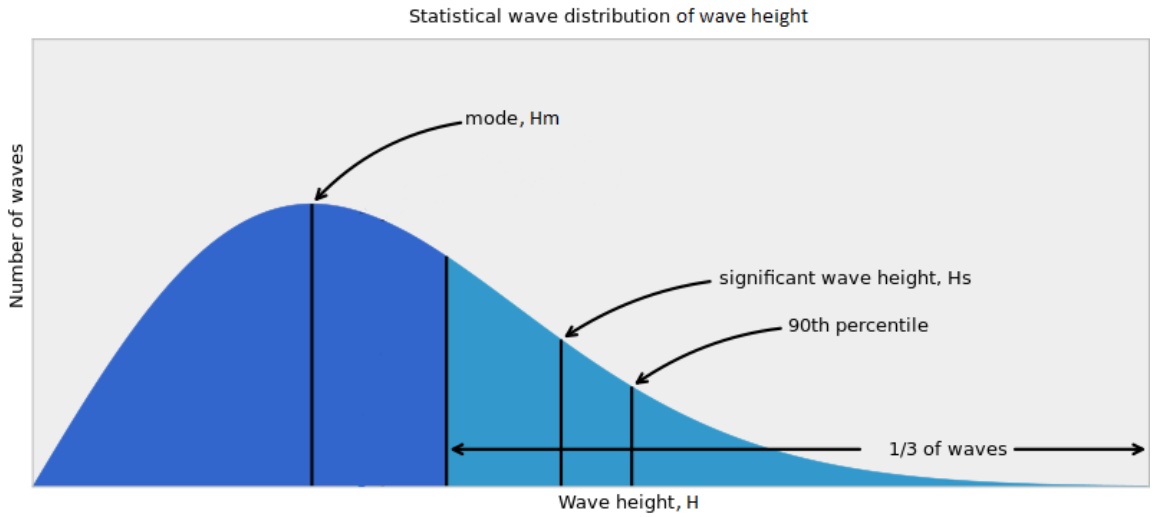

Fig. 1.1 The statistical distribution of wave heights showing various parameters. Copied from [2].

In deep ocean acoustic communication, most of the sources of ambient noise are at or near the sea surface [22]. The analysis of the effects of reflecting boundaries are also related to the parameters of waves. Therefore, with the understanding of sea surface, we can obtain accuracy in the set up of underwater simulations and the prediction of noise.

1.3 Absorption and Noise Distribution

Signal-to-noise ratio (SNR) is the key factor in many analyses in UAC, and it is related to underwater path loss and ambient noise. Their distinguishing property is the fact that they both vary with frequency.

The dependence of the path loss on the signal frequency is a consequence of absorption. In addition to the absorption loss, a signal experiences a spreading loss, which increases with distance. The overall path loss is given by [3]:

$$A(l,f) = (l/l_r)^k a^{(l-l_r)}(f), \tag{1.3}$$

where f is the signal frequency and l is the transmission distance, taken in reference to some distance l_r. The path loss exponent k models the spreading loss, and its usual values are between 1 and 2 (for cylindrical and spherical spreading, respectively). The absorption

coefficient $a(f)$ can be obtained using an empirical formula [41]:

$$8.68 \times 10^3 \left(\frac{SAf_T f^2}{f_T^2 + f^2} + \frac{Bf^2}{f_T} \right) (1 - 6.54 \times 10^{-4} P)[\text{dB/km}], \tag{1.4}$$

where $A = 2.34 \times 10^{-6}$, $B = 3.38 \times 10^{-6}$, S is salinity, P is hydrostatic pressure [kg/cm^2], f is frequency [kHz], and

$$f_T = 21.9 \times 10^{6-1520/(T+273)} \tag{1.5}$$

is a relaxation frequency [kHz], with T the temperature [°C]. While the temperature ranges from 0° to 30°C, f_T varies approximately from 59 to 210 kHz. Fig. 1.2 illustrates its rapid increase with frequency.

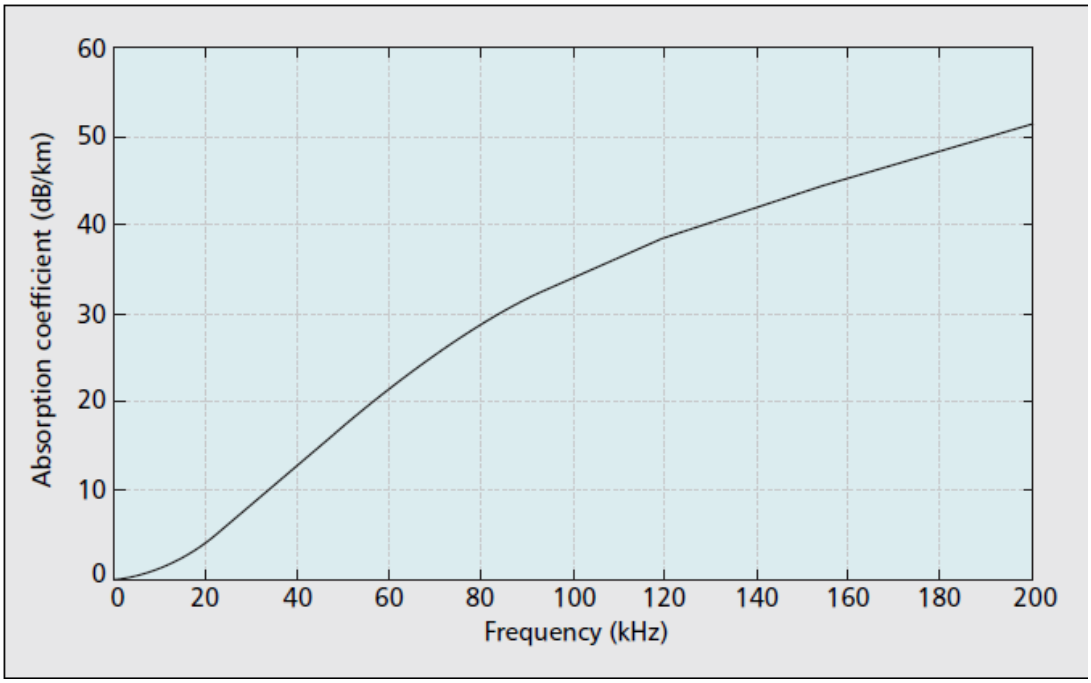

Fig. 1.2 Absorption coefficient. Copied from [3].

Ambient noise in UAC excludes momentary, occasional sounds, such as the noise of a close-by passage of a ship or of an occasional rain squall [42]. While this noise is often approximated as Gaussian, it is not white [3]. Unlike ambient noise, site-specific noise often contains significant non Gaussian components. In general, omnidirectional ambient noise increases at lower frequencies just as the corresponding transmission loss decreases and the power spectral density of ambient noise decays at a rate of approximately 18 dB/decade [43].

The attenuation, which grows with frequency, and the noise, whose spectrum decays with frequency [43], result in a signal-to-noise ratio (SNR) that varies over the signal bandwidth.

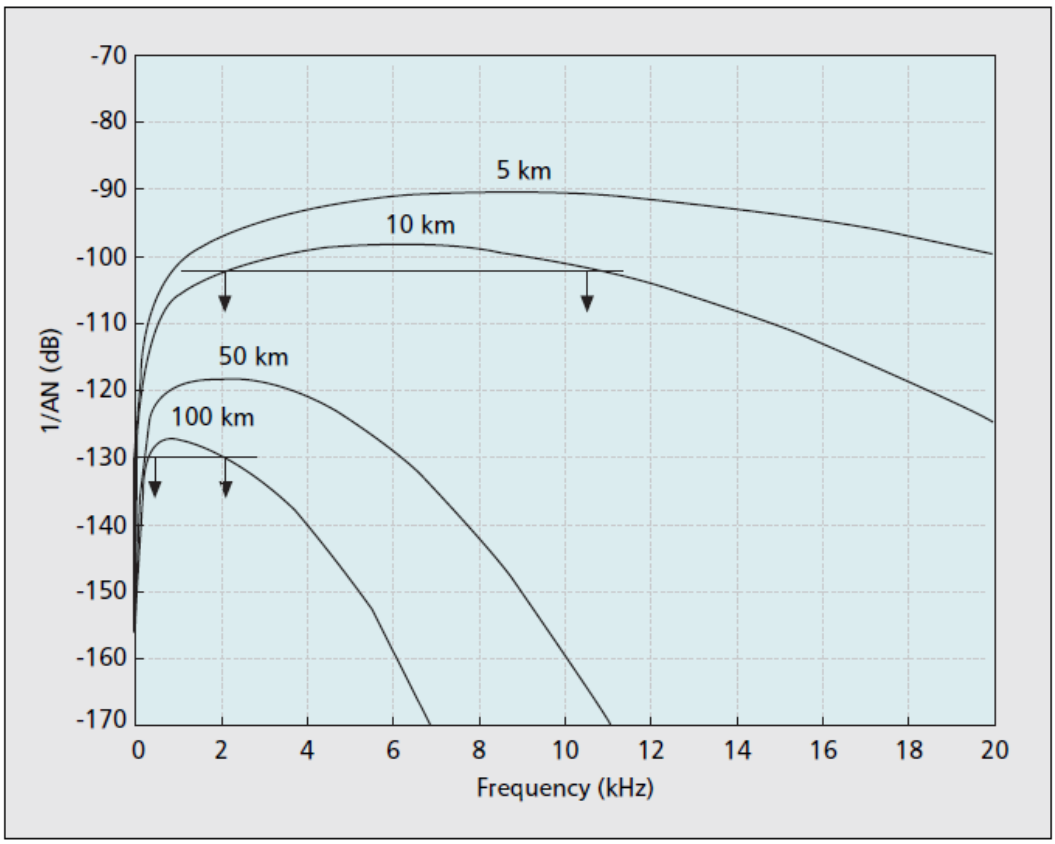

Fig. 1.3 Signal-to-noise ratio in an acoustic channel depends on the frequency and distance through the factor $1/A(l,f)N(f)$, where $N(f)$ is the power spectral density of the ambient noise. Copied from [3]

For any given distance, the narrowband SNR is a function of frequency [3], as shown in Fig. 1.3. From this figure it is apparent that the acoustic bandwidth depends on the transmission distance.

The bandwidth is severely limited at longer distances [44]: at 100 km, only about 1 kHz is available. At shorter distances, the bandwidth increases, but will ultimately be limited by that of the transducer. The fact that bandwidth is limited implies the need for bandwidth-efficient modulation methods[3].

The ambient noise in underwater could be broken up into three frequency domains as shown in Table 1.1 [1]. Although the sources of the ambient noise are mostly near the surface, the changing environmental factors would result in different noise level through the domains.

Table 1.1 Underwater ambient noise in different frequency domains [1]

Frequency domains	
Very high frequency (VHF) domain	$> 100kHz$
High frequency (HF)	$10 - 100kHz$
Sonar frequency (SF)	$200Hz - 10kHz$

For the very high frequency domain (above 100 kHz), the principal noise source is the thermal agitation of the seawater constituent molecules at the hydrophone and this noise is proportional to the absolute temperature [45]. Due to the fact that typical ocean temperature changes small and high attenuation occurs in such high frequency, the investigation of ambient noise in this frequency domain is meaningless except for extreme cases [45].

In the high frequency domain (10 to 100 kHz) the surface sources become dominant. However, attenuation is still more critical [22].

In the next important domain (200 Hz to 10 kHz), experiments at Bermuda during the 1960's showed that relatively higher noise levels at higher angles and a null noise at 0° [46–49].

For downward-refracting environments, i.e., situations in which sound speed decreases with depth, some measurements of vertical directionality of midfrequency surface noise have been made in the Gulf of Mexico (GOM) [50, 4]. It is noted that when the sound-speed-profile (SSP) is downward-refracting as shown in Fig. 1.4, the highest noise arrives at a receiver from upward directions while the noise from downward-looking directions is attenuated according to the nature of the bottom, and there is a significant quiet region at near-horizontal directions as shown in Fig. 1.5.

The investigation in the noise distribution in UACs can contribute to channel modelling, and help us to set up an accurate environment for underwater simulations. The understanding in the directionality of noise in underwater also relates to the noise reduction in the design of receivers.

1.4 Underwater Acoustic Propagation Models

Modelling the underwater acoustic propagation channel has been attracting interest from around the world. One of the earliest papers was published in 1948 and it developed the theory of a simple two-layer model (ocean and sediment) with constant sound speed in each layer. Today, there are many models allow for a more detailed description of both the ocean and sediment SSPs [51, 52]. The most common underwater acoustic propagation models in them are the Kraken [23], the Bellhop [24] and the range-dependent acoustic

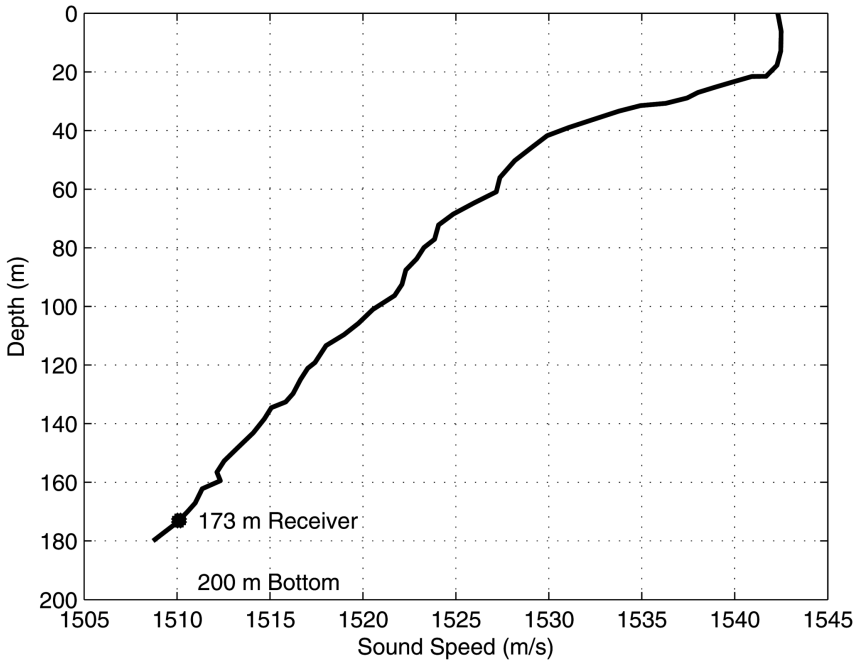

Fig. 1.4 SSP for GOM environment. Copied from [4].

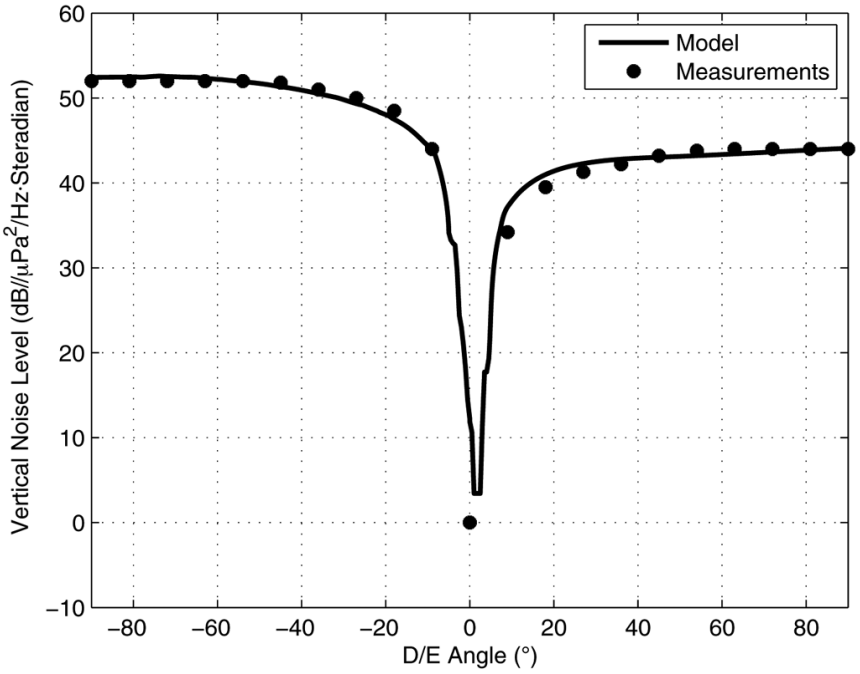

Fig. 1.5 Measured beam noise for the GOM environment. Copied from [4].

model (RAM) [53]. The models are well suited to simulate and analyze both range dependent and range independent acoustic propagation. They also allow an accurate definition of the velocity profile, range, depth, as well as a good characterization of the seabed properties such as roughness.

It is often useful to be able to plot the multipath rays for a given environment for illustrative purpose. There have been a number of approaches to model multipath, for example, using a static channel impulse response obtained from acoustic field computation [23, 54], or a model based on random fluctuations of complex amplitudes of paths [20]. A promising approach for dealing with underwater environmental effect is the 'virtual' signal transmission [55, 56].

Bellhop [24] is a widely known open-source Gaussian beam ray-tracing program model in the underwater acoustic modelling community. It is designed in order to perform acoustic ray tracing for a given sound speed profile $c(z)$ or a given sound speed field $c(r,z)$, where z is the depth of the receiver and r is the relative distance (range) from the receiver to the transmitter, in ocean waveguides with flat or variable absorbing boundaries [24]. The output of Bellhop includes ray coordinates, travel time and the corresponding amplitude of each eigenray, acoustic pressure or transmission loss [57]. The calculation of acoustic pressure is based on the theory of Gaussian beams [54].

Bellhop is suitable for high-frequency signals propagating in a deep water area. It is not suitable for very low frequency signals propagating in shallow water areas.

RAM [53] is suitable for strongly range-dependent environments with variable bathymetry and spatially varying sound speed profiles. It can handle very low frequency propagation in shallow water environments.

Kraken has two modes: The adiabatic mode and the coupled mode [23]. The adiabatic mode is suited for weakly range-dependent cases (the bathymetry is relatively flat) and the coupled mode is used for the strongly range-dependent case. In Kraken, when given a dynamic scenario, the arrival information can be pre-calculated. The disadvantage of Kraken is that, when dealing with highly variable bathymetric data (non-flat bathymetry), the approximation to the undersea landscape must be accurate, dramatically increasing the computer disk space and computation time required.

The three ocean acoustic propagation models (Bellhop, Kraken, and RAM) are often used to produce 2-D sound transmission loss plots for visualization of the sound fields. Given its relatively low computation complexity and memory demand, Bellhop is also used to produce a 3-D sound field display based on the N$\times$2D paradigm—a set of 2-D sound fields from different bearings merged into a 3-D sound field. Note that the azimuthal sectors must be

narrow enough to adequately sample the environment; otherwise, the simulation results may not have adequate accuracy.

For high-frequency problems the ray model provides results more rapidly and Bellhop can handle this computation more convenient than other models [56]. In this thesis, Bellhop is used in the design of the simulator, and underwater applications in localization, trajectory estimation and transmit beamforming.

1.5 Acoustic Channel Simulators for Underwater Communications

To assess the communication performance, sea experiments are often performed. However, to set up the infrastructure of sea experiments is usually expensive and difficult. To reduce the cost, a simulation of the signal transmission can be used. To simulate communications in UAC, acoustic channel simulators are applied. The channel simulator takes into account physical aspects of acoustic propagation. The basic model of an acoustic channel is that of a multipath channel with a low-pass filter, which accounts for energy absorption. The signal also attenuates with distance, according to the energy spreading law. In a multipath channel, all the paths can be approximated as having the same reference transfer function, but a different gain and delay. Some existing UWA channel simulators are presented below.

1.5.1 VirTEX

The VirTEX model [55] and extensions to it [56] uses a regular grid to describe the volume of water that the signal propagates through. The resolution of the grid is set up according to the required accuracy. In the example given in [55], three wavelengths in depth and several hundred in range give satisfactory results. The interpolation is performed in VirTex on the amplitude and time of arrivals of the multipath components. An interpolated point between the grid points is the weighted sum of the arrivals at the four surrounding points. So for instance if there were two multipath arrivals at each of the surrounding grid points then the interpolated point would comprise of eight multipath arrivals. The delays are adjusted according to the local speed of sound, the geometric distance and incident angle from the interpolated point to the grid point. The amplitude has a linear weighting according to that distance. VirTEX can simulate the transmission of relatively short signals between moving transmitter and receiver, and it requires computation of the channel impulse response from the acoustic field computations at every signal sample, which is complicated when dealing with signals at a high carrier frequency.

1.5.2 Waymark

A common promising approach in the virtual signal transmission [55, 56] is the Waymark simulator [58], which allows modelling the signal transmission for moving transmitter and receivers. The motion-induced channel time variations are modelled by sampling the transmitter/receiver trajectory at a rate much lower than the signal sampling rate and calculating, for each Waymark position, the channel impulse response from the acoustic field computation. The Waymark impulse responses are then used for interpolation of the time-varying channel impulse response at a sampling rate chosen with respect to the highest frequency in the spectrum of the transmitted signal. The high sampling frequency may result in a high running time for the original Waymark simulator.

1.5.3 Baseband Waymark

A further development of the Waymark model [58] with the aim to significantly reduce the simulation time is based on baseband processing. The baseband equivalent representation of the channel and signal is used in this model, which allows the processing on the signal propagating through the channel also to be at baseband frequencies [5]. The processing therefore is performed at a lower sampling rate depending on the signal bandwidth. In addition, this model has the ability to model longer channel impulse responses with the same resource, which helps to deal with more extreme underwater environments. However, the efficiency of the baseband Waymark model is now limited by the ray tracing (the Bellhop program [24] in our case) used for computing the impulse responses at waymarks.

Due to the disadvantages of these acoustic channel simulators, it is desirable to develop a more computationally efficient channel model simulator to speed up the computation.

1.6 Underwater Sensor Networks

To enable unexplored applications and to enhance the ability to observe and predict the ocean, underwater networks of sensors have been widely used [25]. Unmanned or Autonomous Underwater Vehicles (UUVs, AUVs), equipped with underwater sensors, are also envisioned to find application in exploration of natural undersea resources and gathering of scientific data in collaborative monitoring missions [59]. Underwater Acoustic Sensor Networks (UW-ASNs) consist of sensors and vehicles deployed underwater and networked via acoustic links to perform collaborative monitoring tasks [15]. These potential applications will be made viable by enabling communications among underwater devices.

UW-ASNs can enable a broad range of applications, including [15]:

- Ocean Sampling Networks. Networks of sensors and AUVs can perform synoptic, cooperative adaptive sampling of the 3D coastal ocean environment.
- Environmental monitoring. UW-ASNs can perform pollution monitoring (chemical, biological, and nuclear), monitoring of ocean currents and winds, improved weather forecast, detecting climate change, understanding and predicting the effect of human activities on marine ecosystems, and biological monitoring such as tracking of fishes or micro-organisms.
- Undersea Exploration. Underwater sensor networks can help detect underwater oil-fields or reservoirs, determine routes for laying undersea cables, and assist in exploration for valuable minerals.
- Disaster Prevention. Sensor networks that measure seismic activity from remote locations can provide tsunami warnings to coastal areas, or study the effects of submarine earthquakes (seaquakes).
- Assisted Navigation. Sensors can be used to identify hazards on the seabed, locate dangerous rocks or shoals in shallow waters, mooring positions, submerged wrecks, and to perform bathymetry profiling.
- Distributed Tactical Surveillance. AUVs and fixed underwater sensors can collaboratively monitor areas for surveillance, reconnaissance, targeting, and intrusion detection.
- Mine Reconnaissance. The simultaneous operation of multiple AUVs with acoustic and optical sensors can be used to perform rapid environmental assessment and detect minelike objects.
- Infrastructure Monitoring. UW-ASNs can be used to monitor a large amount of underground infrastructure (pipes, electrical wiring and liquid storage tanks). For example, sensors can be deployed along the path of pipes so that leaks can be quickly localized and repaired.

With the broad range of applications, UW-ASNs have been attracting interest from around the world. Challenges, such as localization and trajectory estimation, have been introduced by UW-ASNs. The monitoring information collected from a sensor node would be meaningless if the locations of the node or the trajectory of the UUV and AUV is unknown to the user. The work in this thesis contributes to the localization problem of the underwater nodes, and the the trajectory estimation of the UUVs and AUV, thus enhance the performance of UW-ASNs.

1.7 Underwater Localization and Trajectory Estimation

Underwater localization, also considered as navigation technology, is highly needed in underwater communications such as UW-ASNs [59]. The monitoring information collected from a sensor node would be meaningless if the locations of the node is unknown to the user. This also introduces the requirement of trajectory estimation in some applications related to underwater mobile nodes or AUV sensors.

Navigation technologies in underwater communications include depth sensing [60], orientation sensing [61], time-of flight acoustic navigation [62], Doppler navigation [63], inertial navigation [64] and satellite navigation [62].

In depth sensing, vehicle depth is usually computed from the direct measurements of ambient sea water pressure via standard equations for the properties of sea water [60]. The overall accuracy attained by depth sensing is about 0.1% of full-scale [65]. Attaining full accuracy requires calibration and compensation for thermal variation in sensor gain and offset.

In orientation sensing, rapid innovation in the technology of attitude sensing over the past two decades has resulted in new families of attitude sensors that offer dramatic improvement in accuracy, size, power consumption, interfaces, and operational lifetime [62]. A great variety of commercially available single-axis (heading only) and three-axis flux-gate magnetometers provide heading accuracies (when properly calibrated) on the order of 1°–3° with respect to local magnetic North, update rates on the order of 1–10 Hz, and power consumption typically less than 1 W [66]. A variety of systematic errors, such as errors due to the magnetic disturbance of the vehicle, can reduce the accuracy of these magnetic sensors. Low-cost roll and pitch sensors are most commonly based upon measuring the direction of the acceleration due to gravity with either pendulum sensors, fluid-level sensors, or accelerometers [67]. The accuracy provided by them is on the order of 1°-5° [67].

Acoustic time-of-flight navigation methods pioneered in the 1960's and 1970's continue to be employed today [68]. Long Baseline (LBL), in which a vehicle triangulates its position from acoustic ranges within a network of transponders are routinely used today [62]. A

high-frequency (typically 300 kHz or greater) LBL system is capable of sub-centimeter precision and update rates up to 10 Hz [69]. Unfortunately, due to the rapid attenuation of higher frequency sound in water, high-frequency LBL systems typically have a very limited maximum range which is less than 100 m [69]. The 12 kHz Long Baseline (LBL) acoustic navigation typically operates at up to 10 km ranges with a range-dependent precision of 0.1-10 m and update periods as long as 20 seconds or more [70]. All acoustic time of flight navigation methods require: careful placement of transponders fixed or moored on the sea floor, on the hull of a surface ship, or on sea-ice; accurate knowledge of the sound velocity; and are fundamentally limited by the speed of sound in water [71].

An acoustic navigation system combining LBL navigation techniques with transponder based Doppler velocity sensing is reported in [63]. Relative navigation errors are 0.4% of the distance travelled. There are two principal error sources arising in the Doppler navigation of underwater vehicles. The first one is heading, in terms of attitude sensor accuracy and precision [67, 61]. The second error source is sensor calibration alignment errors between the Doppler sonar and the attitude sensor [61, 64]. All navigation methodologies that employ Doppler measurements require accurate knowledge of the Doppler adjustment; accurate sound velocity estimates; and attitude measurements from gyrocompasses for accurate position estimates. The range suitable for Doppler measurements is also very limited (less than 100 m) [72].

Inertial measurement units (IMUs) are often employed in high-precision surveys, but their power consumption (ranging from 12–30 W) and cost (often in excess of $100,000 U.S.) have precluded their widespread use in civilian oceanographic vehicles [73].

The global positioning system (GPS) provides superior 3-D navigation capability for both surface and air vehicles, and is widely employed by oceanographic research surface vessels [74]. However, the GPS system's radio-frequency signals are blocked by sea water, thus GPS signals cannot be directly received by deeply submerged ocean vehicles [75]. A common solution for underwater vehicles to navigate through the GPS system is occasionally surfacing or connecting to a surface platform to obtain the GPS baseline, which is often impractical in oceanic environment [62].

Due to the high cost in the set up of infrastructure and impracticality in some underwater environment, it is useful to develop some advanced underwater localization techniques and trajectory estimation approaches.

1.8 Transmit Beamforming in Underwater Communications

The capacity of an underwater multiuser system is often limited by the co-channel interference (CCI) and intersymbol interference (ISI). CCI is the interference caused by users sharing the same channel. If the delay spread in a multipath channel is larger than a fraction of a symbol, the delayed components will cause ISI.

In radio communications, adaptive beamforming has been widely used at the receiver to reduce both CCI and ISI and to improve the capacity by adjusting the beam pattern such that the effective signal-to-interference-plus-noise ratio (SINR) at the output of the beamformer is increased [26]. In order to reduce CCI, the beamformer places nulls at the directions of interference, while the gain at the direction of the desired transmitter is maintained constant [76]. If multipath signals with large delay spread arrive at different angles, the single-tap beamformer rejects the ISI terms by placing nulls at the directions of multipath signals. In underwater environment, deploying antenna arrays at underwater receiver node is often impractical due to the size of the receiver. However, transmit beamforming can be deployed at underwater base station transmitter to improve the channel capacity. In scenarios where antenna arrays are used at transmitters, the beam-pattern of each antenna array can be adjusted to minimize the induced interference to undesired receivers, thus introducing the transmit beamforming.

Transmit beamforming and receiver beamforming are substantially different in nature. Receiver beamforming can be implemented independently at each receiver, without affecting the performance of other links, while transmit beamforming at each transmitter will change the interference to all other receivers. Therefore, transmit beamforming has to be done jointly in the entire network [77]. Moreover, in receiver beamforming, local feedback from the receiver output is used to adjust the beamformer vector. In transmit beamforming, channel estimation has to be done at the receiver and a feedback channel should be used to transmit the Channel State Information (CSI) to the transmitter.

The design of a transmit beamformer in multiuser channels is an area with increasing interest in modern wireless communication systems with SDMA [78]. The early concepts underlying digital beamforming (DBF) were first developed for applications in sonar [79] and radar systems [80]. The beamforming is then carried out by weighting the digital signals, thereby adjusting their amplitudes and phases such that when added together they form the desired beam. The most commonly used configuration is the linear array, in which the antenna elements are spaced along a straight line. The main difficulty in such systems is that coordinated receive processing is not possible and the processing must be employed at the transmitter side [81]. Linear precoding schemes provide a promising trade-off between performance and complexity [82–85]. The zero-forcing (ZF) beamforming

is the most common linear precoding scheme, which decouples the multiuser channel into multiple independent subchannels [86–92]. OFDM communication is considered as a promising technology for high data-rate communications in UAC [93–96]. It can be efficiently combined with SDMA to improve the system throughput [93, 97–99]. In this thesis, we will be investigating transmit beamforming based on linear precoding in an OFDM communication system.

1.9 Motivation and Contribution

The contribution of this thesis is summarized as follows:

The existing underwater acoustic channel models are investigated first, then an advanced channel model [7] for signal transmission in fast-varying UWA channels is proposed. In this model we propose to pre-compute ray parameters on a space (depth-range) grid, similarly to how it is done in the known VirTEX simulator, and use the ray parameters for the waymark impulse response computation, thus speeding up the simulation. In particular, this model can be used for numerical investigation of UWA communication systems with moving transmitter and/or receiver. Numerical examples show that this approach can reduce the simulator running time by 10-20 times compared to the baseband Waymark simulator, and, for some scenarios, make the simulation time even close to the real time.

An underwater localization technique [8] is proposed with the idea of pre-computing the acoustic field. The localization is based on pre-computation of acoustic channel parameters between a transmitter-receiver pair on a grid of points covering the area of interest. In this case, every receiver is assumed to have a single hydrophone, while multiple transducers transmit (pilot) signals known at a receiver. The receiver processes the received pilot signal to estimate the Channel State Information (CSI) and compares it with the CSI pre-computed on the grid; the best match indicates the location estimate. This localization could be applied in two-dimensional (Depth-Range) plane to present the location estimate by depth and relative distance (Range) to the transmitter, and it can also be applied to achieve the location estimate in three-dimensional (X-Y-Z) space,

A trajectory estimation technique [9] is proposed based on the proposed localization technique and data smoothing approach. For a dynamic receiver moving in the area of interest, with location estimates along the receiver trajectory, a smoothing approach based on P-splines is applied to recover the trajectory. This trajectory estimation approach can reduce the cost of infrastructure compared to the acoustic beacon networks.

The proposed localization technique also enables an efficient solution to the inherent problem of informing a transmitter about the CSI available at the receiver for the purpose

of transmit beamforming [8]. The receiver only needs to send a grid point index to enable the transmitter to obtain the pre-computed CSI corresponding to the particular grid point, thereby significantly reducing transmission overheads.

1.10 Thesis Outline

This thesis explores the techniques of channel modelling, localization, trajectory estimation and transmit beamforming in UAC.

Following the introduction and literature review presented in this Chapter, Chapter 2 describes the fundamentals of Grid Waymark Baseband underwater acoustic transmission simulator. Numerical simulation results are presented to show that this approach can reduce the simulator running time by 10-20 times compared to the baseband Waymark simulator, and, for some scenarios, make the simulation time close to the real time.

Chapter 3 presents an advanced underwater receiver localization technique based on grid computation. This method is applied and investigated in two cases: estimate the location of the receiver in two-dimensional (Depth-Range) plane and three-dimensional (X-Y-Z) space. Numerical results demonstrate that the proposed localization technique is effective in terms of accuracy of localization are presented.

Chapter 4 introduces an estimation method for the trajectory of an underwater dynamic receiver. This method is based on the proposed localization technique and smoothing approach. The combination of the localization and the smoothing approach is described. Numerical results are presented to show that this method allows accurate trajectory estimation in both two-dimensional plane and three-dimensional space cases.

In Chapter 5, we propose to apply this localization technique in UAC with SDMA to inform the transmitter of the CSI when designing the transmit beamformer, thus greatly reducing the size of the feedback message from the receiver to the transmitter. A transmit beamformer is also proposed, that exploits multiple channel estimates for the same user to improve the detection performance. Numerical results are presented to demonstrate that the proposed transmit beamformer achieves a high detection performance.

Finally, Chapter 6 presents the main conclusions of the thesis and ideas for future work are discussed.

Chapter 2

Grid Waymark Baseband Underwater Acoustic Transmission Model

2.1 Introduction

The performance of underwater acoustic communication systems is heavily dependent on the propagation environment, such as the SSP, the sea surface, and the bottom. To assess the communication performance, sea experiments are often required. However, to set up the infrastructure for sea experiments is usually expensive and difficult. To reduce the cost, a simulation of the signal transmission can be used. A simulation of the signal transmission can guarantee similar conditions when comparing different systems and provide reliable monitoring of the environment and thus give a valuable interpretation of experimental results. Therefore, it is highly desirable for researchers to have an efficient simulator for underwater acoustic signal transmission [3, 59]. There have been a number of approaches to deal with this problem, for example using a static channel impulse response [20] obtained from acoustic field computation, or a model based on random fluctuations of complex amplitudes of paths [23, 54]. Some models introduce frequency shifts in paths and a statistical model for multipath amplitudes [100]. Some approaches use a measured time-varying channel response and random local displacements based on direct replay [101, 3].

The first underwater acoustic signal transmission simulator introduced in this chapter is the VirTEX (Virtual Timeseries Experiment) simulator [55], which operates by post processing the outputs produced by the Bellhop ray tracing program [24]. This simulator approximates the environment by a snapshot or freeze frame, then it performs Bellhop ray tracing computation in the snapshot, the ray parameters are then obtained at computation points in the freeze frame [55]. VirTEX can simulate the transmission of relatively short

signals between moving transmitter and receiver, and it requires computation of the channel impulse response from the acoustic field computations at every signal sample, which is complicated when dealing with signals at a high carrier frequency.

Another promising approach in the virtual signal transmission [55, 56] is the Waymark simulator [58], also allowing modelling of the signal transmission for a moving transmitter and receiver. The motion-induced channel time variations are modelled by sampling the transmitter/receiver trajectory at a rate much lower than the signal sampling rate and calculating, for each waymark position, the channel impulse response from the acoustic-field computation. The Waymark impulse responses are then used for interpolation of the time-varying channel impulse response at a sampling rate chosen with respect to the highest frequency in the spectrum of the transmitted signal. The high sampling frequency may result in a high running time for the original Waymark simulator.

A further development of the Waymark model [58] with the aim to significantly reduce the simulation time is based on baseband processing [5]. However, the efficiency of the baseband Waymark model is now limited by the ray tracing program (the Bellhop program [24] in our case) used for computing the impulse responses at every waymark.

In this chapter, to further speed-up the simulation, it is proposed to pre-compute the ray parameters on a space (depth-range) grid, similarly to how it is done in the VirTEX simulator [55], then save this grid map with arrival information at every grid point in memory. When in simulation, the ray parameters at every waymark are approximately computed by combining the pre-computed arrivals at four grid points around the waymark location rather than running Bellhop, thus speeding-up the computations.

2.2 Grid Waymark Model

In a time-varying channel, the noise-free signal at a receiver is described as a convolution [102],

$$y(t) = \int_{-\infty}^{\infty} h(t,\tau)s(t-\tau)\mathrm{d}\tau, \quad t \in [0, T_{sig}], \tag{2.1}$$

where $h(t,\tau)$ is the passband channel impulse response at time t, $s(t)$ is the transmitted signal and T_{sig} is the signal duration. At time t the channel impulse response can be represented as the sum of multipath components [103]:

$$h(t,\tau) = \sum_{p=1}^{L} A_p(t)\delta(\tau - \tau_p(t)), \tag{2.2}$$

where L is the number of arrivals, $A_p(t)$ is the time-varying amplitude of the pth path, $\delta(t)$ is the Dirac delta function and $\tau_p(t)$ represents the corresponding delay. The time-varying delay $\tau_p(t)$ is defined by the path geometry, which encompasses any movement in the system ultimately representing the Doppler effect.

In the Waymark model [58], a set of points (waymarks) are set along the receiver/transmitter trajectory, and the impulse response at every waymark is calculated using the arrivals computed by the Bellhop ray-tracing program [24]. The time interval in the trajectory between waymarks is typically much longer than the signal sampling interval due to the slow variation of the channel impulse response from one signal sample to another. This long waymark interval reduces the simulation time greatly when compared to ray-tracing for every signal sample interval.

Local splines are used in Waymark model to reduce the complexity and memory requirement for the computation of the impulse response. When using cubic B-splines, only four arrival coefficients are needed to compute the impulse response at any sampling instant [58]. For the computation of the signal at the output of the channel at any instant, only a few waymark impulse responses are needed. This approach significantly reduces the modeling complexity and it allows a recursive computation of the output signal with reduced and fixed memory consumption, independent of the signal duration.

To reduce the simulation time further, an extension to the Waymark model in [58] creates a time-varying channel model using the baseband equivalent representation of the signals and channel, which allows the processing on the signal propagating through the channel also to be at baseband frequencies [5]. The processing therefore is performed at a lower sampling rate depending on the signal bandwidth. In addition, this approach has the ability to model longer channel impulse responses with the same resources, which helps to deal with more extreme underwater environments.

In the baseband Waymark model, as described in [5], the original signal spectrum is shifted to center around zero and a low pass filter applied. The low pass filter chosen is the raised cosine filter [104].

The baseband equivalent transmitted signal $s_e(nT_s)$ can be approximated by:

$$s_e(nT_s) = \sum_{k=-K/2}^{K/2-1} [s(kT_s)e^{-j2\pi f_c kT_s}] r(nT_s - kT_s), \quad n = 0, ..., N-1, \tag{2.3}$$

where the raised cosine impulse response [104] is given by:

$$r(nT_s) = \text{sinc}(f_0 nT_s) \frac{\cos(\pi f_0 \alpha nT_s)}{1 - (2f_0 \alpha nT_s)^2}, \tag{2.4}$$

where T_s is the original sampling period of the passband signal, f_c is the carrier frequency, $N = T_{sig}/T_s$, K is the raised cosine filter length, α represents the roll-off factor, and f_0 is the upper bound of the baseband frequencies.

Once the transmitted signal has been transformed into the baseband equivalent $s_e(nT_s)$, the sampling interval T_s then can be increased to a longer sampling period T_d. The baseband signal at the receiver is then obtained via the baseband filtering:

$$y_e(n_dT_d) = \sum_{i=0}^{I-1} h_e(n_dT_d, iT_d)s_e(n_dT_d - iT_d), \quad n_d = 0, ..., N_d - 1, \tag{2.5}$$

where $h_e(n_dT_d, iT_d)$ is the baseband channel impulse response at time $t = n_dT_d$, $N_d = T_{sig}/T_d$, I is the number of channel taps and i is the index of channel tap. The channel impulse response $h_e(n_dT_d, iT_d)$ at every sample n_dT_d is computed by a spline approximation [58] using the channel impulse responses $h_{e,m}(iT_d)$ calculated at waymark points. Once passed through the channel, the output baseband signal $y_e(n_dT_d)$ is upsampled back to the original sampling frequency as $y_e(nT_s)$, and upshifted back to passband. Due to the relatively slow speed of sound, the channel delay variations are very important in the restoration of the signal to the passband. Therefore, the upshift of the signal needs to take into account the delay that was applied to the input signal at each sample point. The upshifted post channel signal is then calculated as:

$$y(nT_s) = \Re\left\{y_e(nT_s)e^{j2\pi f_c(nT_s - \tau_n)}\right\}, \tag{2.6}$$

where $y(nT_s)$ is the output passband signal sample, $y_e(nT_s)$ is upsampled baseband output signal and τ_n represents the estimated additional delay at each output sample instant. The delays τ_n are computed using the spline interpolation between the delays computed at waymarks.

To speed up the computations in the Waymark model further, the Grid Waymark model is proposed here. Similar to the VirTEX model in [55], we are using a regularly spaced grid to describe the volume of water that the signal propagates through. The interpolation is performed on the amplitude and delay of arrivals of the multipath components. An interpolated point (waymark) between the grid points is gathering the weighted arrivals at the four surrounding grid points as shown in Fig. 2.1 and Fig. 2.2.

The attenuations from the four grid points are weighted and gathered to obtain complex amplitudes $\mathbf{A}_G$ at the waymark (trajectory) point (x, y), and the corresponding delays τ_G are adjusted by the ray path travel time differences between the corners of the computational grid and the interpolated point (see [55] for more details). The arrival amplitudes at each of the grid points are weighted and combined as:

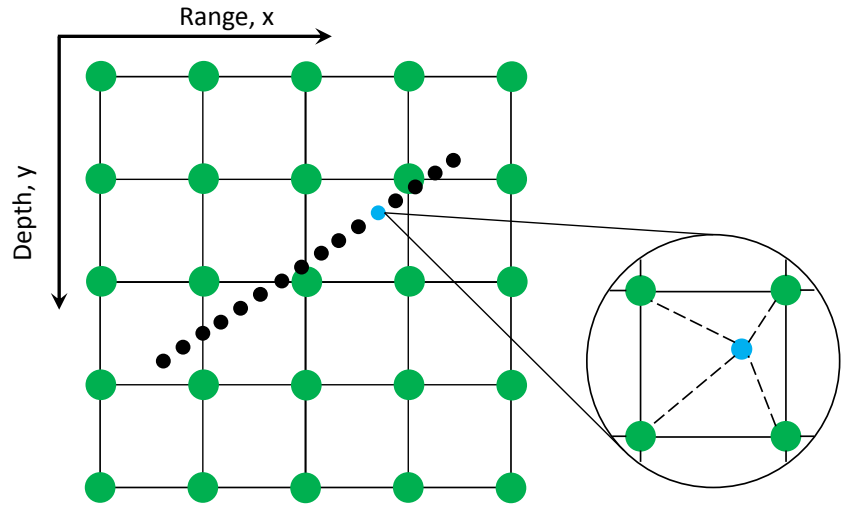

Fig. 2.1 Receiver trajectory with waymarks (black, blue) in a grid field (green). The acoustic field at a waymark point is combined with the weighted arrivals at four grid points around it.

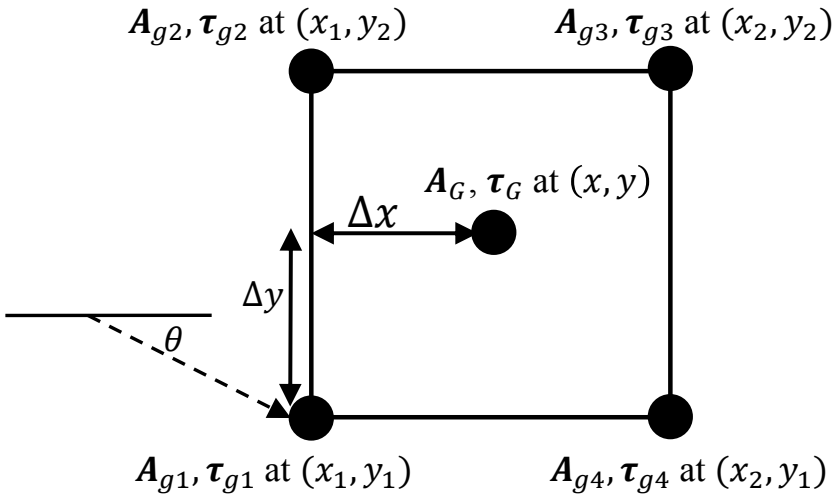

Fig. 2.2 Four points of the grid for a ray tracing computation at a waymark. The arrivals are pre-computed at the four corners and any point in the interior is computed through interpolation of the weighted amplitudes and adjusted delays at grid points. A sample arrival is shown traveling at angle θ.

$$\mathbf{A}_G = \begin{bmatrix} (1-w_x) \times (1-w_y) \times \mathbf{A}_{g1} \\ (1-w_x) \times w_y \times \mathbf{A}_{g2} \\ w_x \times w_y \times \mathbf{A}_{g3} \\ w_x \times (1-w_y) \times \mathbf{A}_{g4} \end{bmatrix} . \tag{2.7}$$

Here we assume that the maximum number of arrivals at each grid point is L, then $\mathbf{A}_{g1}$, $\mathbf{A}_{g2}$, $\mathbf{A}_{g3}$, and $\mathbf{A}_{g4}$ are column vectors of length L; they represent the arrival amplitudes at each of four grid points around the waymark point (x,y). The weights w_x and w_y are given by [55]:

$$\begin{aligned} w_x &= (x-x_1)/(x_2-x_1), \\ w_y &= (y-y_1)/(y_2-y_1). \end{aligned} \tag{2.8}$$

Thus, w_x represents a proportional distance in the x direction and w_y represents a proportional distance in the y direction.

As shown in Fig. 2.2, the dashed line represents an arrival traveling at angle θ at the lower left grid point. The delay time for that arrival is adjusted from position (x_1,y_1) to position (x,y) by the distance divided by the sound speed [55]. The adjusted delay is given by

$$\Delta_{delay} = (\Delta x \cos\theta + \Delta y \sin\theta)/c, \tag{2.9}$$

where $\Delta x = x - x_1$, $\Delta y = y - y_1$ for the grid point (x_1,y_1) in this example, and c is the sound speed at (x_1,y_1). The corresponding delays of arrival at (x,y) are then given by

$$\tau_G = \begin{bmatrix} \tau_{g1} + \Delta_{\tau 1} \\ \tau_{g2} + \Delta_{\tau 2} \\ \tau_{g3} + \Delta_{\tau 3} \\ \tau_{g4} + \Delta_{\tau 4} \end{bmatrix}, \tag{2.10}$$

where τ_{g1}, τ_{g2}, τ_{g3} and τ_{g4} are column vectors of length L; they represent the delays of arrival at grid points corresponding to $\mathbf{A}_{g1}$, $\mathbf{A}_{g2}$, $\mathbf{A}_{g3}$, and $\mathbf{A}_{g4}$. Vectors $\mathbf{\Delta}_{\tau 1}, \mathbf{\Delta}_{\tau 2}$, $\mathbf{\Delta}_{\tau 3}$ and $\mathbf{\Delta}_{\tau 4}$ contain adjusted delays $\mathbf{\Delta}_{delay}$ of all arrivals at (x_1,y_1), (x_1,y_2), (x_2,y_2), (x_2,y_1).

With the complex amplitudes of arrivals $\mathbf{A}_G$ and corresponding delays τ_G, which characterize the acoustic-field, we can find the channel frequency response $H_e(\omega)$ at that waymark (x,y). The baseband channel impulse response $h_e(iT_d)$ is obtained from $H_e(\omega)$ by the inverse Fourier transform.

At waymark m, the channel frequency response $H_{e,m}(\omega_q)$ at a frequency ω_q is computed as

$$H_{e,m}(\omega_q) = \sum_{l=1}^{M} C_l e^{-j2\pi(\tau_{G,l} - \tau_{min})\omega_q}, \tag{2.11}$$

where M is the number of eigenpaths (distinct curved direct paths linking the transmitter and receiver) gathered for the waymark point, τ_{min} is the minimum delay (the common propagation delay) for all the paths, which is removed from all arrivals to reduce the size of the impulse response at waymark point as described in [58]. C_l is the baseband complex

amplitude of the lth arrival and $\tau_{G,l}$ is the corresponding delay. The complex amplitude of the multipath arrival at the baseband is given by [103]:

$$C_l = \mathbf{A}_{G,l} e^{-j2\pi f_c \tau_{G,l}}, \tag{2.12}$$

where $\mathbf{A}_{G,l}$ is the complex amplitude of the lth arrival gathered at waymark m, and f_c is the carrier frequency.

Assuming Q frequencies of interest ω_q, the impulse response $h_{e,m}(iT_s)$ is then obtained by the inverse Fourier transform:

$$h_{e,m}(iT_d) = \sum_{q=0}^{Q-1} H_{e,m}(\omega_q) e^{j\omega_q iT_d}. \tag{2.13}$$

The structure of the proposed simulator is shown in Fig. 2.3, as a development from the original system in [5]. In this development, the acoustic field at waymark m is computed by gathering the weighted arrivals at four grid points around the waymark point, rather than calling the Bellhop program. The channel frequency response $H_{e,m}(\omega_q)$ in (2.12) and the impuse response $h_{e,m}(iT_d)$ in (2.13) are then computed. With the baseband equivalent representation, the processing is allowed to be at baseband frequencies and performed at a lower sampling rate, thus reducing the simulation time. The splitting of the channel into two components, the composite delay and impulse response, allows more accurate interpolation of the channel impulse response between waymarks. Since the variation of the channel impulse response from one signal sample to another is considered slow, the sampling interval is increased from T_s to $T_d = \eta \times T_s, (\eta \gg 1)$, to give a lower sampling rate, and consequently reduce the computation. The local spline interpolation is then used for recovering the impulse response for all signal sampling instants. The local interpolation between waymarks allows removal of any constraints on the duration of the signal transmission simulation session.

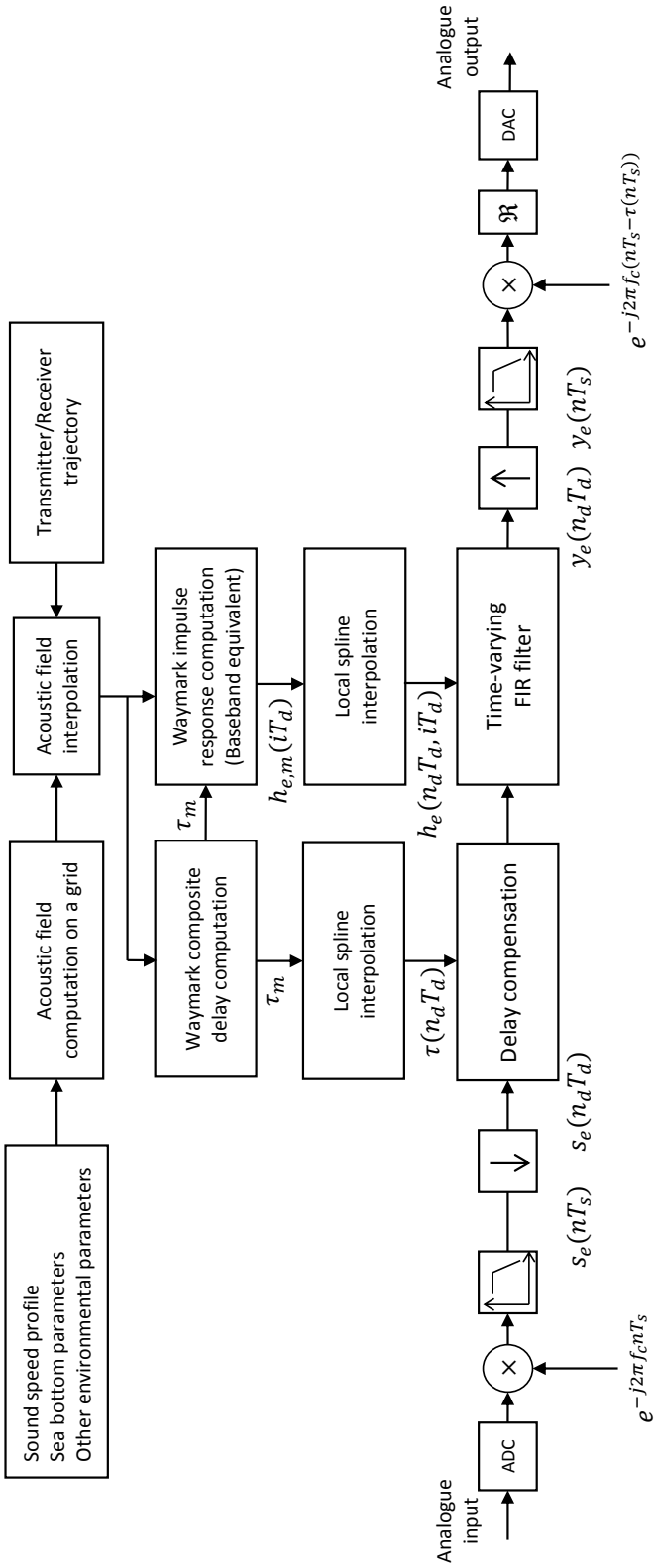

Fig. 2.3 A block diagram of the underwater acoustic channel simulator as a development on the system presented in [5].

2.3 Numerical Simulation in Shallow Water

In this section, some examples are given to illustrate the proposed simulator and compare it with the original baseband Waymark and VirTEX models.

1. Simplified Environment Test: The simulation environment is as follows.

   A 10 kHz tone signal is transmitted. It is sampled at a 40 kHz sample frequency. The signal duration is 100 seconds. The underwater environment is described by a flat Sound Speed Profile (SSP); the speed of sound is constant 1500 m/s from the bottom to surface. The sea bottom is flat at 200 meters depth and the surface is flat calm. Both the receiver and transmitter are at a depth of 100 meters. The range between them varies as 1000 m $+ v_c t$ m, (v_c = 5m/s). The decimation factor is η =64, giving the signal sample interval $T_d = 64 \times T_s = 1.6$ ms.

   With a 10 kHz tone, the motion was expected to result in a Doppler shift of around -33.3 Hz. The waymark interval was set to 0.0512 seconds. Fig. 2.4 shows the spectrum of the channel output from the original baseband Waymark, VirTEX and proposed Grid Waymark models. The peaks in the figure are due to multipath components with slightly different Doppler spreads due to different angles of arrival. The normalized root-mean-square error (NRMSE) between the spectrum of the channel output from the original baseband Waymark and the proposed Grid Waymark models is 10%, and also 10% between VirTEX and the proposed Grid Waymark models.

   The simulation was running in Matlab (version R2017a) under Windows 7 operating system with a 3.4 GHz Intel Core i7 CPU and 8 GB of RAM. For the original baseband Waymark model, simulating 120 seconds of transmission time requires 4662 seconds, this number is mostly due to the Bellhop ray-tracing called at every waymark. For the proposed Grid Waymark model with grid step of 0.25 m, the same as the waymark step in the original baseband Waymark model, this simulation only takes 226 seconds, which is almost a real time simulation (120 s signal duration). This is a significant reduction in computation compared to the original baseband Waymark model, it is about 20 times faster with the proposed Grid Waymark model.

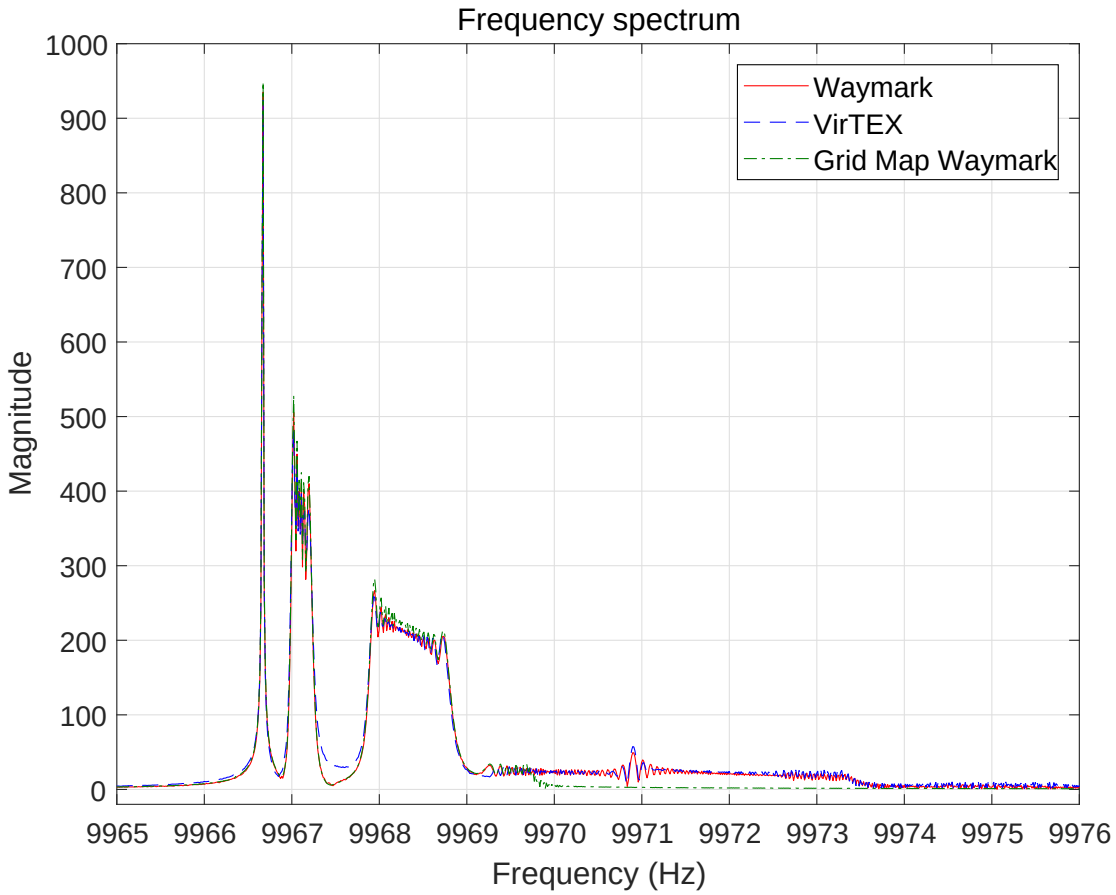

Fig. 2.4 The received signal spectrum from the Waymark, VirTEX and Grid Waymark models for a scenario with a flat SSP sound environment.

2. Complex Environment Test: To compare these three models with a more complex and realistic environment, the 10 kHz tone is transmitted in the SWellEx-96 SSP and a section of the trajectory from Event S5 [105]. The simulation environment is as follows.

   A 10 kHz tone of 100 s duration is transmitted, sampled at 40 kHz sampling frequency. The sea bottom is flat and the surface is flat calm. Speed, locations and motions of the transmitter and the receiver are from the SWellEx-96 event S5 localized data [106]. Fig. 2.5 shows a map of the source track during event S5 and the location of the receiver hydrophone array, a vertical line array (VLA) used for data collection. During the experiment, a source at a supposed depth of 54 m was towed along an isobath by a source ship [106]. The source ship started its track from the south of the array and proceeded northward at a speed of about 2.5 m/s. The decimation factor is η =64.

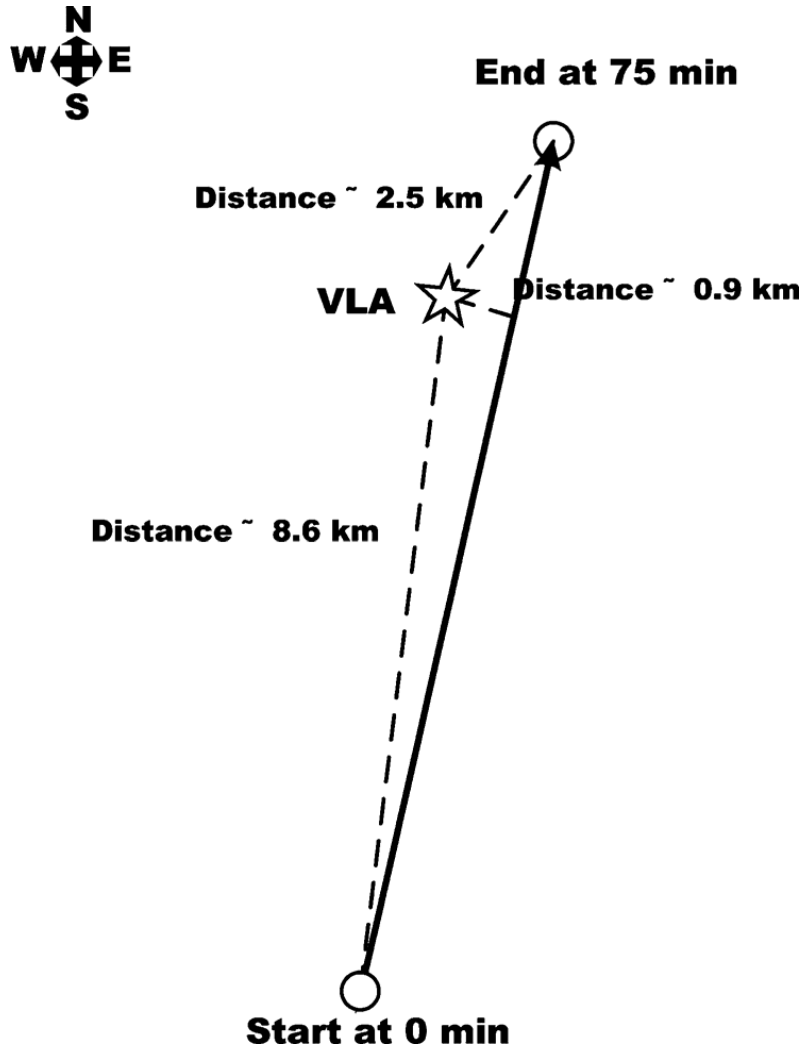

Fig. 2.5 Map of the source track and the location of the VLA. Copied from [6]

Fig. 2.6 shows the spectrum of the channel output from the original baseband Waymark, VirTEX and the proposed Grid Waymark models. The waymark interval for the Waymark model [5] and the Grid Waymark model was 0.0512 seconds. The Doppler spreads around the main peaks are again generally agree. The NRMSE between the spectrum of the channel output from the original baseband Waymark and the proposed Grid Waymark models is 0.11%, and 6.2% between VirTEX and the proposed Grid Waymark models. For the Waymark model, 14009 seconds is required in this simulation, while the proposed Grid Waymark requires 1476 seconds, which shows about 10 times faster computation.

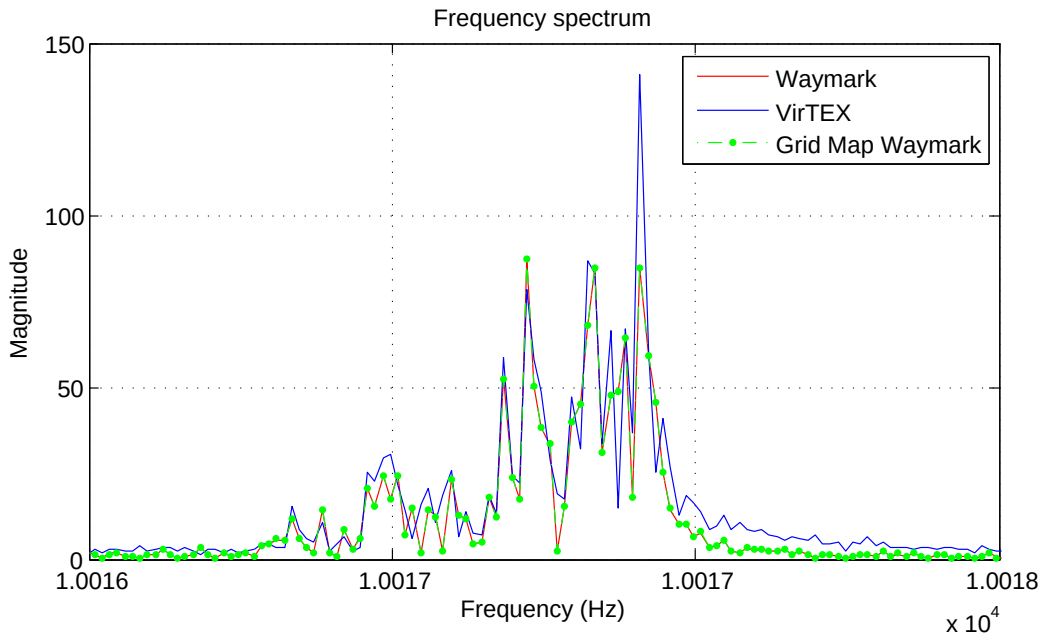

Fig. 2.6 The received signal spectrum from the Waymark, VirTEX and Grid Waymark models for a scenario with the SWellEx environment and trajectory. The red line overlaps the green line since they are very close to each other.

Simulations were carried out to investigate the effect of the grid step size on the NRMSE between the spectrum of the channel output from the original baseband Waymark and the proposed Grid Waymark models, and the simulation time required for the proposed Grid Waymark model. It can be seen in Table 2.1 that the simulation time and the accuracy of the Grid Waymark model are improved with a reduction in the grid step. However, the simulation time increases insignificantly. The storage memory for the acoustic field information and the computation time for pre-computing a space grid is then investigated and this is described in Section 3.4.

Table 2.1 The NRMSE between the spectrum of the channel output from the original baseband Waymark and the proposed Grid Waymark models with different grid step sizes

Grid step	NRMSE	Simulation time
5 m	3.12%	1392 s
2.5 m	1.20%	1411 s
1 m	0.54%	1427 s
0.5 m	0.31%	1453 s
0.25 m	0.11%	1476 s
0.1 m	0.11%	1491 s

2.4 Conclusions

In this chapter, a further extension to the Waymark model proposed in [58] and [5] is described as the Grid Waymark model. This model combines the Waymark model with the idea of pre-computing the acoustic field on a space grid. It computes the waymark impulse responses by gathering weighted ray parameters from the grid points around the waymark. The Grid Waymark model has a significant advantage in computation speed compared to the original baseband Waymark model.

The original baseband Waymark, VirTEX and Grid Waymark have been compared. The results show similarity with the major features of the Doppler shifts. The computation time taken with the Grid Waymark model is significantly less than that of the original Waymark model. Therefore, the Grid Waymark model simulator is also applied in the simulations in this thesis.

With this proposed channel model and the idea of pre-computing the arrival parameters in a grid map and storing them at the transmitter and the receiver, an advanced receiver localization technique and a trajectory estimation method are proposed in the following chapters.

Chapter 3

Receiver Localization Based on Grid Computation

3.1 Introduction

Determining the location of a transmitter/receiver has attracted interest from around the world. In many applications such as sensor networks, the sensing information is meaningless if the location of the sensor node is unkown to the user. The measurement of the position of an emitter/receiver is usually done with sensors, which can sense the depth, acceleration, or orientation. The target can be in a terrestrial or underwater environment. In the terrestrial environment, existing systems and technologies for precise localization are costly and time consuming to develop and deploy, and lack the flexibility to make cost-effective enhancements once deployed. Existing systems mostly rely on the global positioning system (GPS), which is unable to be accessed in underwater.

In the underwater environment, location estimation for underwater vehicles/sensors in the oceanic medium has been attracting the interest of researchers for decades [107]. Underwater localization is widely used in offshore applications such as deep sea exploration, environmental monitoring, geological and ecological research, sample collection [108]. Propagation delays, a motion-induced Doppler shift, phase and amplitude fluctuations, multipath interference, and so on, are all significant factors in location measurement, and they have introduced challenges in UWA localization.

The well-known GPS system, which can accurately estimate geographical locations of sensor nodes, does not work in underwater. A common method to apply a GPS system in UACs is that the AUV has to occasionally reach the surface, or connect to other vehicles on the surface, to obtain a GPS baseline and update its location [109, 110]. However, this is

either dangerous or impractical in many cases [109]. Another common solution is applying acoustic beacon networks for triangulation [111]. However triangulation system requires overwhelming support infrastructures located in different positions in underwater, resulting in high cost especially in long distance, When errors are accumulated in the location estimates and a wrong trajectory estimation is recovered, the receiver can easily be lost.

To overcome these problems, we propose an advanced receiver localization technique based on grid computation. In the localization, a database of possible Channel State Information (CSI) is pre-computed for a grid in space (grid of range/depth points), and saved at both the transmitter and receiver. Such a database is built based upon acoustic field computation for a specific environment, where the receiver is navigated. To estimate the location of the receiver, the CSI measured at the receiver is compared with the CSI on the grid covering the area of interest; the location estimate is indicated by the best match.

The approach based on pre-computing the acoustic field using a wave equation is similar to localization using matched field processing (MFP) often based on processing of a priori unknown signals received by an array of hydrophones. There have been a number of studies and experiments related to MFP [112–116] and the general idea is to search over a parameter space for the unknown parameters of the signal source [117, 118]. As a development of MFP, the environmental focalization technique was proposed [119, 120], which is based on adjustment of environmental parameters within a search space which, after being optimized under a particular objective function, generates physical parameters that correspond to the acoustic field replica best matching the observed acoustic field. In the recent work [121], the localization technique was used to improve the channel estimation in UAC.

MFP is often based on processing a priori unknown signals received by an array of hydrophones. However, in our case, every receiver is assumed to have a single hydrophone, while an array of transducers transmits (pilot) signals known at a receiver. For a dynamic receiver, the grid map localization is applied at sample points along the receiver trajectory to obtain a set of estimated locations, which are represented by relative distance (range) to the transmitter and depth of the receiver.

3.2 Receiver Localization in Depth-Range Plane

Consider a (geographical) area of interest presented in Depth-Range plane, for example as shown in Fig. 3.1. The Channel State Information (CSI) between a transducer and a receiver hydrophone located within this area can be pre-computed, e.g., using standard acoustic field computation programs. This computation can be repeated for every grid point as illustrated in Fig. 3.1, thus producing a grid map. The receiver can estimate the CSI using a pilot signal

transmitted from the transducer. By comparing the estimated CSI with the CSI in the grid map, the best match can be identified and the position of the corresponding grid point can be treated as an estimate of the receiver position.

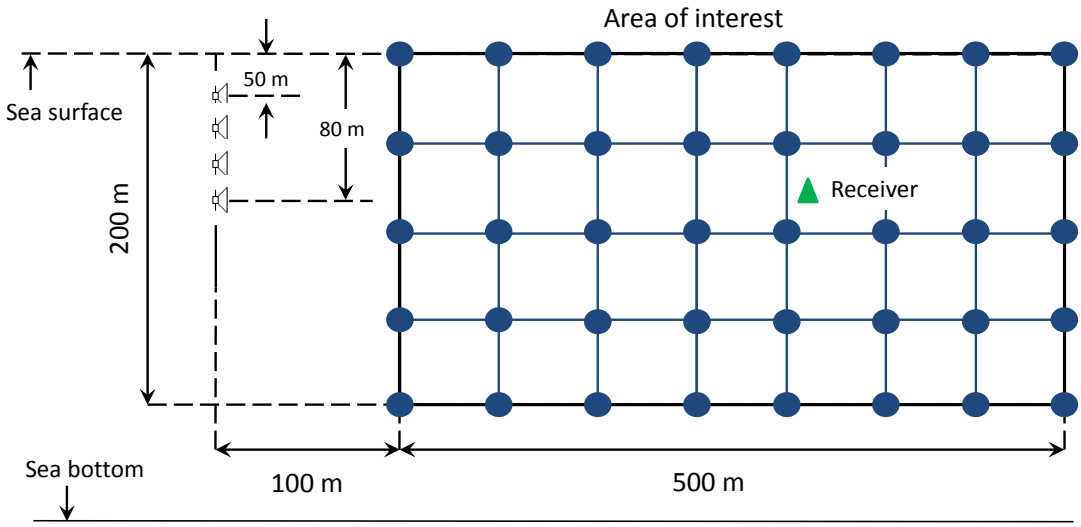

Fig. 3.1 An example scenario, the receiver is located in an area of interest 200 m $\times$ 500 m. The sea depth is 220 m. The transducers are equally spaced from a depth of 50 m to 80 m.

Let $\mathbf{g}_m$ be a $K \times 1$ channel frequency response vector representing the CSI for the mth grid point; the vector length K is the number of (subcarrier) frequencies at which the frequency response is defined. UAC typically operates at relatively high frequencies, for which ray tracing is an efficient method to solve the wave equation and thus compute the vector $\mathbf{g}_m$. For our numerical examples, we use the ray-tracing program Bellhop [24]. Based on knowledge of the acoustic environment, such as the sound-speed profile (SSP) and acoustic parameters of the sea bottom, the depth of the transducer, and the (range-depth) position of the grid point, the program computes the complex-valued amplitudes $A_{m,i}$ and delays $\tau_{m,i}$ for multiple (L_m) rays (eigenpaths), $i = 0, \ldots, L_m - 1$, connecting the transducer and hydrophone at the mth grid point. Based on these channel parameters, the channel frequency response can be computed as

$$g_m(f) = \sum_{i=0}^{L_m-1} A_{m,i} \exp(-j2\pi f \tau_{m,i}), \tag{3.1}$$

where the computations are made at subcarrier frequencies $f = f_0, \ldots, f_{K-1}$ covering the frequency range of the communication system; the values $g_m(f)$ are elements of the vector $\mathbf{g}_m = [g_m(f_0), \ldots, g_m(f_{K-1})]^T$.

Let $\hat{\mathbf{h}}$ be a $K \times 1$ vector representing the channel estimate at the same subcarrier frequencies. In the frequency domain, at a frequency f, the received signal is given by

$$y(f) = h(f)p(f) + n(f), \tag{3.2}$$

where $h(f)$, $p(f)$ and $n(f)$ are the channel frequency response, transmitted signal and noise, respectively. The least-square channel estimate is then given by [122]:

$$\hat{h}(f) = \frac{y(f)}{p(f)}, \;\; f = f_0, ..., f_{K-1}. \tag{3.3}$$

Thus, elements of the $K \times 1$ vector $\hat{\mathbf{h}}$ are the values $\hat{h}(f_k), k = 1, \ldots, K$, i.e. $\hat{\mathbf{h}} = [\hat{h}(f_0), ..., \hat{h}(f_{K-1})]^T$.

The vector $\mathbf{g}_m$ represents a 'signature' of the mth grid point, and $\hat{\mathbf{h}}$ is a 'signature' measured at the receiver. By comparing $\hat{\mathbf{h}}$ with the M signatures in the database $\{\mathbf{g}_m\}_{m=1}^{M}$, we can find the best match resulting in an estimate of the receiver location.

We can find the best match between the vector $\hat{\mathbf{h}}$ and M vectors $\{\mathbf{g}_m\}_{m=1}^{M}$ representing the grid map by computing the normalised covariance

$$c_m = \frac{\left|\mathbf{g}_m^H \hat{\mathbf{h}}\right|^2}{||\mathbf{g}_m||_2^2 \, ||\hat{\mathbf{h}}||_2^2}, \;\; m = 1, \ldots, M, \tag{3.4}$$

where c_m is also considered as the match level of $\hat{\mathbf{h}}$ and $\mathbf{g}_m$, $||\hat{\mathbf{h}}||_2^2 = \hat{\mathbf{h}}^H \hat{\mathbf{h}}$, and finding the maximum amongst all the covariances:

$$m_{\text{best}} = \arg \max_{m=1,...,M} c_m. \tag{3.5}$$

However, since the pilot transmission and reception are not synchronized, there is an unknown delay between the channel impulse responses estimated at the receiver and those pre-computed using the wave equation. In application to the channel frequency responses, this is equivalent to replacing $\hat{\mathbf{h}}$ with $\mathbf{\Lambda}_\tau \hat{\mathbf{h}}$, where $\mathbf{\Lambda}_\tau$ is an $K \times K$ diagonal matrix with diagonal elements

$$\mathbf{\Lambda}_\tau = \text{diag}\left[e^{-j2\pi f_0 \tau}, \ldots, e^{-j2\pi f_{K-1} \tau}\right],$$

and τ is the unknown propagation delay. Additionally, with multiple transducers, the localization performance can be improved by combining the coherence coefficients for all (N_T) transducers. More specifically, $\{\mathbf{g}_{t,m}\}_{m=1}^{M}, t = 1, ..., N_T$, with N_T grid maps are pre-computed, and N_T channel estimates $\hat{\mathbf{h}}_t, t = 1, ..., N_T$, are obtained at the receiver. Therefore,

the covariance in (3.4) is modified as

$$c_m = \sum_{t=1}^{N_T} \frac{\max_{\tau \in [\tau_{\min}, \tau_{\max}]} \left| \mathbf{g}_{t,m}^H \mathbf{\Lambda}_\tau \hat{\mathbf{h}}_t \right|^2}{||\mathbf{g}_{t,m}||_2^2 \, ||\hat{\mathbf{h}}_t||_2^2}. \tag{3.6}$$

where we use the fact that $||\mathbf{\Lambda}_\tau \hat{\mathbf{h}}||_2^2 = ||\hat{\mathbf{h}}||_2^2$, and $[\tau_{\min}, \tau_{\max}]$ is an interval of possible delays. Note that the quantities $\mathbf{g}_{t,m}^H \mathbf{\Lambda}_\tau \hat{\mathbf{h}}$ in (3.6) can be efficiently computed for a range of delays using the fast Fourier transform (FFT). The grid point m_{best} then is found as the maximum c_m over the M grid points. The idea of using multiple transducers to improve the localization performance is similar to a beacon network system, which estimates the location of the receiver with precise distance measurements made by multiple beacon nodes [123]. The difference is that a beacon system requires the beacon nodes to be installed at different positions on the sea-bed, while the proposed localization technique only needs a vertical array of transducers [107].

Geographical coordinates of the grid point m_{best} are considered as an estimate of the receiver location. The accuracy of this localization method is investigated in Section 3.4.

In the following chapter, we show how this localization technique combined with a smoothing technique can be used to recover the trajectory of a receiver in the Depth-Range plane. An advanced transmit beamforming technique in a multiuser communication system will also be proposed based on this grid localization method in Chapter 5.

3.3 Receiver Localization in Three-Dimensional Space

With the localization technique described in the previous section, one can estimate the location of the receiver represented in the two-dimensional (Depth-Range) plane with one transmit antenna or an array of transducers. To have the location estimated in the three-dimensional (X-Y-Z) space, as an extension to the localization in the two-dimensional plane, we propose to place multiple transducers around the space of interest, and apply the proposed localization for the receiver with each transducer, then the location estimates are combined to obtain the estimated location represented in X-Y-Z space.

Let M denote the number of transmit transducers/antennas. For each transmit antenna, we pre-compute a grid map, and the receiver estimates its depth and relative distance to the transmit antenna using the grid map localization method proposed in the previous section. The depth of the receiver, also considered as the Z component of the receiver location, is estimated M times with M transducers, and these depth estimates should be the same if the estimates are correct. The X and Y components of the receiver location can be achieved by

combining the estimated distances to the transmit antennas as:

$$(x_0, y_0) = \arg\min_{(x,y)} \sqrt{\sum_{m=1}^{M} \left[\sqrt{(x_m - x)^2 + (y_m - y)^2} - r_m \right]^2}, \tag{3.7}$$

where (x_0, y_0) is the estimated position of the receiver in X-Y plane, M is the number of transmit antennas, (x_m, y_m) is the coordinates of the mth transmit antenna in X-Y plane, and r_m is the estimated distance (range) of the receiver to the mth transmit antenna. As in (3.7), the position of the receiver in X-Y plane is found with its distances to the transducers match the measurements.

With this grid localization method used in X-Y-Z space, one can recover the trajectory of a moving receiver in the three-dimensional space, which is described in Chapter 4. The accuracy of the proposed localization technique is demonstrated in the following section.

3.4 Numerical Results

Discussion

In the existing triangulation system, the receiver must 'see' at least three beacons to localize itself in a plane [124, 125]. Therefore, the set up of a beacon network for a triangulation system requires placement of anchor nodes at different positions on sea-bed, which introduces the problem of accurate installation of the structures [126]. This problem is more challenging in the deepwater environment. The accuracy of a classical triangulation system has been investigated in [107, 127]. For 1 km $\times$ 1 km area with four beacon nodes, the accuracy is 1 to 10 m between the true location and the estimated location.

The commonly used GPS technique does not require the installation of beacons and the accuracy of it is considered high (within 5 m) [128]. However, it needs the receiver to reach the surface, or connect to other vehicles at the surface, which is not possible in many applications [109, 110].

With the proposed receiver localization technique using a pre-computed grid map, the only installation needed is a vertical sensor array, which can be connected to a ship or an anchor node on sea-bed, thus reducing the cost of the infrastructure.

In this section, numerical examples are presented to illustrate the accuracy of the proposed receiver localization technique.

Simulation setup

In the investigation, we use the Waymark simulator [58, 5, 7] for the virtual signal transmission in scenarios with N_T transducers.

The following scenario is considered. The sea depth is 220 m, and the area of interest is as shown in Fig. 3.1. The SSP and sea bottom parameters are taken from [105] and shown in Fig. 3.2. Every receiver is equipped with a single receive antenna. The signals are transmitted at the carrier frequency 3072 Hz with a frequency bandwidth of 1024 Hz, so that the frequency band is from 2560 Hz to 3584 Hz.

To estimate the CSI at the receiver, a pilot is transmitted from the transmitter to the receiver. It is performed using OFDM signals with $K = 1024$ subcarriers, an orthogonality interval of 1 s, and subcarrier spacing of 1 Hz. The cyclic prefix (CP) of the OFDM symbols is 1 s long to avoid the intersymbol interference due to long channel delays (see Fig. 3.4). When searching over delays τ in (3.6), the search interval $[\tau_{\min}, \tau_{\max}]$ is set to the OFDM orthogonality interval $[-0.5, 0.5]$ s. The pilot and data symbols used for modulation of OFDM subcarriers are BPSK symbols.

In the experiments, a grid map, with 1 m or 0.5 m resolution, is generated and stored in memory for every transducer. The grid maps are pre-computed in Matlab (version R2017a) under the Windows 7 operating system with a 3.4 GHz Intel Core i7 CPU and 8 GB of RAM. The 1 m resolution grid map with $201 \times 501 \approx 10^5$ grid points is computed within 5 mins, and it requires a storage memory of 37 MB. The 0.5 m resolution grid map with about 4×10^5 grid points is computed within 20 mins, and it requires a storage memory of 148 MB. The average computation time and storage memory for one grid point is approximately 3 ms and 370 bytes, respectively.

3.4.1 Receiver Localization in Two-Dimensional Plane

To investigate the performance of the localization technique in the Depth-Range plane (two-dimensional plane), transducers are equally spaced from a depth of 50 m to 80 m (for $N_T = 4$) or to 100 m (for $N_T = 6$). The transducers emit acoustic signals in the interval of vertical angles $[-50^\circ, +50^\circ]$. A pilot signal is transmitted from each of the four (or six) transmit antennas sequentially in time. The pilot signal is a single OFDM symbol with a predefined BPSK sequence modulating the subcarriers. At the receiver, channel estimation is carried out as described by (3.3). Using the channel estimates, the best combined coherence of the channel frequency responses estimated at the receiver and those computed at the grid points is calculated using equation (3.6). The position of this best grid point is treated as an estimate

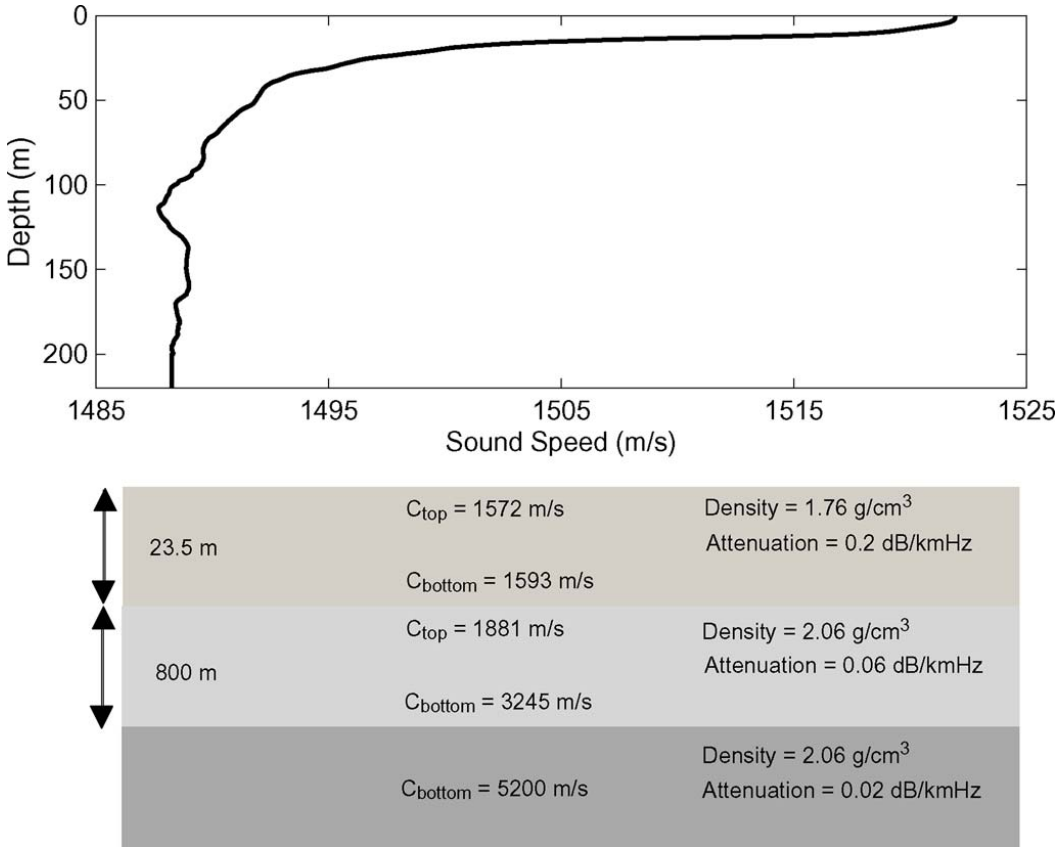

Fig. 3.2 The SSP and the layered sea bottom parameters.

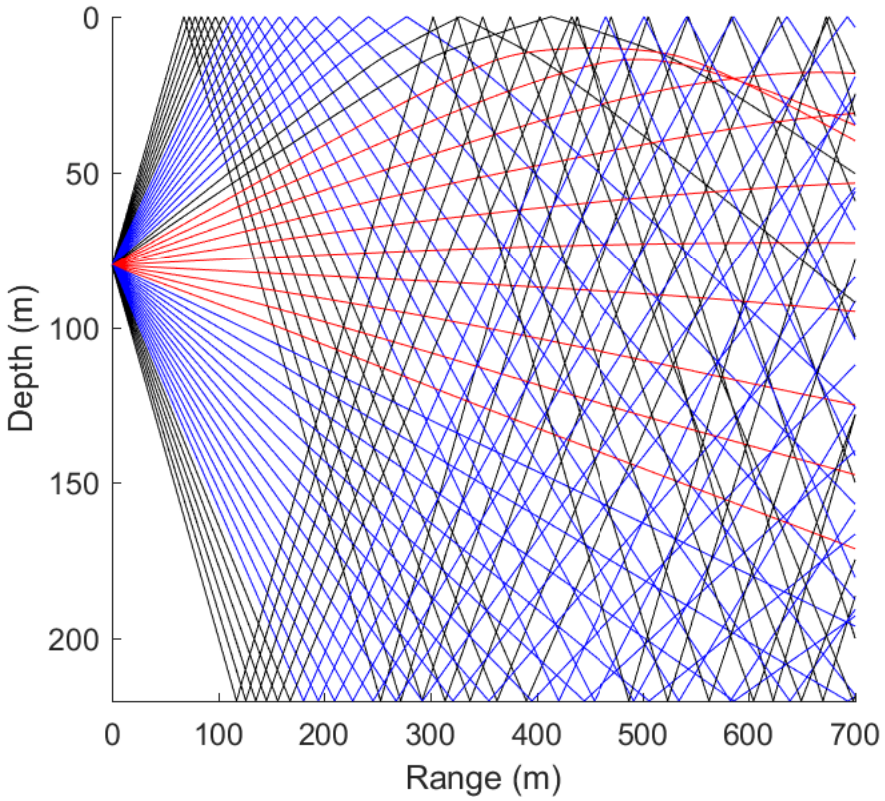

Fig. 3.3 Ray tracing computation for the area of interest. The rays are plotted using different colors to improve the visualization.

of the receiver position. The grid map is computed with a resolution of either 1 m or 0.5 m in both the depth and range.

To illustrate the acoustic field in the area of interest, Fig. 3.3 shows results of the ray tracing in this area. Fig. 3.4 shows examples of the channel impulse response for the four grid points within this area. It is seen that most of the acoustic rays experience reflections from the sea surface or bottom. As a result (as can be seen in Fig. 3.4), the multipath delay spreads can be as high as 0.5 s.

To investigate the probability of correct localization, the localization is performed for 100 different positions of the receiver within the area of interest. The tested positions uniformly cover the area. We consider two cases. In the first case, the received signal is not distorted by the additive noise, i.e., the signal-to-noise ratio is SNR = ∞ dB. In the second case, white Gaussian noise of the same power as the signal power in the frequency bandwidth of the communication system is added to the received pilot signal, so that SNR $= 0$ dB; we repeat the experiment 10 times, every time adding a new noise realization, and averaging simulation results over the 10 trials.

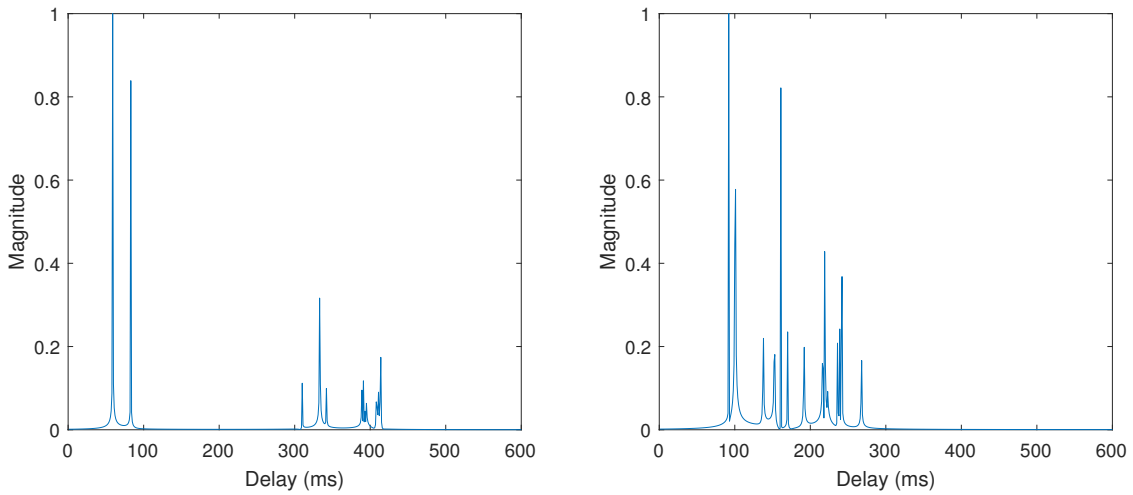

(a) $d = 50$ m, $r = 200$ m.

(b) $d = 50$ m, $r = 500$ m.

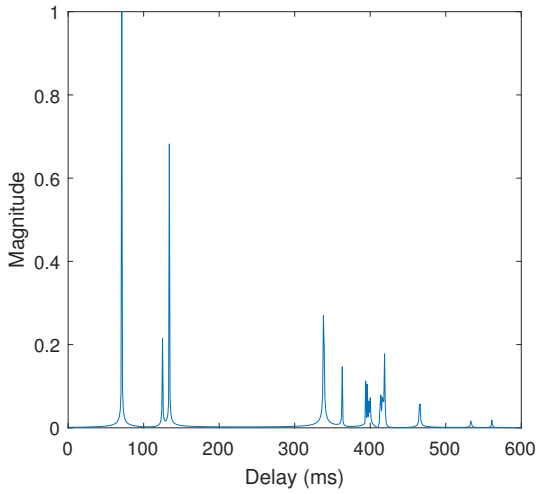

(c) $d = 150$ m, $r = 200$ m.

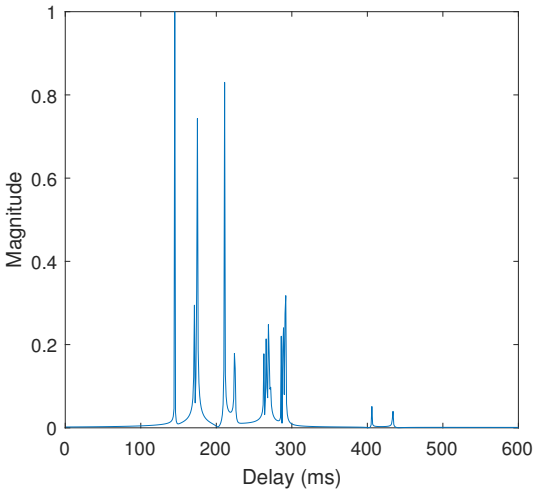

(d) $d = 150$ m, $r = 500$ m.

Fig. 3.4 Examples of the channel impulse response magnitude for a receiver within the area of interest and for the transducer depth 80 m. The receiver is positioned at a depth d and range r from the transducer.

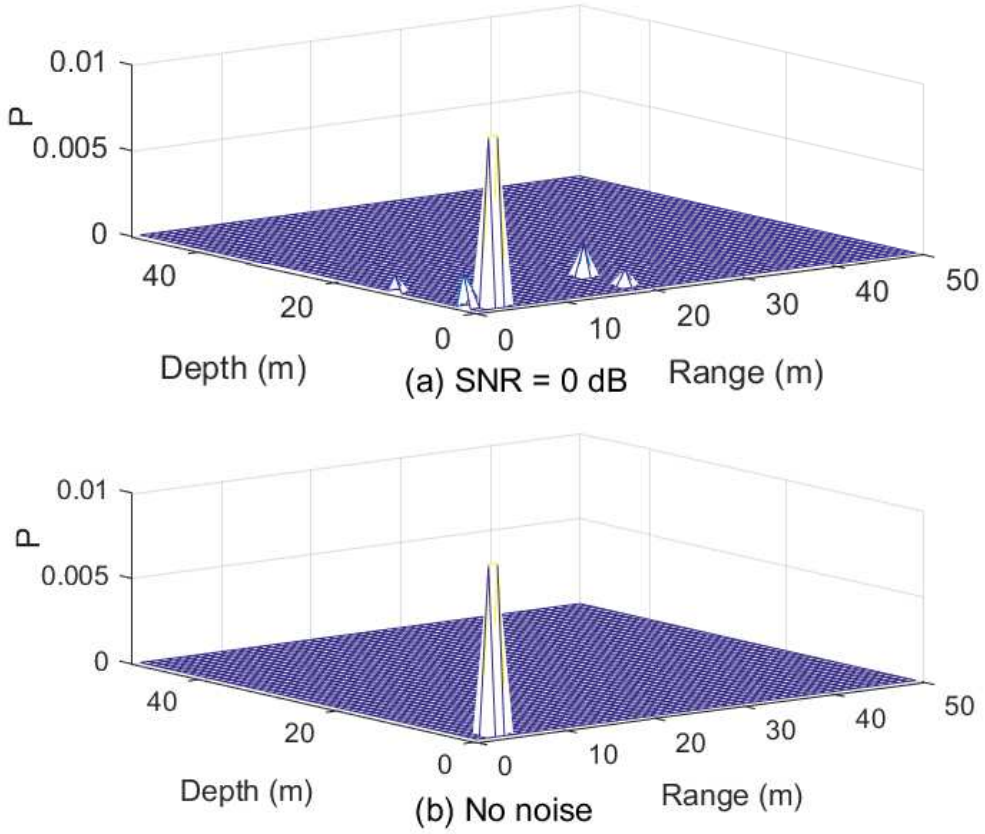

Fig. 3.5 Distribution of localization errors in the scenario with the flat sea surface. The grid map resolution is 1 m.

Experiments are done in the scenarios as follows.

Flat Sea Surface

The sea surface is flat. The receiver is located exactly on a grid point; more specifically, the set of the receiver depths is given by the vector [11 32 53 74 95 116 137 158 179 199] m and the set of ranges from the transducers is given by the vector [100 150 200 250 300 350 400 450 500 550] m. In both cases (low and high SNR) around 91% of estimates are located at the true locations. Fig. 3.5 shows the probability of incorrect localization P as function of the difference (in range and depth) between the estimated location and the true location. It can be seen that the incorrect location estimates are mostly close (within a few meters) to the true location.

Sinusoidal Sea Surface

In UWA channels, propagated signals interact with the sea surface. As can be seen in Fig. 3.3, in the area of interest, many multipath arrivals are reflected from the sea surface, i.e., the sea surface plays an important role in the propagation. Therefore, another test is carried out where the pilot signals are transmitted in the environment with a 'frozen' sinusoidal sea surface, while the channels at grid points are pre-calculated in the environment with a flat calm surface. The amplitude and the wavelength of the sea surface waves are set to be 5 m and 8 m respectively. The other conditions of the experiment are the same as in the previous scenario. As in the experiment with the flat sea surface, in this experiment for both cases (low and high SNR) around 91% of estimates are equal to the true location. Fig. 3.6 shows the probability of incorrect estimates against distances to the true location. It can be seen that the location accuracy is high and similar to that in the experiment with the flat sea surface, despite the mismatch of the grid map computation to the true acoustic environment where the pilot signals propagate.

Receivers are located between grid points

To investigate the localization technique in a more practical scenario, an experiment is carried out with the receiver located between grid points; the receiver locations in the experiment with the flat sea surface are now shifted randomly with a uniform distribution within the grid resolution interval. Fig. 3.7 shows the probability of incorrect localization P as a function of the difference between the estimated location and the true location. In this case, over 70% of location estimates still have a distance to the true location less than 5 m, which can be acceptable for some applications. However, it is clear that compared to the two previous scenarios with the receiver at a grid point, the error probability increases. For some receiver positions, the location estimate can differ significantly (of the order of tens of metres) from the true location, even without the noise.

To achieve better localization, we can improve the resolution of the grid map and/or increase the number of transmit antennas. Fig. 3.8 shows the cumulative distribution function (CDF) of distance between the estimated and true positions for the four combinations of the resolution and number of transmit antennas. White Gaussian noise of the same power as the signal power in the frequency bandwidth of the communication system is added to the received pilot signal, so that SNR $= 0$ dB. An increase in the number of transducers from $N_T = 4$ to $N_T = 6$ greatly improves the localization performance. However, an equivalent effect is achieved with the same number of transmit antennas and an improved resolution of

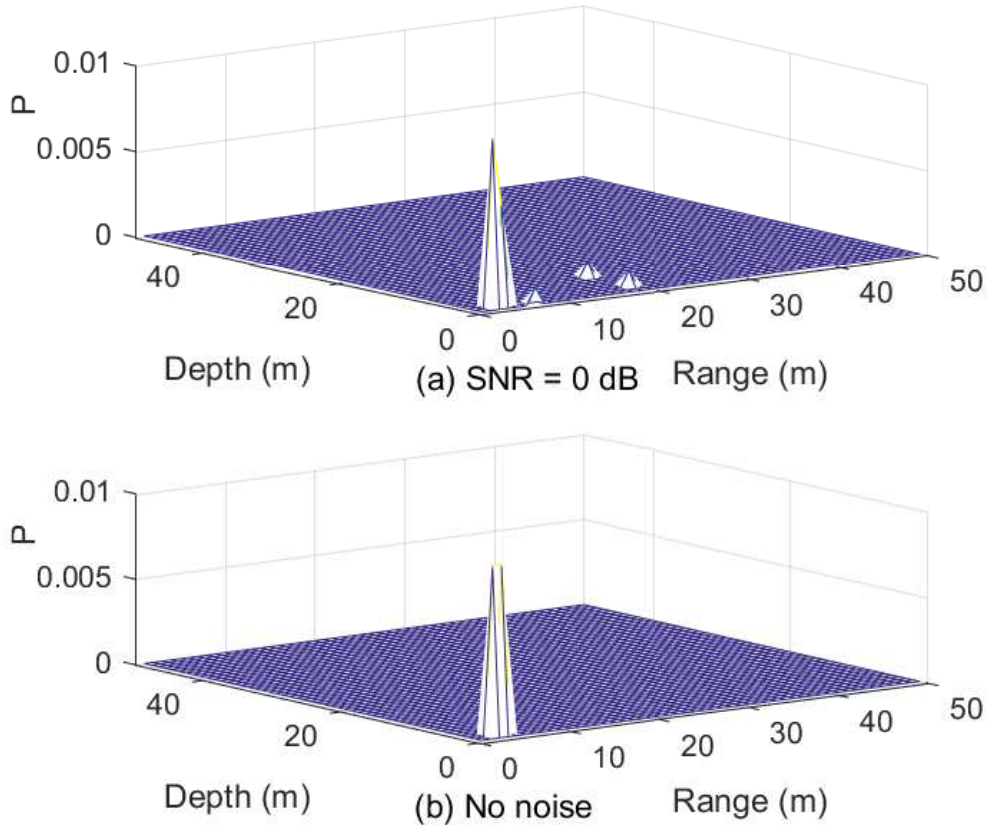

Fig. 3.6 Distribution of localization errors in the scenario with transmission of pilot signals in an environment where the surface is a sine wave, while the grid map is computed for the flat sea surface. The grid map resolution is 1 m.

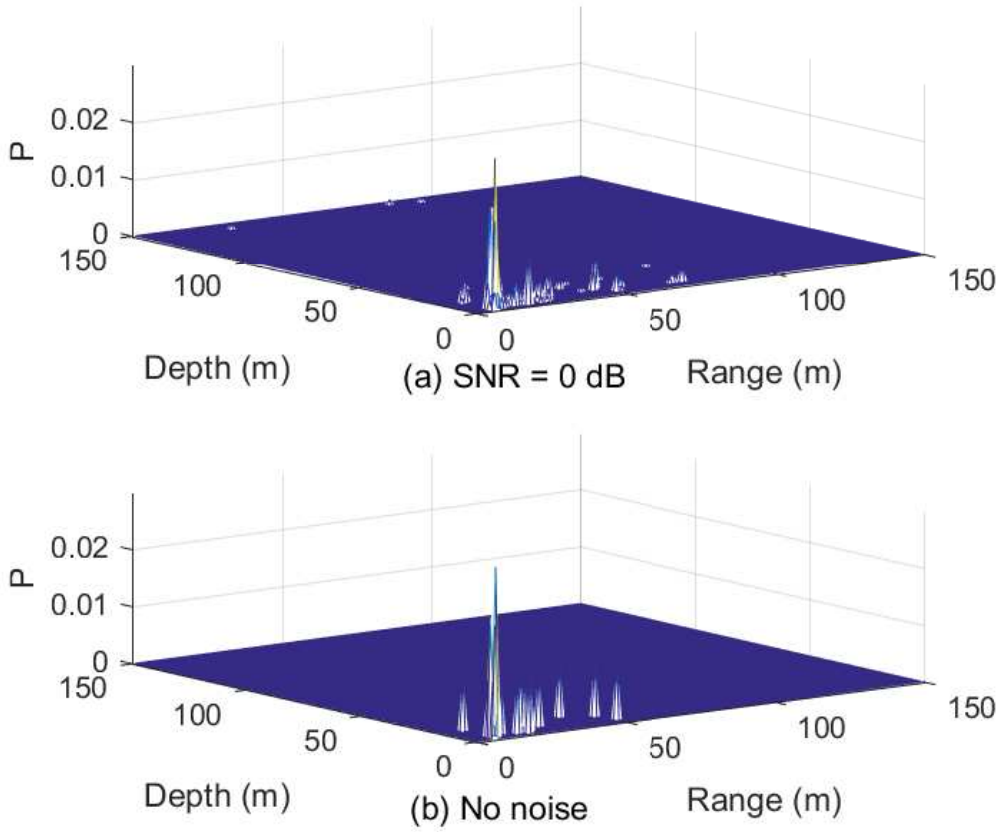

Fig. 3.7 Distribution of localization errors in the scenario with the receiver at random positions between grid points. The grid map resolution is 1 m.

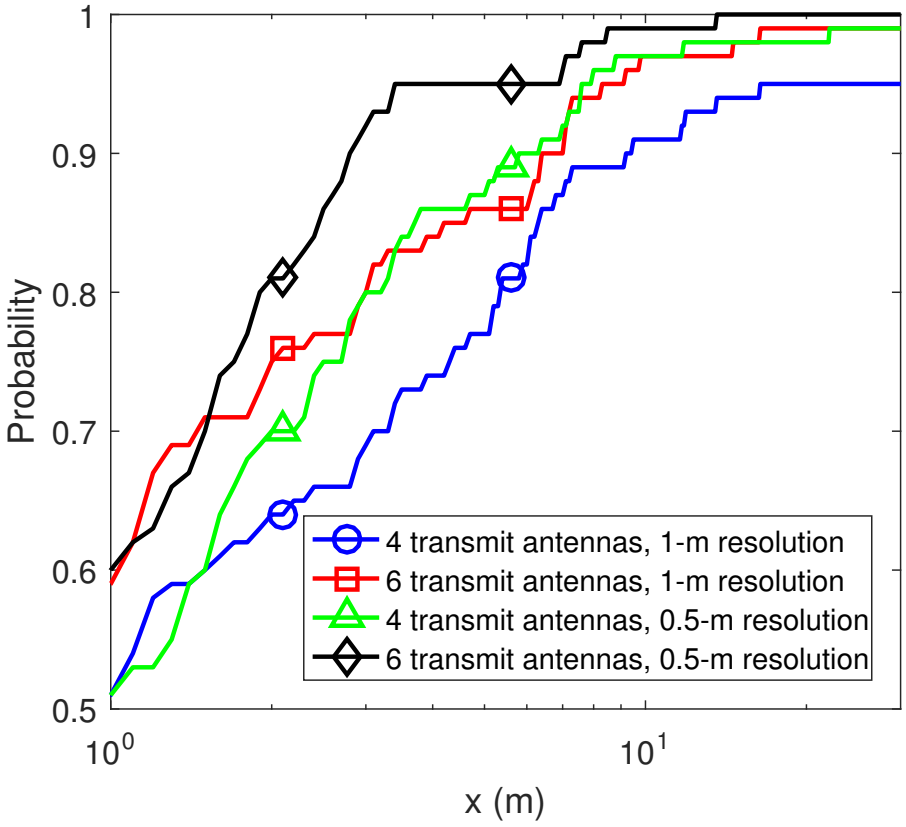

Fig. 3.8 CDF for the position error x (meters), calculated as $x = \sqrt{\Delta_d^2 + \Delta_r^2}$, where Δ_d is the depth error and Δ_r is the range error, for experiments with different grid map resolution and different numbers of transmit antennas. SNR = 0 dB.

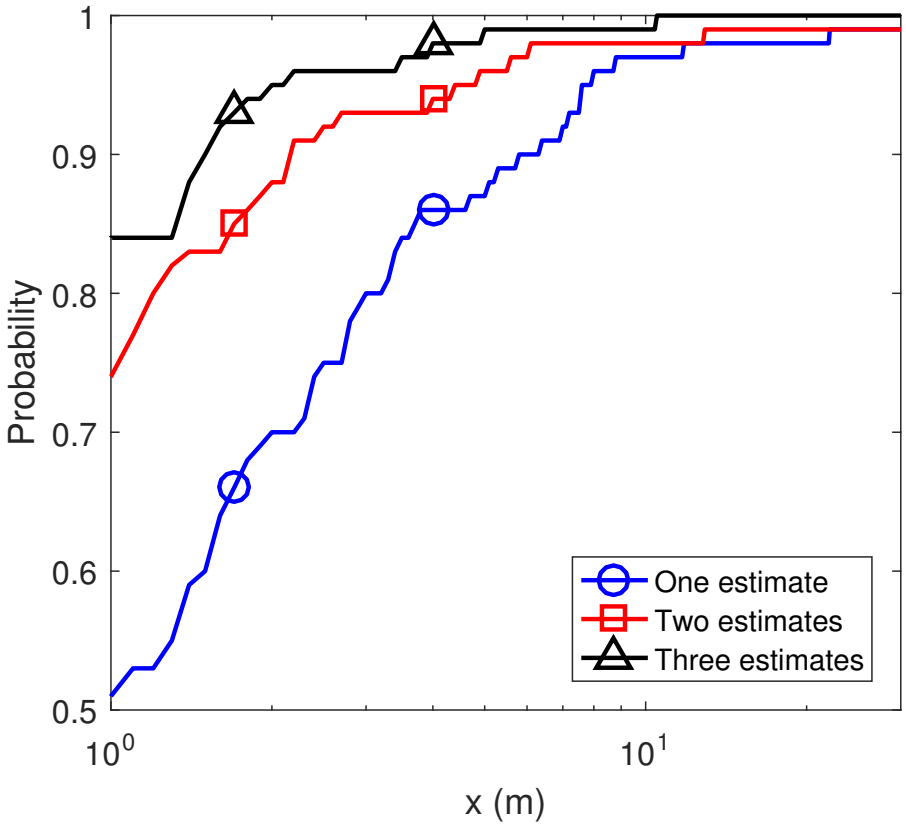

Fig. 3.9 CDF for the position error x (meters) for the best location estimate of one, two, or three estimates. The grid map is calculated with a resolution of 0.5 m. $N_T = 4$. SNR = 0 dB.

the grid map. The latter can be a more practical approach since it does not require additional hardware at the transmitter.

In the design of transmit beamformer described later in this thesis, it is proposed to use several location estimates (several estimated grid points) when designing the transmit beamformer to improve the detection performance. We now investigate the CDF (see Fig. 3.9) of the distance between the best of two (or three) location estimates and the true location for $N_T = 4$. The grid map is calculated with a resolution of 0.5 m, SNR $= 0$ dB. It is seen that it is highly probable (about 80%) that the best of two and best of three position estimates is within 1 m to the true location, while with a single estimate, the probability is only about 50%.

Localization of receivers at a higher frequency

In the previous experiments, the signals are transmitted at the carrier frequency 3072 Hz with a frequency bandwidth of 1024 Hz, so that the frequency band is from 2560 Hz to 3584 Hz. However, in practice, the signals are often transmitted at higher frequencies when the distance between the transmitter and the receiver is less than 1 km. To investigate the performance of the localization technique at higher frequency, another test is carried out where the carrier frequency is increased from 3072 Hz to $3072 \times 2 = 6144$ Hz. The frequency bandwidth remains 1024 Hz, so the frequency band is from 5632 Hz to 6656 Hz. The number of subcarriers remains $K = 1024$, subcarrier spacing is 1 Hz and the orthogonality interval is 1 s. The other conditions of the experiment are the same as in the previous scenario.

When SNR = 0 dB, in the experiment with the carrier frequency of 3072 Hz, with 4 transmit antennas and 1 m resolution of grid maps, around 75% of location estimates have a distance to the true location less than 5 m as shown in Fig. 3.8. In this experiment with a higher carrier frequency, with 4 transmit antennas and 1 m resolution of grid maps, over 60% of location estimates have a distance to the true location less than 5 m, which indicates a decrease in the localization performance. This is because the wavelength in water is reduced and the channel frequency response varies faster at higher frequencies, which results in a decrease in the localization performance when using the grid map with the same size resolution as before. Fig. 3.10 shows the CDF of distance between the estimated and true positions with different grid map resolution and different numbers of transmit antennas. It is seen that, although the performance of the localization is decreased with the higher carrier frequency, an equivalent effect can be achieved by increasing the number of transmit antennas or an improved resolution of the grid map.

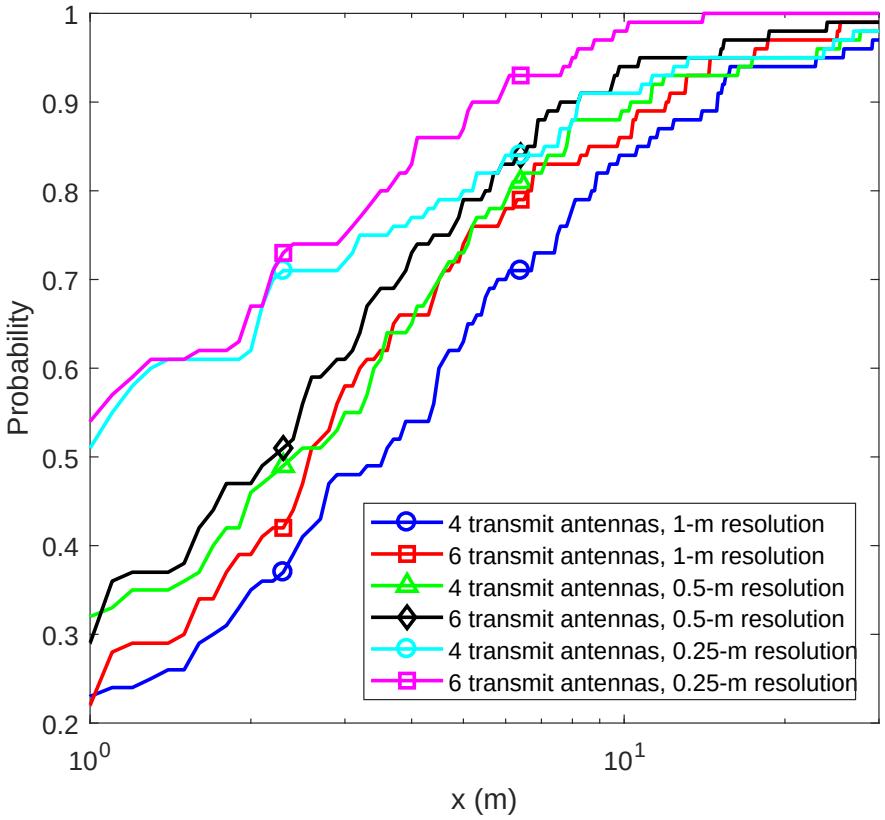

Fig. 3.10 CDF for the position error x (meters), for experiments at high frequency with different grid map resolution and different numbers of transmit antennas. SNR = 0 dB.

Localization of receivers at longer distance

In many practical scenarios in UAC, the distance between the transmitter and the receiver can be longer than a thousand meters. To investigate the localization technique in such a scenario, an experiment is carried out with the area of interest shown in Fig. 3.1 being shifted horizontally by 2 km. Therefore, the area of interest in this experiment is in distances from 2 km to 2.5 km. The other conditions of the experiment are the same as in the scenario with the area of interest shown in Fig. 3.1, the receivers are located between grid points and the carrier frequency is 3072 Hz. Fig. 3.11 shows the CDF of distance between the estimated and true positions with differing grid map resolutions and differing numbers of transmit antennas. It can be seen that, at longer distances, the performance of the localization with different number of transmitters and different resolution of grid maps are generally better than in the scenario at a distance of a hundred meters. This is because the multipath effect in UAC is stronger at longer distances, which improves the diversity in the arrivals at the receiver, and results in a better performance in the receiver localization.

Numerical results considered in this subsection demonstrate that the proposed localization technique is capable of achieving highly accurate position estimates represented in Depth-Range plane.

3.4.2 Receiver Localization in Three-Dimensional Space

To investigate the performance of the localization technique in three-dimensional (X-Y-Z space), an experiment is carried out with $N_T = 4$ transducers located evenly around the space of interest and they are placed at the depth of 50 m. We present the space by (x, y, z) coordinates, where z denotes the depth, (x, y) denotes the position projection on the X-Y plane. The four transducers then are located at (-350, 0, 50), (0, 350, 50), (350, 0, 50), and (0, -350, 50). The transducers emit acoustic signals in the interval of vertical angles $[-50^\circ, +50^\circ]$. A pilot signal is transmitted from each of the four transmit antennas sequentially in time. The pilot signal is a single OFDM symbol with a predefined BPSK sequence modulating the subcarriers.

The localization is performed for 125 different positions of the receiver within the space of interest. Similar as in the simulations for the localization in Depth-Range plane, white Gaussian noise of the same power as the signal power in the frequency bandwidth of the communication system is added to the received pilot signal, so the signal-to-noise ratio is SNR $= 0$ dB; we repeat the experiment 10 times, every time adding a new noise realization, and averaging simulation results over the 10 trials.

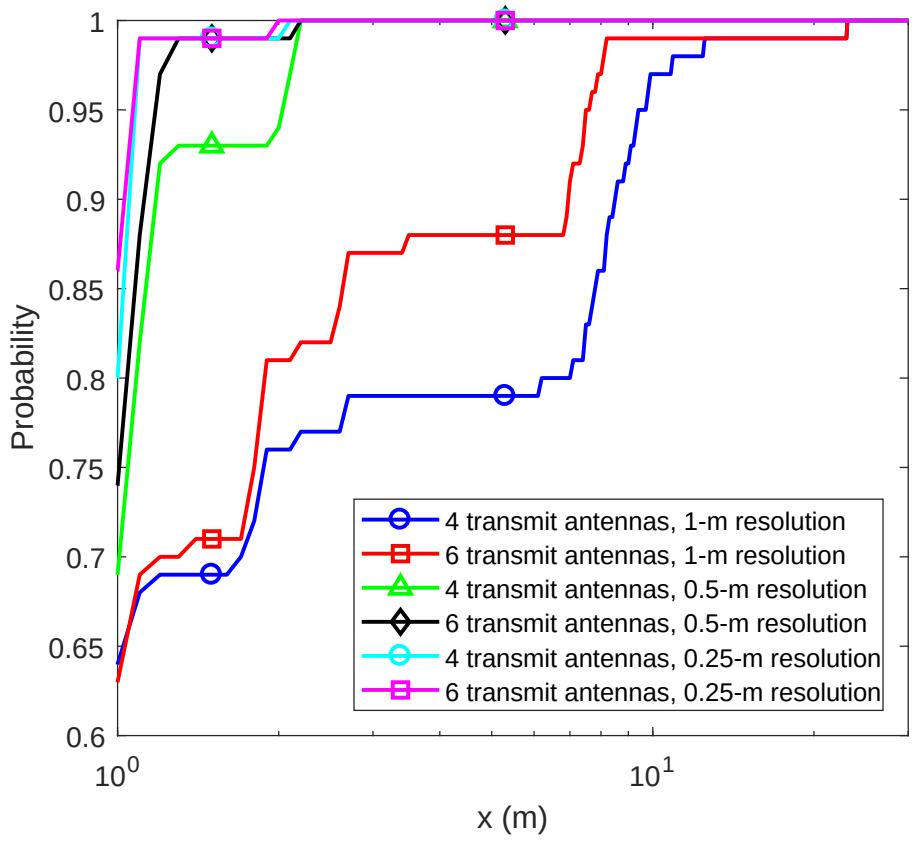

Fig. 3.11 CDF for the position error x (meters), for experiments at long distance with different grid map resolution and different numbers of transmit antennas. SNR = 0 dB.

The sea surface is flat. The tested positions uniformly cover the area. The receiver is first located exactly on a grid point; more specifically, the set of the receiver depths, also described as Z components of the receivers, is given by the vector [11 53 95 137 179] m, the set of X components of the receivers is given by the vector [-150 -50 50 150 250] m and the set of Y components of the receivers is given by the vector [-150 -50 50 150 250]. To illustrate the proposed localization technique in a more practical scenario, the receiver locations are then shifted randomly with a uniform distribution within the grid resolution interval. The localization is applied to each tested position of the receiver.

As described in (3.3), for each position of the receiver, four estimates are obtained based on four transducers, they are considered as correct and are combined only if they have the same depth component. However, when the grid maps used for each transducer are calculated with a resolution of 1 m, only around 20% estimates are considered as correct, which is acceptable for direct estimation of location but not enough for the trajectory estimation proposed in the next chapter.

To achieve better localization, we can improve the resolution of the grid maps used for each transducer. Two different simulations are carried out with an improvement in the resolution of the grid maps as 0.5 m and 0.25 m. When the resolution is improved from 1 m to 0.5 m, as a result, 50% estimates are considered as correct, which is acceptable for the trajectory estimation technique proposed in Chapter 4. When updating the grid maps for each transducer to 0.25 m resolution, over 70% estimates are considered as correct, which is acceptable for some underwater applications. However, the computation time and the storage memory for a grid map of 0.25 m resolution is increased by 16 times compared to the grid map of 1 m resolution.

As shown in Fig. 3.8, the localization performance in the two-dimensional plane can be improved by an improved resolution of the grid map or an increase in the number of transducers. Therefore, we consider localization with more transducers.

Another two simulations are carried out with an increase in the number of transducers as $N_T = 4 \times 2 = 8$ and $N_T = 4 \times 4 = 16$, where the single transducers in the previous simulation are set to be antenna arrays with multiple transducers placed in vertical. The transducers in the antenna arrays are equally spaced from a depth of 50 m to 60 m (for $N_T = 4 \times 2 = 8$) or 80 m (for $N_T = 4 \times 4 = 16$). For an example, when $N_T = 4 \times 2 = 8$, the 8 transducers are located at (-350, 0, 50), (-350, 0, 60); (0, 350, 50), (0, 350, 60); (350, 0, 50), (350, 0, 60); (0, -350, 50), (0, -350, 60). In these two simulations, the grid maps used for each transducer are calculated with a resolution of 1 m. As a result, around 40% estimates are considered as correct with $N_T = 4 \times 2 = 8$ transducers and around 80% estimates are considered as correct with $N_T = 4 \times 4 = 16$ transducers, which indicate the improvements in the localization

performance. However, increasing the number of transducers requires additional hardware at the transmitter, which increases the cost.

As shown in Fig. 3.8, the localization performance in the two-dimensional plane can be improved by an increase in the number of transducers or an improved resolution of the grid map. Therefore, we consider the grid map of higher resolution.

Another two simulations are carried out with an improvement in the resolution of the grid maps used for each transducer. When $N_T = 4$ transducers and The resolution of the grid maps used for each transducer is improved from 1 m to 0.5 m, and as a result, 50% estimates are considered as correct, which is still not enough for underwater localization, but is acceptable for the trajectory estimation technique proposed in Chapter 4.

When updating the grid maps for each transducer to 0.25 m resolution, over 70% estimates are considered as correct, which is acceptable for some underwater applications. However, the computation time and the storage memory for a grid map of 0.25 m resolution is increased by 16 times compared to the grid map of 1 m resolution.

Table 3.1 shows the accuracy under different scenarios. It can be seen that, the percentage of estimates considered as correct can be improved by an increase in the number of transducers or an improved resolution of the grid map. The latter can be a more practical approach since it does not require additional hardware at the transmitter. For practical three-dimensional localization approaches, a grid map of 0.25 m resolution is suggested since it provides accurate localization. For practical three-dimensional trajectory estimation approaches such as AUV tracking, a grid map of 0.5 m resolution is suggested since the accuracy of it is high enough to recover the trajectory.

Table 3.1 The accuracy under different scenarios

Number of transducers	Resolution	Percentage of estimates considered as correct
4	1 m	20 %
8		40 %
16		80 %
4	0.5 m	50 %
	0.25 m	70 %

After the correct location estimates in Depth-Range plane are achieved, they are combined and calculated as in (3.7) to achieve the projection of the receiver location to the X-Y plane, thus obtaining the estimated position of the receiver in the X-Y-Z space.

Fig. 3.12 shows the CDF of distance between the estimated and true positions for different grid map resolution and different numbers of transducers. It can be seen that for all scenarios, after determining the correct location estimates, over 80% of the receiver location estimates have the distance to the true receiver location less than 1 m. Thus we can only focus on

the percentage of location estimates being considered as correct in different scenarios. As described above, the percentage of location estimates being considered as correct is related to the number of transducers and the resolution of grid maps. For four transducers, 50% estimates are considered as correct when the resolution of the grid maps used for each transducer is 0.5 m, which is acceptable for the trajectory estimation proposed in Chapter 4, and it is a more practical approach since it does not require additional hardware at the transmitter.

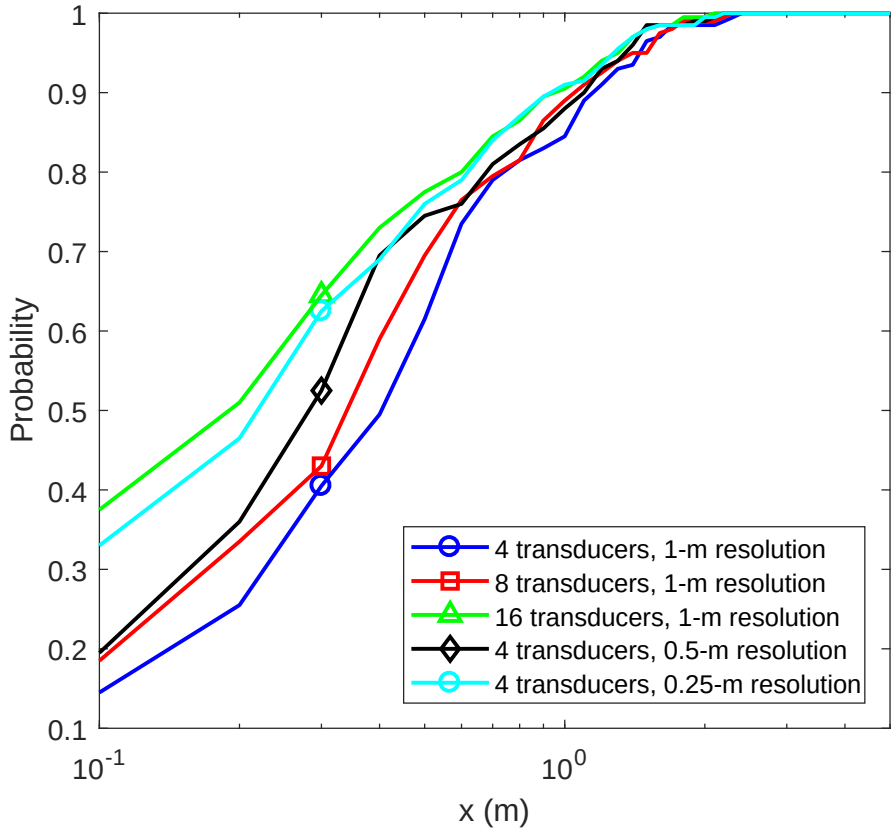

Fig. 3.12 CDF for the position error x (meters), for experiments with different grid map resolution and different numbers of transducers. SNR = 0 dB.

3.5 Conclusions

In this chapter, underwater receiver localization techniques in Depth-Range plane and X-Y-Z space have been proposed, which are based on pre-computation of a grid map with CSI defined by the acoustic environment. In the localization in Depth-Range plane, a database of possible CSI is pre-computed for a grid in space (grid of range/depth points) covering the

area of interest, and saved at both the transmitter and receiver. To estimate the location of the receiver, the CSI measured at the receiver is compared with the CSI on the grid; the location estimate is indicated by the best match. The localization in the three-dimensional space is proposed as an extension to the localization in Depth-Range plane. Multiple transducers are suggested to be placed around the investigation geography space. The localization in Depth-Range plane is applied for the receiver with each transducer to obtain the location estimates, then they are combined to obtain the location estimate in X-Y-Z space. Numerical examples have shown that the receiver localization in Depth-Range plane can achieve an acceptable accuracy while reduce the cost of infrastructure compared to the acoustic beacon networks, and surfacing for GPS navigation is no longer necessary. With the sacrifice in the computation time and the storage memory, the receiver localization in X-Y-Z space can also achieve an acceptable accuracy.

Based on the localization described in this chapter, an advanced underwater receiver trajectory estimation approach is proposed in Chapter 4, and a transmit beamforming technique is proposed in Chapter 5.

Chapter 4

Underwater Trajectory Estimation Based on Grid Map Localization

4.1 Introduction

Compared to other major ocean observing equipment such as ships and buoys, unmanned or autonomous underwater vehicles (UUVs or AUVs) are characterized by easy deployment and low operational costs for ocean applications, and they can be treated as oceanic mobile sensing platforms. These oceanic mobile sensing platforms are capable of long-term monitoring tasks over a course of weeks to months for data collection in large-scale environments. They are also capable of a wide-range of ocean applications, such as ocean monitoring [129–131], underwater cavity exploration [132] and biological research [133, 134]. To operate an AUV, trajectory estimation is one of the most important issues since in surveying missions, data collected from an AUV is only meaningful with its localization information. Besides, an underwater surveying mission often requires AUVs to navigate to a pre-determined destination and it is essential for an AUV to localize and adjust its orientation to reach the destination. An AUV has to continuously update its location during the mission. The investigation of underwater trajectory estimation (navigation) has to meet many challenges since the standard technologies for aerial and terrestrial systems, including the Global Positioning System (GPS), are not available [74]. Traditional underwater positioning systems such as long baseline (LBL) [62], short baseline (SBL) [135], and ultra-short baseline (USBL) [136] use networks of sea-floor mounted baseline transponders as reference points for navigation, are somewhat too expensive and also inconvenient in many of AUV applications. As described in Chapter 3, the existing GPS underwater navigation suffers from impractical, and the classical triangulation method suffers from high cost in the set up of infrastructures.

To overcome the problems of an impractical GPS fix and to reduce the cost, we propose here a trajectory estimation technique based on grid map localization and a data smoothing approach. In the grid map localization proposed in the Chapter 3, a dictionary of possible Channel State Information (CSI) is pre-computed for a grid in space (grid of range/depth points) and saved at both the transmitter and receiver. Such a dictionary is built based upon acoustic field computation for a specific environment, where the receiver is navigated. To estimate the location of the receiver, the CSI measured at the receiver is compared with the CSI on the grid covering the area of interest; the location estimate is indicated by the best match. For a dynamic receiver, the grid map localization will be applied at every sample point along the receiver trajectory to obtain a set of the estimated locations, which can be treated as a set of data with components, such as relative distance (range) to the transmitter and depth of the receiver. According to the power of most types of underwater equipment, the velocity and the acceleration of a AUV receiver is basically low and the trajectory curve of it is smooth. Therefore, smoothing approaches can be applied to the set of estimated locations to reduce the error estimates and recover an estimated trajectory accurately. There exist several smoothing approaches, such as kernel smoothers [137], regression spline [138], B-splines [139, 140] and P-splines [141–143]. The smoothing we apply in the proposed trajectory estimation is P-splines, which are a combination of B-splines and difference penalties on the estimates. As a straightforward extension of (generalized) linear regression models, P-splines conserve moments (means, variances) of the data and have polynomial curve fits. The computations of P-splines are relatively inexpensive and easily incorporated [141–143]. Except for a set of estimated locations, a set of corresponding accuracy levels of the estimates can also be obtained by the grid map localization, and this could be used as weight coefficients in the P-splines to reduce the error estimates and benefit the trajectory performance.

The proposed technique for trajectory estimation requires a transmitter (with multiple transmit antennas), and environment parameters (sound speed profile, sea surface, etc.) in the investigated geographical area to be known at both the transmitter and the receiver. Such a technique reduces the cost of infrastructure compared to the acoustic beacon networks for triangulation and the surfacing for a GPS fix is no longer necessary.

4.2 Trajectory Estimation using Smoothing Approach and Localization

A smoothing approach is commonly used to smooth a data set by creating an approximating function that attempts to capture important patterns in the data, while leaving out noise or

other rapid phenomena. In smoothing, the data points of a signal are modified so points that are higher than the adjacent points are reduced, and points that are lower are increased leading to a smoother signal.

P-splines define a penalty based on the finite difference of the coefficients of adjacent B-splines [141], and the least squares minimization. As described in [139, 140], let the number of the trajectory sample points be X, and each sampling interval be covered by $q+1$ P-splines. As described in the previous chapter, the localization can be applied in Two-Dimensional plane or in Three-Dimensional space, and the location estimates can be represented by depth and range components, or by X,Y and Z components. A component vector of the location estimates can be represented as $\mathbf{y} = [y_0, ..., y_{X-1}]$. Let $B_j(i)$ denote the value at the ith sample point of the jth P-spline. A fitted curve $\hat{\mathbf{y}}$ to data $\mathbf{y}$ is then defined as the linear combination $\hat{y}_i = \sum_{j=1}^{n} a_j B_j(i)$. The objective function to minimize [141] is given by:

$$S = \sum_{i=1}^{X} w_i \left\{ y_i - \sum_{j=1}^{n} a_j B_j(i) \right\}^2 + \lambda \sum_{j=k+1}^{n} (\Delta^k a_j)^2, \tag{4.1}$$

where $n = X + q - 1$, $\Delta a_j = a_j - a_{j-1}$, λ is the regularization parameter that controls the smoothness of the fit, and w_i is the weight coefficient for y_i, the estimated location at ith sample point.

The system of equations that follows from the minimization of S in (4.1) can be written as [141]:

$$\mathbf{B}^T \mathbf{W} \mathbf{y} = (\mathbf{B}^T \mathbf{W} \mathbf{B} + \lambda \mathbf{D}_k^T \mathbf{D}_k)\mathbf{a}, \tag{4.2}$$

where $\mathbf{D}_k$ is the matrix representation of the difference operation Δ^k, the elements of $\mathbf{B}$ are $b_{ij} = B_j(i)$, and $\mathbf{W}$ is a diagonal matrix with the weights w_i on the diagonal.

After the set of location estimates and the corresponding match levels are obtained, the P-splines smoothing approach is applied to recover the trajectory of the receiver. As described in Chapter 3, at the ith sample point the index of the estimated grid point is found by the grid map localization. According to (3.4) and (3.6), this grid point is the one with the maximum combined covariance coefficient, which can be seen as the match level of this estimated location. Therefore, it is possible to consider the match level c_m at the ith sample point as the weight coefficient w_i for P-splines. Additionally, the velocity and the acceleration of the estimated trajectory can be calculated after the smoothing, so the regularization parameter λ can be set according to a maximum possible acceleration level.

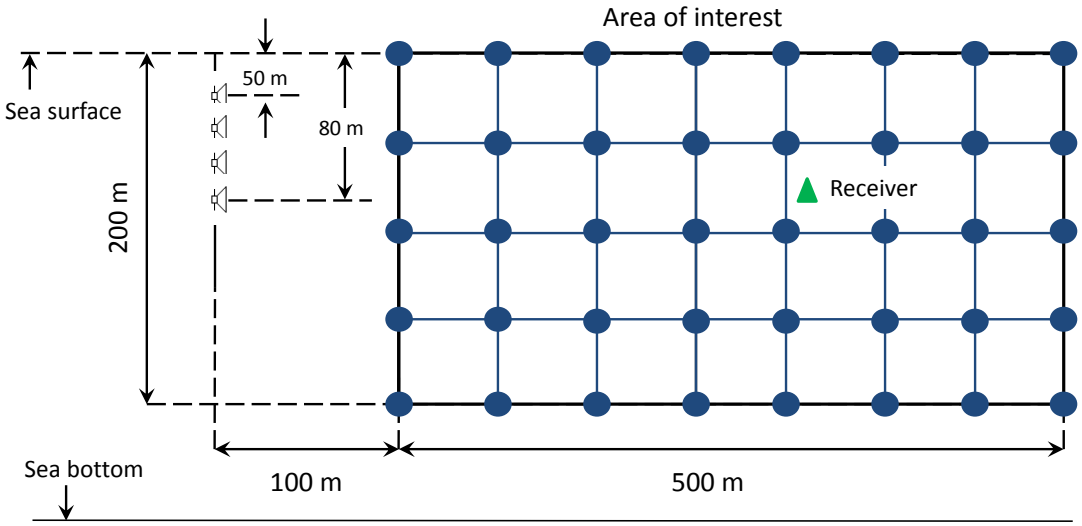

Fig. 4.1 The receiver is located in an area of interest 200 m $\times$ 500 m. The sea depth is 220 m. The transducers are equally spaced from a depth of 50 m to 80 m.

4.3 Numerical Results

4.3.1 Trajectory Estimation in Two-Dimensional Plane

To recover the trajectory using smoothing approaches, it is not necessary to have very accurate location estimates. According to the experimental results shown in [8], for 100 receivers randomly located in the area of interest and for 10 trials of simulation, over 70% of the receivers have location estimates close to true values (with a difference less than 5 m), which is enough for P-splines to recover the trajectory.

With the accuracy of the grid map localization demonstrated, we investigate the accuracy of the proposed receiver trajectory estimation with numerical examples presented in this section. The accuracy of the proposed receiver trajectory estimation is investigated in an example scenario. The sea surface is assumed to be flat. The sea depth in the investigation area is 220 m. The area of interest is shown in Fig. 4.1. The transducers emit acoustic signals in the interval of vertical angles $[-50^\circ, +50^\circ]$. The sound speed profile (SSP) and sea bottom parameters are taken from [105] and shown in Fig. 3.2. The receiver is equipped with a single receive antenna. The pilot signal for channel estimation is transmitted at the carrier frequency 3072 Hz with a frequency bandwidth of 1024 Hz, thus the frequency band is from 2560 Hz to 3584 Hz. The pilot transmission is performed using OFDM signals with $K = 1024$ subcarriers, an orthogonality interval of 1 s, and subcarrier spacing of 1 Hz. When searching over delays τ in (3.6), the search interval $[\tau_{\min}, \tau_{\max}]$ is set to OFDM orthogonality

interval $[-0.5, 0.5]$ s. In the experiments, the transducers are equally spaced from a depth of 50 m to 80 m (for $N_T = 4$) and a grid map with 1 m resolution is generated and stored in memory for every transducer.

To investigate the performance of the trajectory estimation, an experiment is carried out in the scenario where a receiver is moving at a constant speed of 0.5 m/s along a sinusoid curve trajectory and away from the transmitter. The proposed localization is applied at every sampling instant. The location estimates and the related match levels are obtained after the grid map localization and P-splines are applied with them to recover the trajectory of the receiver.

The sinusoidal curve trajectory of the receiver is in Three-Dimensional space as shown in Fig. 4.2, with 5 m amplitude and 50 m wavelength. The relative distance between the transmitter and the receiver is from 200 to 550 m, and the depth of the receiver is from 137.5 to 50 m. The sample rate is set to be 1 Hz and the total number of sample points is approximately 800. The grid map localization is applied to each sample point to obtain the location estimates, which is represented by distance to the transmitter and the depth of the receiver as range and depth components. The estimated trajectory is also represented by the range and depth components, in a two-dimensional plane.

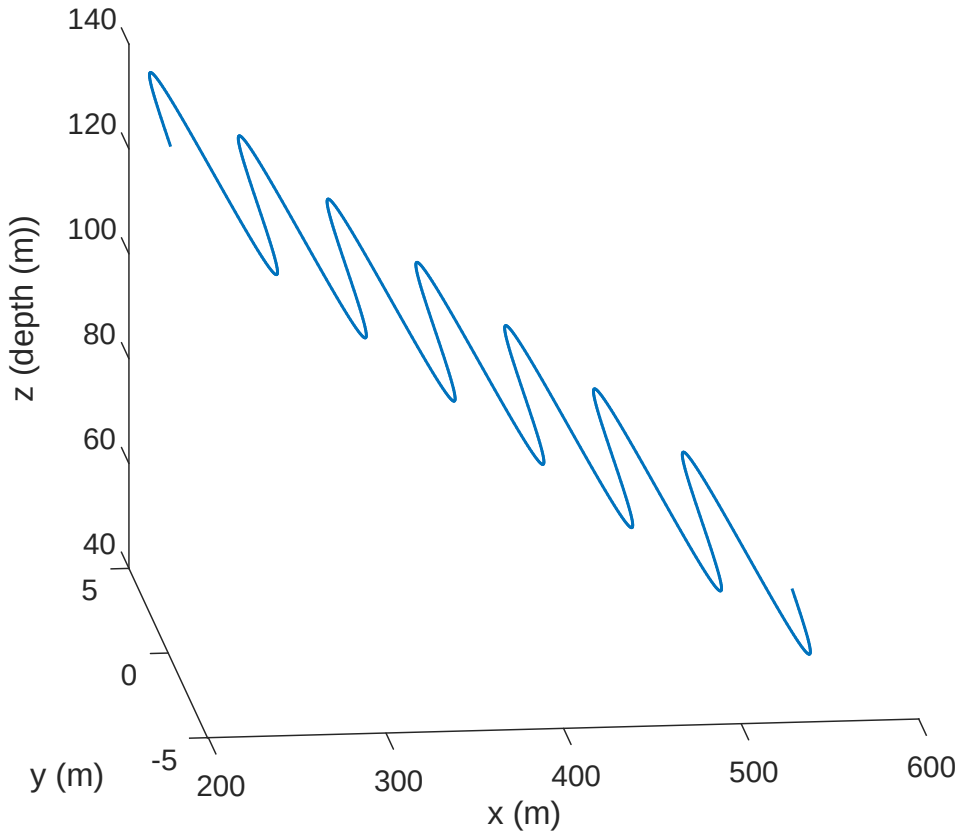

Fig. 4.2 The true trajectory of the receiver in three-dimensional space.

After obtaining the location estimates for the 800 positions, the P-spline smoothing is applied separately to the range and depth components. The weight coefficients in P-splines are set to be the match level on each sampling point, The estimates with low match levels are considered as error estimates and a filter is set to remove them. The threshold of the filter is set to be 70% in the experiments. The maximum acceleration for underwater equipment is assumed to be 1 m/s^2. The regularization parameter λ is set to have the maximum acceleration of the estimated trajectory at both components being under 1 m/s^2. The estimated trajectory and the real receiver trajectory are shown in Fig. 4.3. The estimated trajectory is close to the true trajectory with an error less than 3 m, and the NRMSE between them is 0.73%. Such a high performance of the trajectory estimator is acceptable for AUV applications like seabed observation, environment sensing, subsea infrastructure building, etc [129–134].

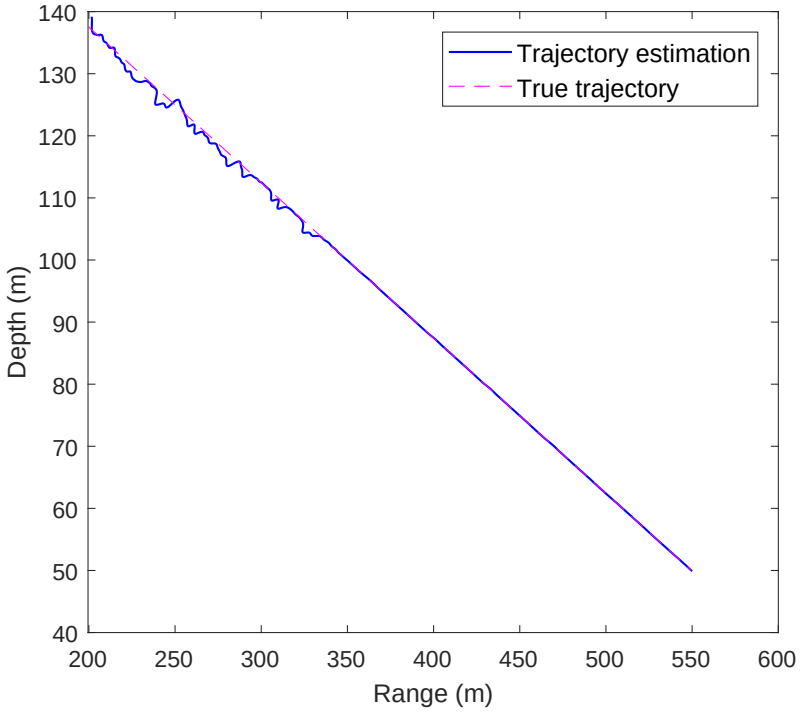

Fig. 4.3 The estimated trajectory and the true trajectory of the receiver, represented by the distance to the transmitter (range) and the depth of the receiver. The sampling rate is 1 Hz.

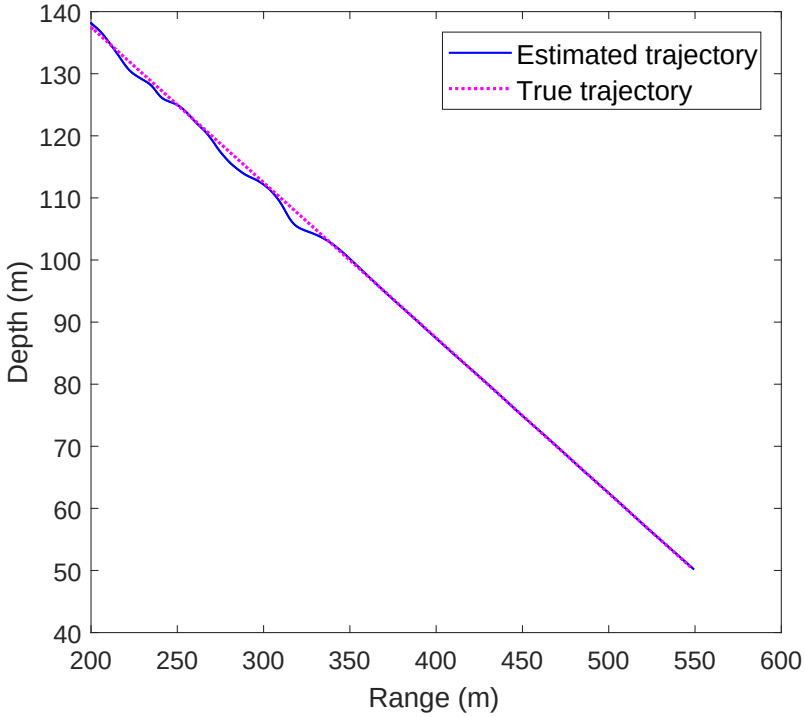

Fig. 4.4 The estimated and true trajectory of the receiver. The sampling rate is 1/5 Hz.

The sample rate of the trajectory is usually low according to the functionality of underwater equipment. Therefore, we repeat the experiment in a more practical scenario where the sampling rate is five times lower than in the previous experiment (1/5 Hz). The trajectory curve obtained by the proposed trajectory estimator is still close to the true trajectory (with less than 3 m distance and the NRMSE is 0.75%) and the performance can be seen in Fig. 4.4.

Another simulation is carried out when the receiver is moving in a sinusoid curve in the range-depth plane, with 2 m amplitude and 20 m wavelength. The receiver is moving at a constant speed of 1 m/s along the trajectory and the sampling rate of the trajectory is 1 Hz. With the estimated locations and the corresponding match levels obtained by the proposed grid map localization algorithm, the estimated trajectory is obtained, and the performance can be seen in Fig. 4.5 with the estimated trajectory being close to the true trajectory (with less than 2 m distance and the NRMSE is 0.93%).

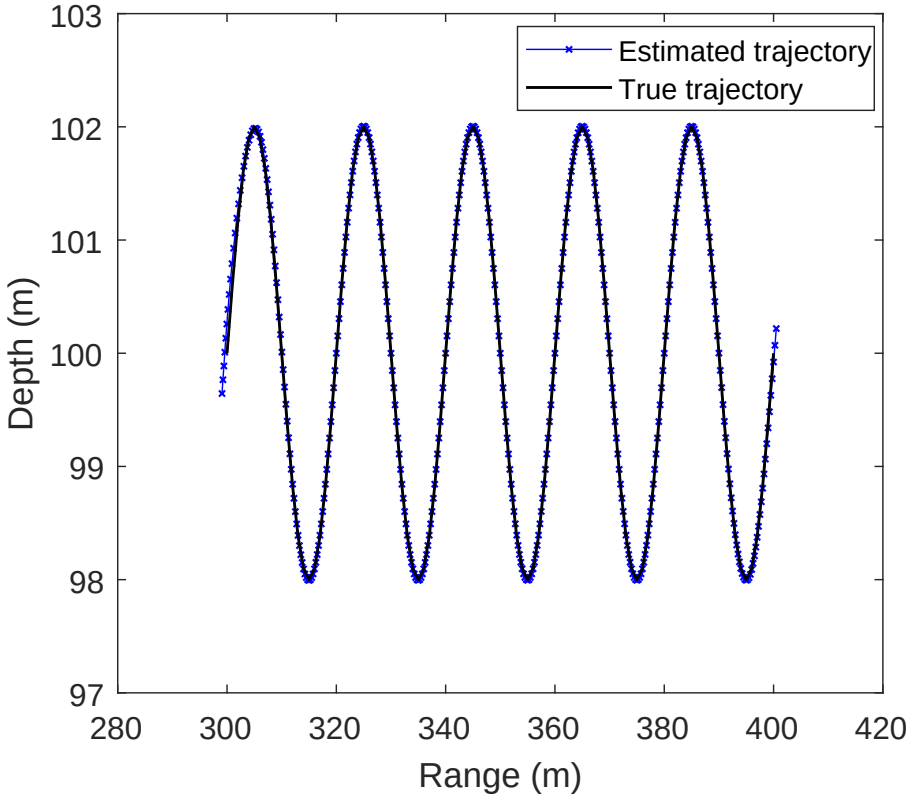

Fig. 4.5 The estimated trajectory and the true trajectory of the receiver moving in a sinusoid curve in the range-depth plane.

4.3.2 Trajectory Estimation in Three-Dimensional Space

As an extension to the trajectory estimation in depth-range plane, trajectory estimation in three-dimensional space is carried out based on the receiver localization in three-dimensional space. To investigate the performance of the trajectory estimation in three-dimensional space, simulations are carried out in this section. According to the simulation results shown in Chapter 3, the resolution of the grid maps used in the three-dimensional trajectory estimation are suggested to be 0.5 m. Similar to the simulation of receiver localization in three-dimensional space, four transmit antennas are located around the space of interest at the depth of 50 m. The positions of these transmit antennas in the X-Y-Z coordinates are (-350, 0, 50), (0, 350, 50), (350, 0, 50), and (0, -350, 50) m.

The set up of the sea parameters are the same as the simulations of trajectory estimation in a Two-Dimensional plane.

To investigate the performance of the trajectory estimation, an experiment is carried out in the scenario where a receiver is moving at a constant speed of 0.5 m/s along a sinusoid curve and away from the transmitter. The location estimates and the corresponding match levels are obtained after the grid map localization and P-splines are applied to recover the trajectory of the receiver.

The true trajectory of the receiver is a sinusoid in space as shown in Fig. 4.6 with 10 m amplitude and 100 m wavelength, the depth of the receiver varies from 150 to 110 m.

The sample rate is set to be 1 Hz and the total number of sample points is approximately 200. For each transmit antenna, the grid map localization is applied to each sample point to obtain the location estimates, represented by the relative range to the transmitter and the depth of the receiver.

The location estimates are considered as correct if they have the same depth component, otherwise they are filtered out and the sample point is removed. In this simulation, with the grid map of 0.5 m resolution, around 50% of location estimates are filtered and the rest are used in the smoothing approach to recover the trajectory. The correct location estimates are combined and calculated as in (3.7) to obtain the position of the sample point and the relative match level. With the P-spline smoothing approach, the trajectory of the receiver is recovered as in the depth-range plane. The output estimated trajectory and the real receiver trajectory are shown in Fig. 4.6 and Fig. 4.7. The estimated trajectory is close to the true trajectory with the maximum distance between them 1 m. The NRMSE between the true trajectory and the estimated trajectory is 1.44%.

To compare the performance of the trajectory estimation for different smoothing approaches, table 4.1 shows the NRMSE between the true trajectory and the estimated trajectory

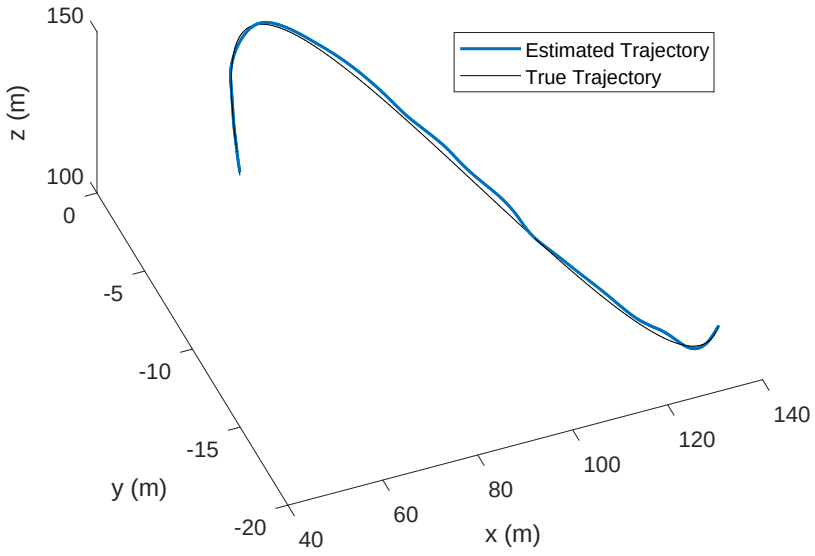

Fig. 4.6 The estimated and true trajectory of the receiver moving in a sinusoid curve in three-dimensional space.

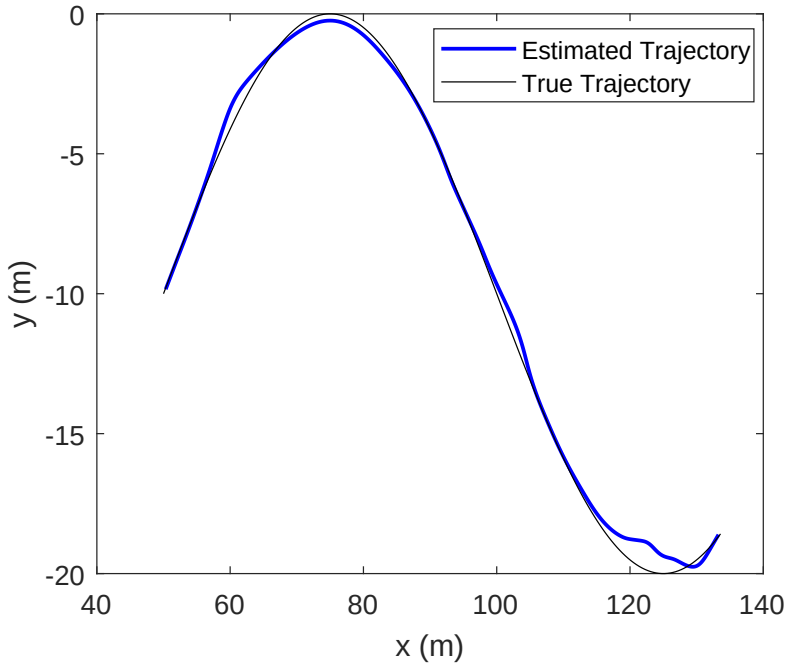

Fig. 4.7 The estimated and true trajectory of the receiver moving in a sinusoid curve in the range-depth plane.

with different smoothing approaches. It is seen that the best performance of the trajectory estimation is achieved by using the P-splines smoothing approach.

Table 4.1 The NRMSE between the true trajectory and the estimated trajectory for different smoothing approaches

Smoothing approaches	NRMSE
P-splines smoothing	1.44%
Moving average filtering	1.83%
Local regression smoothing	2.13%
Savitzky-Golay filtering	2.35%

4.4 Conclusions

In this chapter, receiver trajectory estimation techniques for Two-Dimensional (Depth-Range plane) and Three-Dimensional (X-Y-Z space) are proposed, which are both based on underwater localization using a pre-computed grid map proposed in Chapter 3. In the proposed localization method, the location of the receiver is estimated and a corresponding match level is obtained, which indicates the match level of the estimate and the true value. For a moving receiver, estimated positions and the corresponding match level coefficients are obtained by the localization at each sampling instant. In the P-splines smoothing approach described in this chapter, a smooth curve can be obtained with a data string. The two key parameters of P-splines are the weighting coefficients applied on the data string, and the regularization parameter controls the smoothness. In this chapter, it is proposed to set the weighting coefficients as the match levels of the estimated positions, and the regularization parameter is set according to the maximum acceleration of the receiver. The trajectory of the receiver is then recovered. The numerical investigation has shown that the proposed techniques allow accurate trajectory estimation not only in Depth-Range plane, but also in X-Y-Z space. With the proposed approach to the trajectory estimation, the cost is reduced compared to acoustic beacon networks and it also overcomes the impracticality of the GPS navigation underwater.

Chapter 5

Transmit Beamforming Based on Grid Map Localization

5.1 Introduction

Although acoustic communication is the typical physical-layer technology underwater for distances up to several tens of kilometers, achieving high data rates for video or other transmission through the acoustic channel are difficult to accomplish as acoustic waves suffer from attenuation, limited bandwidth, Doppler spreading, high propagation delay, and time-varying propagation characteristics [3, 144]. For these reasons, the existing acoustic communication solutions are still mostly focusing on enabling delay-tolerant, low-bandwidth/low-data rate transmission or at best low-quality/low-resolution multimedia streaming in the order of few tens of kbps. To achieve higher data rates in the bandwidth-limited underwater acoustic channel, several techniques should be combined together. For example, signal beamforming along with multiple antenna arrays [145] could achieve this goal.

Antenna array processing involves manipulation of signals induced on various antenna elements. Its capabilities of steering nulls to reduce co-channel interference and pointing independent beams toward various mobile users make it attractive to a wireless communications system designer. The difference between steering antenna array and steering distinct aperture antennas is that the antenna array is electrically steered by weighting each antenna element to change phases, while the aperture antennas are steered mechanically. The wide spread interest in the subject area has been maintained over decades. The first issue of IEEE Transaction on Antenna and Propagation was published in 1964 [146] and was followed by a series of special issues of adaptive antennas, adaptive processing and beamforming [147, 76].

The design of a transmit beamformer in multiuser channels is an important problem in modern wireless communication systems with SDMA. The main difficulty in such systems is that coordinated receive processing is not possible and that all the signal processing must be employed at the transmitter side [81]. Linear precoding schemes provide a promising trade-off between performance and complexity [82–85]. Zeroforcing (ZF) beamforming is the most common linear precoding scheme, which decouples the multiuser channel into multiple independent subchannels [86–92]. OFDM communication is considered as a promising technology for high data-rate communications in UAC [93–96]. It can be efficiently combined with SDMA to improve the system throughput [93, 97–99]. In this chapter, we will be investigating transmit beamforming based on linear precoding in an OFDM communication system.

The main challenge in transmit beamforming is the position uncertainty of the users, which leads to inaccuracies in the design of beamformers, and therefore to overall performance degradation. The problem becomes even worse over time if the vehicle remains underwater for long because of the accumulation of its position error, which leads to nonnegligible drifts in the vehicle's position estimation, as attested by many works on underwater localization [148–150]. However, with the grid map localization technique proposed in Chapter 3, one can locate the vehicle without the necessity to surface.

In this chapter, an advanced underwater transmit beamforming technique is proposed in Section 5.2 based on the grid map localization technique. Numerical results are described in Section 5.3 to prove the detection performance of the proposed technique. The conclusions are drawn in Section 5.4.

5.2 Design of the transmit beamformer

We consider a scenario with a transmitter using multiple transmit antennas and multiple receivers using single receive antennas. The transmission technique is OFDM with a transmitted signal described by a set of subcarriers at frequencies $f \in \{f_0, ..., f_{K-1}\}$. A broadcast channel with N_R users can be described in the frequency domain as

$$y_n(f) = \mathbf{h}_n^T(f)\mathbf{x}(f) + n_n(f), \;\; n = 1, \ldots, N_R, \tag{5.1}$$

where $y_n(f)$ is the signal received by the nth receiver at subcarrier f, $\mathbf{h}_n(f) = [h_{n,1}(f), ..., h_{n,N_T}(f)]^T$ is the frequency response of the channel between the transmit antennas and nth receiver at frequency f, $\mathbf{x}(f)$ is the $N_T \times 1$ transmitted signal vector and $n_n(f)$ is Gaussian noise with zero mean and variance $\sigma_n^2(f)$. We also introduce the $N_R \times N_T$ channel matrix

$\mathbf{H}(f) = [\mathbf{h}_1(f), ..., \mathbf{h}_{N_R}(f)]^T$. Then the model in (5.1) can be rewritten as

$$\mathbf{y}(f) = \mathbf{H}(f)\mathbf{x}(f) + \mathbf{n}(f), \tag{5.2}$$

where $\mathbf{y}(f) = [y_1(f), \ldots, y_{N_R}(f)]^T$ are signals received by the N_R receivers and $\mathbf{n}(f) = [n_1(f), \ldots, n_{N_R}(f)]^T$ is the noise vector.

In linear precoding (transmit beamforming) methods, the transmitted signal vector $\mathbf{x}(f)$ is a linear transformation of the information symbols $\mathbf{s}(f) = [s_1(f), \ldots, s_{N_R}(f)]$ [92]:

$$\mathbf{x}(f) = \mathbf{T}(f)\mathbf{s}(f), \quad f = f_0, ..., f_{K-1}, \tag{5.3}$$

where $\mathbf{T}(f)$ is an $N_T \times N_R$ precoding matrix (beamformer).

To design $\mathbf{T}(f)$ achieving zero interference between users, the product $\mathbf{H}(f)\mathbf{T}(f)$ should be a diagonal matrix [92] of size $N_R \times N_R$, e.g., the identity matrix $\mathbf{I}_{N_R}$:

$$\mathbf{H}(f)\mathbf{T}(f) = \mathbf{I}_{N_R}. \tag{5.4}$$

Such a precoder is known as the zero-forcing (ZF) beamformer and it is given by

$$\mathbf{T}(f) = \mathbf{H}^H(f)\left[\mathbf{H}(f)\mathbf{H}^H(f)\right]^{-1}. \tag{5.5}$$

The detection performance of the receivers can be improved using the diagonal loading:

$$\mathbf{T}(f) = \mathbf{H}^H(f)\left[\mathbf{H}(f)\mathbf{H}^H(f) + \alpha\mathbf{I}_{N_R}\right]^{-1}, \tag{5.6}$$

where $\alpha > 0$ is associated with different beamforming designs [151–153]; for the design of ZF beamforming, $\alpha = 0$. When designing the beamformer, the true channel parameters are unavailable and therefore their estimates are used instead.

Every column $\mathbf{T}^{(n)}(f)$ of the matrix $\mathbf{T}(f)$ is an $N_T \times 1$ beamformer vector dedicated to a single receiver. The transmitted OFDM signal for the nth user after beamforming is given by

$$\mathbf{x}_n(f) = \mathbf{T}^{(n)}(f)s_n(f), \quad f = f_0, ...f_{K-1}, \tag{5.7}$$

where $s_n(f)$ is the information symbol for the nth user at subcarrier f.

The design of the transmit beamformer requires the channel frequency response from each transmit antenna to be known by the transmitter. A classical method to obtain this knowledge is to send back the estimated channel frequency response from each receiver to the transmitter. Such feedback represents a significant overhead, however, and can comprise a substantial

portion of the overall capacity for data throughput. With the proposed localization technique using the grid map, the only information that needs to be sent back to the transmitter is the index number of the grid point where the receiver is located.

To obtain more accurate localization and better detection performance, the resolution of the grid map needs to be improved; the influence of the map resolution on the localization is investigated in Section 3.4, and detection performance is investigated in Section 5.3.

Another approach is based on increasing the number of grid points transmission to which is cancelled by the beamformer, as proposed below. With our localization technique, based on grid computation, the full set of position estimates is finite. Therefore, we can find, instead of one location estimate, several estimates, e.g., by finding several (two or three, as in our numerical investigation) grid points with the highest covariances. In this case, the feedback message should contain indices of these grid points. When designing the transmit beamformer, the additional channel estimates can be used to improve the detection performance by cancelling interference of the extra grid points.

To explain the proposed approach in detail, consider an example with $N_T = 4$ transmit antennas and $N_R = 2$ users. When only one location estimate for each user is received at the transmitter in the feedback message, the 2×4 channel matrix is given by $\mathbf{H}(f) = [\mathbf{h}_1(f), \mathbf{h}_2(f)]^T$ and the 4×2 matrix $\mathbf{T}(f)$ is found from (5.6). Here, the vectors $\mathbf{h}_1(f)$ and $\mathbf{h}_2(f)$ are the frequency responses for the best grid points of user 1 and user 2, respectively, as found by using (3.6).

With two location estimates for each user, the beamformer vectors for user 1 and user 2 are found by solving, respectively, the following equations:

$$\mathbf{H}_1(f)\mathbf{T}^{(1)}(f) = [1,0,0]^T, \tag{5.8}$$

$$\mathbf{H}_2(f)\mathbf{T}^{(2)}(f) = [0,0,1]^T, \tag{5.9}$$

where $\mathbf{H}_1(f) = [\mathbf{h}_{1,1}(f), \mathbf{h}_{2,1}(f), \mathbf{h}_{2,2}(f)]^T$, $\mathbf{H}_2(f) = [\mathbf{h}_{1,1}(f), \mathbf{h}_{1,2}(f), \mathbf{h}_{2,1}(f)]^T$, and $\mathbf{h}_{p,q}$ is the channel response vector corresponding to the qth location estimate of the pth user. The beamformer found by solving the equation (5.8) will focus the beam towards the best location estimate of user 1, while focusing zeros to the two location estimates for user 2. The beamformer found by solving the equation (5.9) will focus the beam towards the best location estimate of user 2, while focusing zeros to the two location estimates for user 1. This can significantly reduce the multiuser interference in the case where the best location estimates are incorrect.

With three location estimates for each user, the beamformer vectors for user 1 and user 2 are found by solving, respectively, the following equations:

$$\mathbf{H}_1(f)\mathbf{T}^{(1)}(f) = [1,0,0,0]^T, \tag{5.10}$$
$$\mathbf{H}_2(f)\mathbf{T}^{(2)}(f) = [0,0,0,1]^T, \tag{5.11}$$

where $\mathbf{H}_1(f) = [\mathbf{h}_{1,1}(f), \mathbf{h}_{2,1}(f), \mathbf{h}_{2,2}(f), \mathbf{h}_{2,3}(f)]^T$,
and $\mathbf{H}_2(f) = [\mathbf{h}_{1,1}(f), \mathbf{h}_{1,2}(f), \mathbf{h}_{1,3}(f), \mathbf{h}_{2,1}(f)]^T$.

In the case of two and three location estimates, the beamforming vectors are found as

$$\mathbf{T}^{(1)}(f) = \left[\mathbf{H}_1^H(f)[\mathbf{H}_1(f)\mathbf{H}_1^H(f) + \alpha\mathbf{I}_{N_R}]^{-1}\right]^{(1)}, \tag{5.12}$$
$$\mathbf{T}^{(2)}(f) = \left[\mathbf{H}_2^H(f)[\mathbf{H}_2(f)\mathbf{H}_2^H(f) + \alpha\mathbf{I}_{N_R}]^{-1}\right]^{(2)}. \tag{5.13}$$

With the location of the receiver estimated using the proposed grid map technique, there is no need to have a long feedback message sent back to the transmitter to design the beamformer. Assuming that the total number of grid points in the area of interest (see Fig. 4.1) is $201 \times 501 < 2^{17}$ (with the 1 m resolution grid map), only 17 bits are required to represent the receiver position on the grid. For two users, the feedback messages contain 34 bits. This is significantly less compared to the case when the CSI estimate is transmitted. Indeed, to transmit frequency responses for $K = 1024$ subcarriers, $N_T = 4$ transducers and $N_R = 2$ users, and with 16 bits representing a complex-valued sample of frequency response, a feedback message comprising $16KN_TN_R = 16 \times 1024 \times 4 \times 2 = 2^{17}$ bits is required. This requires an UAC system with a very high throughput, and such transmission would be impractical. The proposed approach allows the feedback messages to be reduced in size by $2^{17}/34 \approx 4000$ times. For the grid map with a 0.5-meter resolution, 38 bits (only slightly higher than 34 bits in the case of 1-m resolution) are required for the feedback messages. Thus, UAC with the proposed transmit beamforming allows for a significant reduction in the length of feedback messages.

5.3 Numerical Results

In this subsection, we consider scenarios with $N_T = 4$ transmit antennas and $N_R = 2$ users (receivers). An experiment contains two stages. At the first stage, the transmitter transmits one pilot OFDM symbol from each transmit antenna, and the receivers process the received pilot signals as described in Chapter 3 to identify the receiver positions on the grid map. These positions (grid point indices) are sent back to the transmitter, which recovers the CSI of the receivers from the grid map and designs the beamformer $\mathbf{T}$ as explained in Section 5.2.

At the second stage, the transmitter generates $N_T = 4$ signals for transmission by the four transmit antennas from two data packets, represented by vectors $\mathbf{d}_1$ and $\mathbf{d}_2$ in Fig. 5.1, and intended for the two users. Every 512 bits of each information data packet are encoded into a 1024-bit message using a rate 1/2 convolutional encoder with a generator polynomial matrix [23 35] in octal. The message bits are interleaved and transformed into $K = 1024$ BPSK symbols, corresponding to 1024 subcarriers of a single OFDM symbol for a single user, $s_1(f_k)$ and $s_2(f_k)$, respectively. The BPSK symbols intended for simultaneous transmission to the two users are applied to two jointly developed beamformers, $\mathbf{T}^{(1)}(f_k)$ and $\mathbf{T}^{(2)}(f_k)$. The beamformer outputs are combined at corresponding subcarriers and corresponding transmit antennas and transformed into the time domain using the inverse FFTs (IFFTs).

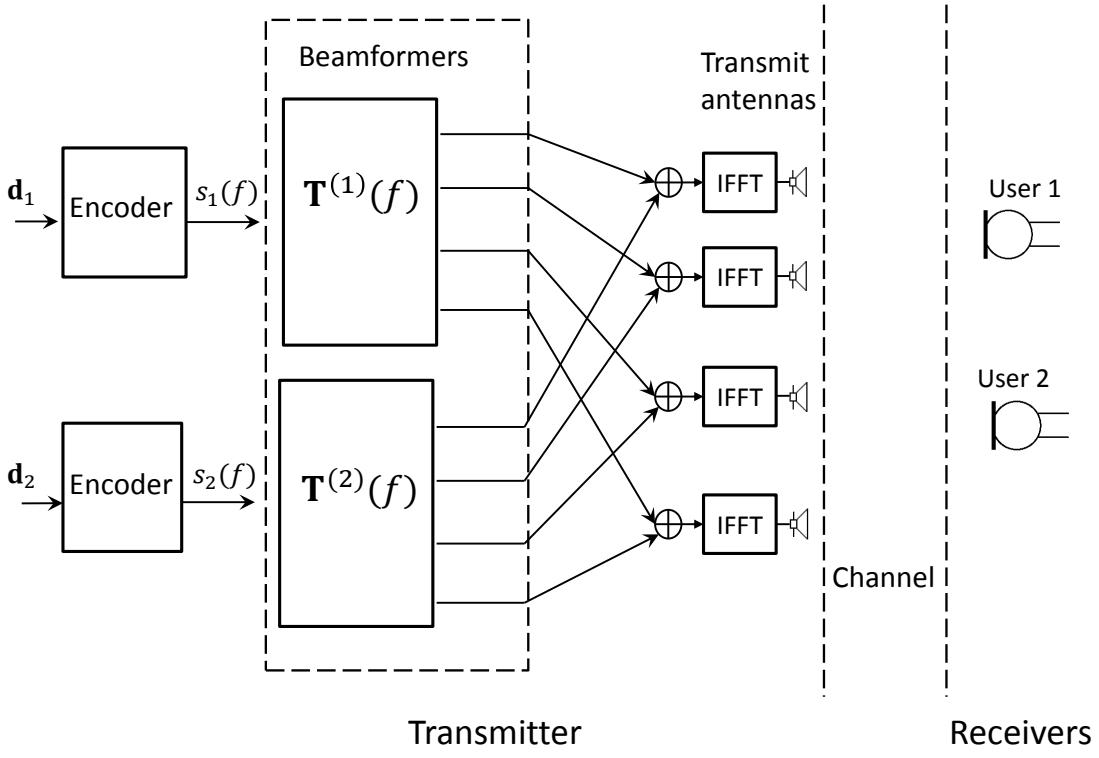

Fig. 5.1 Transmit beamforming experiment set up with four transmit antennas and two users.

A data packet comprising 65536 data bits generates 128 consecutive OFDM symbols as shown in Fig. 5.2. The 128-length sequence of the information OFDM symbols is appended with 8 pilot OFDM symbols as shown in Fig. 5.2. In the pilot OFDM symbols, all $K = 1024$ subcarriers are allocated for pilot symbols. At the receiver, eight channel estimates obtained from the eight pilot OFDM symbols are averaged to reduce the noise level in the final

estimates. These channel estimates are used for minimum mean-squared error (MMSE) equalization of the information OFDM symbols in the frequency domain and further decoding by the soft-input Viterbi decoder [154].

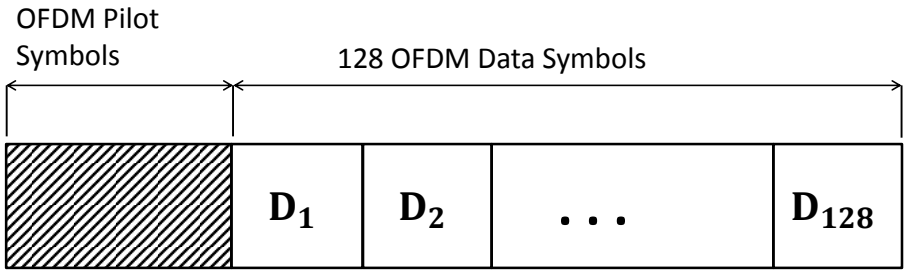

Fig. 5.2 The OFDM signal structure.

Experiments are carried out for the following four scenarios.

Scenario 1 - The receivers are located at grid points with perfect localization provided by the first estimates

In this scenario, both the receivers are located at grid points with perfect localization provided by the first estimates. User 1 is located at a depth of 74 m and range of 200 m from the transmitter, user 2 is located at a depth of 95 m and range 200 m from the transmitter. The BER performance for user 1 is shown in Fig. 5.3. In this scenario, the best BER performance is achieved by the beamformer designed using the first location estimate for each user, since the first estimates provide true locations of the receivers. Indeed, the BER performance degrades with more location estimates used for the design of the beamformer.

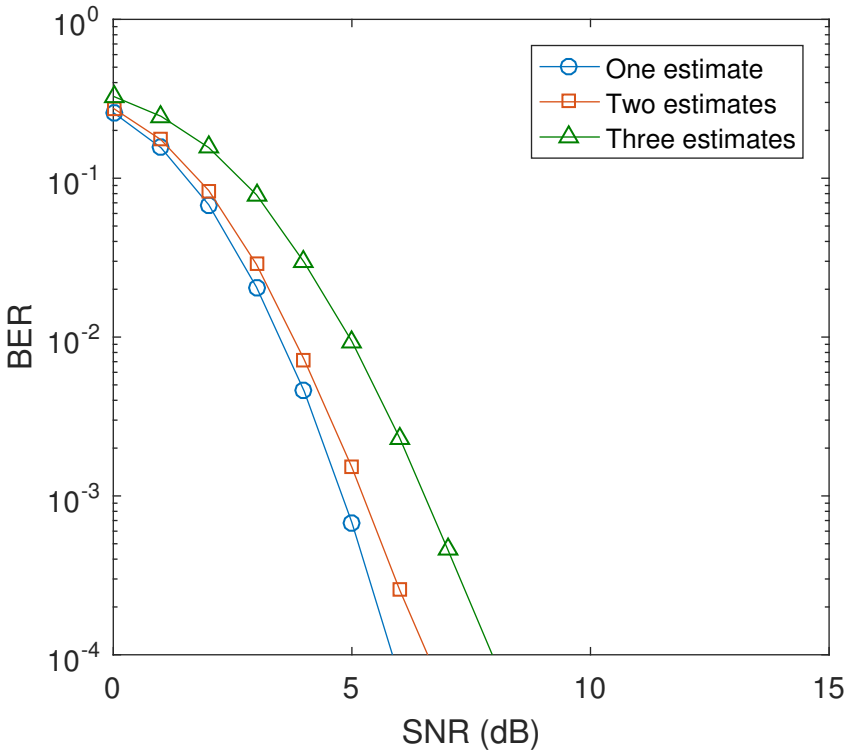

Fig. 5.3 BER performance in Scenario 1. Both the receivers are located at grid points with perfect localization provided by the first estimates.

Scenario 2 - The receivers are located at grid points with perfect localization provided by the second estimate

In this scenario, both the receivers are located at grid points with perfect localization provided by the second estimate. User 1 is at a depth of 116 m and range of 200 m from the transmitter, while user 2 is at a depth of 74 m and range of 250 m. The BER performance for user 1 is shown in Fig. 5.4. The BER performance for the beamformer designed with the first location estimate is poor since the first estimates are not accurate. The beamformer designed with the first and second position estimates has significantly better detection performance. This is because the second estimates are correct in this scenario. When using three position estimates the performance degrades but not significantly.

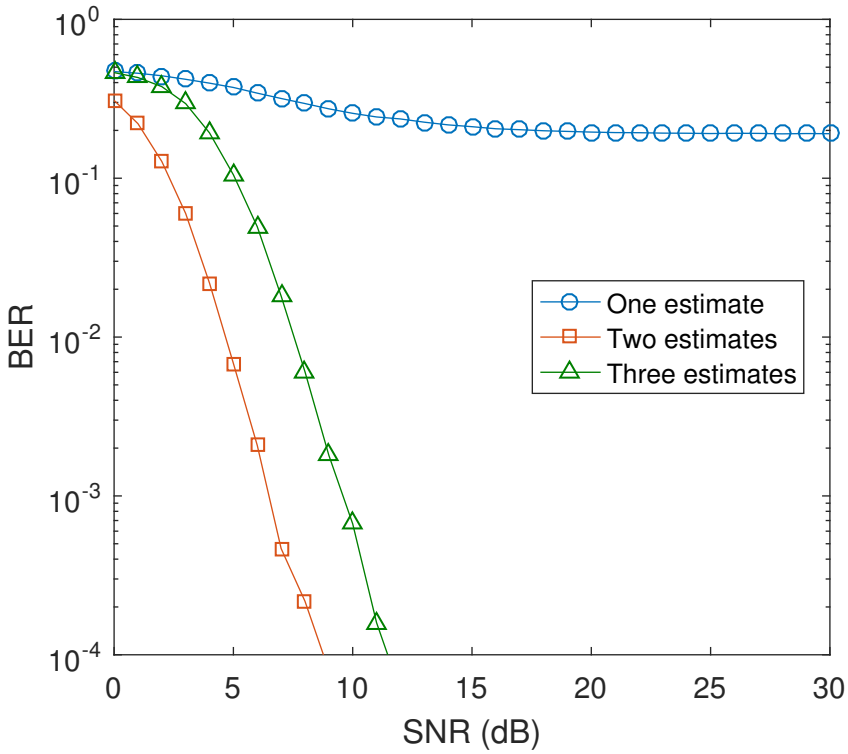

Fig. 5.4 BER performance in Scenario 2. Both the receivers are located at grid points with perfect localization provided by the second estimates.

Scenario 3 - The receivers are located between grid points

A more practical situation is considered in this scenario, where the receivers are located between grid points. User 1 is located at a depth of 116.2m and range of 200.4 m from the transmitter, while user 2 is located at a depth of 74.1 m and range of 250.3 m. Both the users are located between grid points, and therefore, all estimated grid points have displacements to the true user positions.

The difference between an estimate and a true position results in time shifts (phase distortions) and amplitude differences in the channel frequency responses used for designing the transmit beamformer. Fig. 5.5 shows the BER performance for this scenario. It can be seen that the beamformers designed using the 1-m resolution grid map cannot provide high detection performance, since the position errors are high. To reduce the position errors, a simple idea is to improve the resolution of the grid map. Fig. 5.6 shows the BER performance for the 0.5 m resolution grid map. It can be seen that in this case, the performance significantly improves.

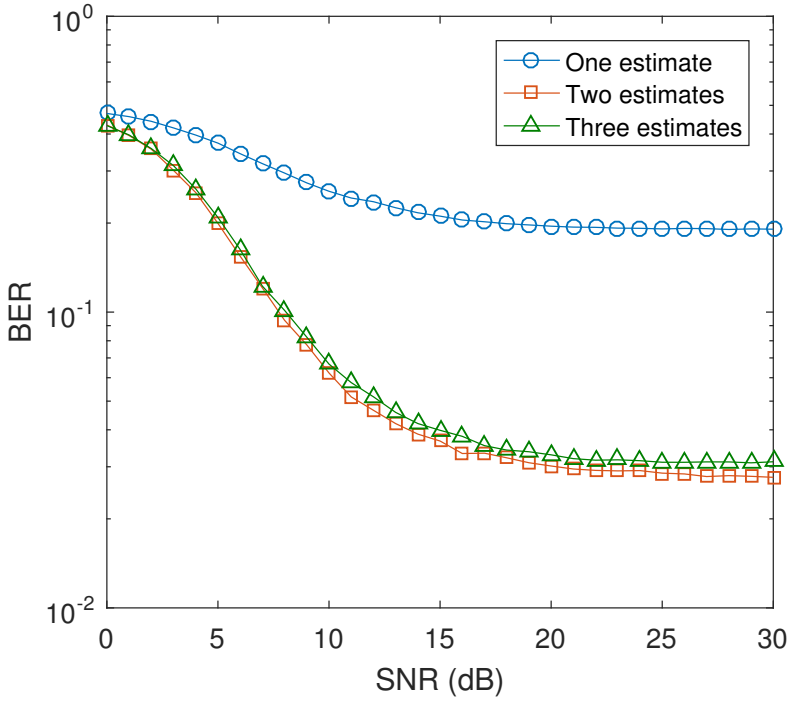

Fig. 5.5 BER performance of beamformers designed in Scenario 3. The receivers are located between grid points. The grid map resolution is 1 m.

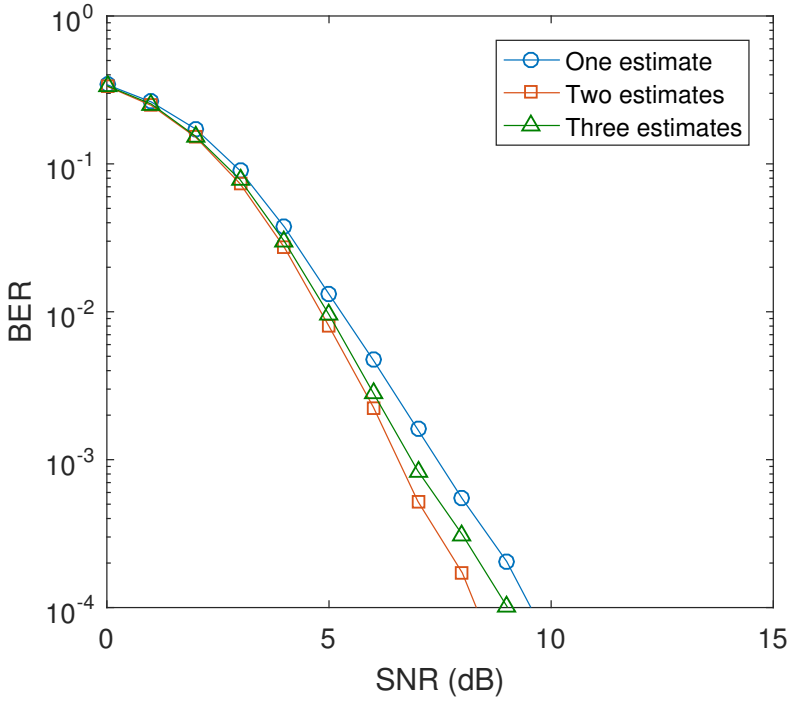

Fig. 5.6 BER performance of beamformers designed in Scenario 3. The receivers are located between grid points. The grid map resolution is 0.5 m.

Scenario 4 - The SSPs are different for signal transmission and for the grid map computation

In this scenario, the propagation channel described by the SSP shown in Fig. 5.7 is used for signal transmission in the Waymark model. It differs from the assumed channel described by the SSP shown in Fig. 3.2 which is still used for computation of the grid map. The other simulation parameters are the same as in Scenario 3. It can be seen that the two SSPs significantly differ at depths close to the sea surface. Fig. 5.8 shows the BER performance for the case of the code rate 1/2, the same as used in Scenario 3. By comparing results in Fig. 5.8 and Fig. 5.6, one can see that the detection performance of the receiver degrades; more specifically, there is now a floor level due to the multiuser interference that is not cancelled by the beamformer, which is now designed based on the mismatched CSI. However, the receiver can still operate with a BER as low as BER = 10^{-3} . With some sacrifice in the system throughput in this scenario, the detection performance can be significantly improved by using a code rate of 1/3, as illustrated in Fig. 5.9. Results in Fig. 5.8 and Fig. 5.9 also show that the proposed beamformer with multiple channel estimates provides better performance than the single-estimate beamformer.

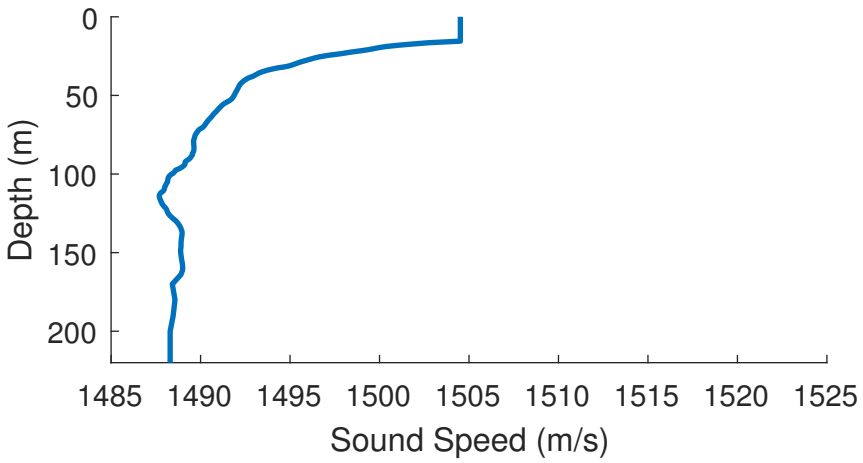

Fig. 5.7 The SSP used for signal transmission in Scenario 4.

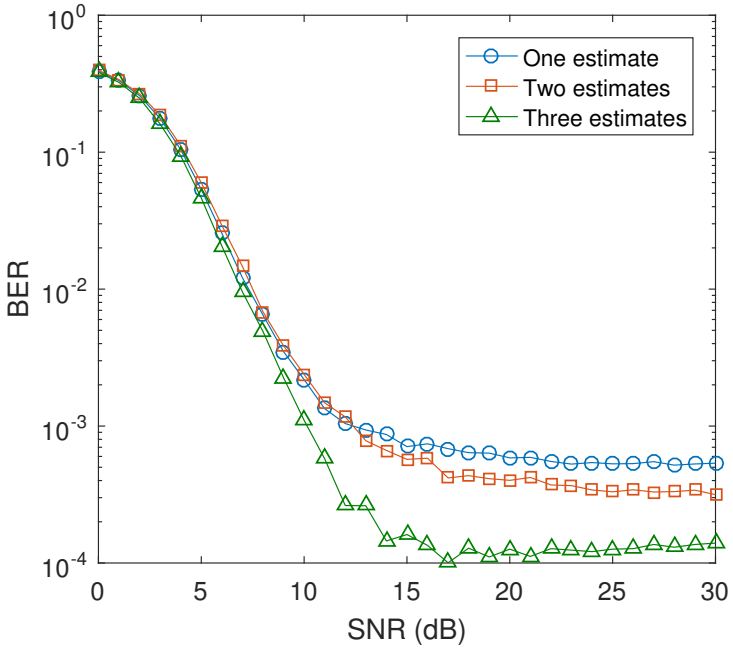

Fig. 5.8 BER performance of beamformers designed in Scenario 4. The receivers are located between grid points. The grid map resolution is 0.5 m. The real SSP (shown in Fig. 5.7) is different from the SSP used for the grid map computation. Code rate 1/2.

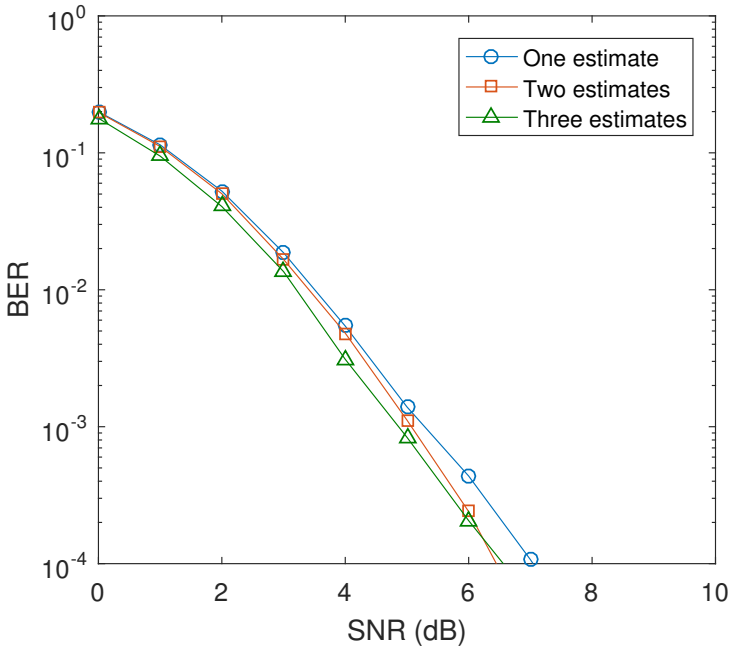

Fig. 5.9 BER performance of beamformers designed in Scenario 4. The receivers are located between grid points. The grid map resolution is 0.5 m. The real SSP (shown in Fig. 5.7) is different from the SSP used for the grid map computation. Code rate 1/3.

5.4 Conclusions

In this chapter, a transmit beamforming technique is proposed, which is based on the proposed receiver localization in the depth-range plane. This technique has been applied to multiuser UACs with multiple transmit antennas. As described in Chapter 2, the acoustic field can be pre-computed on grid points in a grid map and the grid map can be stored at both the transmitter and the receiver. In the receiver localization proposed in Chapter 3, the location estimate of the receiver (a grid point on the grid map) are obtained and included in the feedback message to be sent to the transmitter. After receiving the feedback message, the transmitter accesses the CSI of the receiver with the location estimate and the stored grid map, and the transmit beamformer is designed. To improve the detection performance of the transmit beamformer, multiple location estimates (multiple grid points on the grid map), instead of the single location estimate, are suggested to be obtained in the localization, and they are incorporated in the design of the transmit beamformer by cancelling interference in the extra grid points. High detection performance are shown in numerical investigation. Importantly, the feedback messages only contain indices of the grid points indicating the estimated location, which significantly reduces the size of feedback messages required for designing the beamformer.

Chapter 6

Conclusions and Future Work

6.1 Summary of the Work

This work is motivated by the on-going expansion of human activities in underwater environments and the growing demands for underwater high rate multiuser communication networks. The main aim of this work is to propose an advanced underwater localization method and to use it to make feasible underwater acoustic communication networks based on transmit beamforming.

The contributions in this thesis include:

- An underwater channel modelling simulator is proposed as a combination of the Waymark model with the idea of pre-computing the acoustic field on a space grid. The computation time taken with it is significantly less than that of the existing simulators.
- An underwater receiver localization technique is proposed, which is capable of achieving highly accurate position estimates. This receiver localization technique can be applied on both the Two-Dimensional plane and the Three-Dimensional space. Besides, this proposed localization technique makes feasible underwater communication network by exploiting the transmit beamforming. The complexity of infrastructure installation of the proposed localization technique is reduced compared to existing underwater receiver localization techniques.
- An underwater receiver trajectory estimation technique based on the proposed localization technique and data smoothing approach is proposed. It can recover the trajectory of the receiver accurately in both the Two-Dimensional plane and the Three-Dimensional

space. The cost of it is reduced compared to other common underwater trajectory estimation techniques.

- A transmit beamformer based on the proposed localization technique is proposed, that exploits multiple channel estimates for the same user to improve the detection performance, and the length of the feedback message is significantly reduced.

In Chapter 2, a further extension to the Waymark model proposed in [58] and [5] is proposed as the Grid Waymark model. In this model, we propose to pre-compute ray parameters on a space (depth-range) grid, similarly to how it is done in the known VirTEX simulator, and use the ray parameters for the waymark impulse response computation, thus speeding up the simulation. The Grid Waymark model has a significant advantage in computation speed compared to the original and baseband Waymark models. The baseband Waymark, VirTEX and Grid Waymark have been compared. The results show similarity with the major features such as the Doppler shifts. The computation time taken with Grid Waymark model is significantly less than that with other simulators.

In Chapter 3, an advanced underwater receiver localization technique is proposed, based on matching the CSI estimated at the receiver to the CSI pre-computed at grid points in an area of interest (over depth and range). This technique has been applied to multiuser UACs with multiple transmit antennas; more specifically, the localization method has been used for receiver trajectory estimation and designing the transmit beamforming. Numerical results demonstrate that the proposed localization technique is capable of achieving highly accurate position estimates.

In Chapter 4, an advanced underwater trajectory estimation approach is proposed based on the proposed localization technique. With location estimates on sample points along the trajectory and the corresponding match level coefficients, the trajectory can be recovered using a smoothing approach such as P-splines. The numerical investigation has shown that both in Depth-Range plane and X-Y-Z space, the proposed technique allows highly accurate trajectory estimation.

In Chapter 5, we have proposed a transmit beamforming technique that incorporates multiple location estimates, which are multiple grid points on the grid map, for improving the detection performance. With the proposed localization technique, the indexes of multiple grid points are included in the feedback message sent back to the transmitter for designing the beamformer. Numerical investigation has shown that the proposed technique allows high detection performance. Importantly, this has been achieved with significant reduction in the size of feedback messages required for designing the beamformer.

6.2 Future Work

In this section, some suggestions for future work, based on this thesis, are given below.

1) In Chapter 2, a further extension to the Waymark model is described as the Grid Waymark model. It has a significant advantage in computation speed compared to the original baseband Waymark model. In the proposed Grid Waymark model, the pre-computed grid map is in a fixed environment. However, random signal variations result from surface waves, internal turbulence, fluctuations in the sound speed, and other small-scale phenomena. Thus the pre-computed grid map used in the Grid Waymark model cannot represent the practical time-varying environment in the simulation. To have the simulation more accurate, it is useful to develop the Grid Waymark model to be able to represent the time-vary transmission environment.

2) In Chapter 3, the receiver localization technique is proposed based on the grid computation. As described in Chapter 2, the grid map covering the area of interest contains the arrival information (amplitudes and corresponding delays of arrival) on grid points, and it could be pre-computed and stored in both the transmitter and the receiver. Numerical examples have shown that the computation time and the storage memory of a grid map are acceptable for an underwater equipment such as AUV. To localize the receiver with the proposed localization technique we need to calculate the CSI on the grid points using the arrival information, which is considered as the signature of the corresponding grid point. The computation time for the signatures on the grid points can be high in some situations. For example, for a grid map covering the investigation area shown in Chapter 3 with 4×10^5 grid points, and the CSI computation is made at each of the 1024 subcarriers the computation time for the CSI computation is around 40 minutes. Therefore, it could be useful to develop the grid computation and localization to decrease the computation complexity when calculating the signatures of the grid points.

In this chapter the receiver localization technique in X-Y-Z space is also proposed, which is an extension to the localization technique in X-Z plane. This method combines the location estimates calculated with different transducers, and the transducers are placed around the investigation space. However, as shown in the examples in Chapter 3, with grid maps of 0.5 m resolution, only 50% of location estimates are considered as correct estimates, which is enough for the trajectory estimation in X-Y-Z space but not enough for localization in the three-dimensional space. Improving the resolution of the grid map to 0.25 m can help us to reach an acceptable accuracy in localization. However, the sacrifice (computation time and storage memory) is unacceptable for some underwater equipments. Therefore, it could be useful to develop some methods to increase the accuracy of the localization in Three-Dimensional space.

3) In Chpater 4, a method to recover the trajectory of an underwater receiver using the proposed localization technique and an existing smoothing approach is proposed. In the smoothing approach (P-spline is suggested in this thesis), the key parameters, weight coefficients of the estimates and the regularization parameter, are obtained from the proposed localization. As described in Chpater 4, the weight coefficients are set according to the match levels of the location estimates, and the regularization parameter is set according to the acceleration of the receiver. In the simulation results shown in Chpater 4, the receiver is assumed to be an AUV and the acceleration of it is considered under 1 m/s^2. However, the receiver in a practical underwater communication can be a stable sensor node or a hydrophone attached to a high-power AUV. In other words, it is difficult to approximate the acceleration level of a real underwater receiver, which results in inaccuracy in the setting of the regularization parameter. Therefore, it could be useful to optimize the setting of the regularization parameter in the proposed trajectory estimation.

4) In Chapter 5, an advanced transmit beamforming technique in multiuser UACs is proposed, and the receivers are assumed to be fixed. However, in practical UACs, the locations of the underwater receivers are unstable due to the internal waves. In the experiments shown in Chapter 5, with the proposed beamforming method with multiple estimates considered, a high detection performance can be achieved even if the receiver locations are shifted randomly with a uniform distribution within the grid resolution interval, but it is still useful to develop the beamforming method to improve the detection performance.

In this chapter we also investigated that, when the real SSP in the transmission is different with the one used for the grid map computation, the detection performance of the receiver degrades; more specifically, there is a floor level due to the multiuser interference that is not cancelled by the beamformer, which is designed based on the mismatched CSIs. In this thesis, to improve the detection performance in this scenario, we suggested using a code rate of 1/3, with some sacrifice in the system throughput. In the practical ocean environment, the SSP changes with temperature, salinity and other ocean parameters. In the future work, it is worth investigating the effect of the SSP and develop the beamforming method to improve the detection performance

References

[1] D. Ross, *Mechanics of underwater noise*. Elsevier, 2013.

[2] C. L. Bretschneider, *The Ash Wednesday East Coast Storm, March 5-8, 1962: A Hindcast of Events, Causes, and Effects*. Defense Technical Information Center, 1964.

[3] M. Stojanovic and J. Preisig, "Underwater acoustic communication channels: Propagation models and statistical characterization," *IEEE Communications Magazine*, vol. 47, no. 1, pp. 84–89, 2009.

[4] D. Wilson and R. Kneipfer, "Preliminary results of experiment to measure vertical directionality of ambient noise in shallow water," Naval Undersea Warfare Cntr.(NUWC), Washington, DC, Tech. Rep, Tech. Rep., 1995.

[5] B. Henson, J. Li, Y. V. Zakharov, and C. Liu, "Waymark baseband underwater acoustic propagation model," in *IEEE Underwater Communications and Networking (UComms)*, Sestri Levante, Italy, Sept. 2014, pp. 1–5.

[6] T. Chen, C. Liu, and Y. V. Zakharov, "Source localization using matched-phase matched-field processing with phase descent search," *IEEE Journal of Oceanic Engineering*, vol. 37, no. 2, pp. 261–270, 2012.

[7] L. Liao, B. Henson, and Y. Zakharov, "Grid Waymark baseband underwater acoustic transmission model," in *Underwater Acoustics Conference and Exhibition*, Skiathos, Greece, September 2017, pp. 343–350.

[8] L. Liao, Y. V. Zakharov, and P. D. Mitchell, "Underwater localization based on grid computation and its application to transmit beamforming in multiuser UWA communications," *IEEE Access*, vol. 6, pp. 4297–4307, 2018.

[9] L. Liao, B. Henson, and Y. Zakharov, "Underwater trajectory estimation based on grid localization and smoothing," in *the Tenth IEEE Sensor Array and Multichannel Signal Processing Workshop*, Sheffield, UK, July 2018.

[10] J. Li, L. Liao, and Y. V. Zakharov, "Space-time cluster combining for UWA communications," in *IEEE OCEANS*, Shanghai, China, 2016, pp. 1–6.

[11] L. Lanbo, Z. Shengli, and C. Jun-Hong, "Prospects and problems of wireless communication for underwater sensor networks," *Wireless Communications and Mobile Computing*, vol. 8, no. 8, pp. 977–994, 2008.

[12] R. Headrick and L. Freitag, "Growth of underwater communication technology in the US Navy," *IEEE Communications Magazine*, vol. 47, no. 1, pp. 80–82, 2009.

[13] S. Al-Dharrab, M. Uysal, and T. M. Duman, "Cooperative underwater acoustic communications," *IEEE Communications Magazine*, vol. 51, no. 7, pp. 146–153, 2013.

[14] K. Chen, M. Ma, E. Cheng, F. Yuan, and W. Su, "A survey on MAC protocols for underwater wireless sensor networks," *IEEE Communications Surveys & Tutorials*, vol. 16, no. 3, pp. 1433–1447, 2014.

[15] Y. Xiao, *Underwater acoustic sensor networks*. CRC Press, 2010.

[16] D. Pompili and I. F. Akyildiz, "Overview of networking protocols for underwater wireless communications," *IEEE Communications Magazine*, vol. 47, no. 1, pp. 97–102, 2009.

[17] M. Stojanovic, "Recent advances in high-speed underwater acoustic communications," *IEEE Journal of Oceanic engineering*, vol. 21, no. 2, pp. 125–136, 1996.

[18] M. Stojanovic, "Underwater acoustic communications," in *IEEE Electro/95 International. Professional Program Proceedings.*, Boston, MA, USA, June 1995, pp. 435–440.

[19] M. A. Abidi and R. C. Gonzalez, *Data fusion in robotics and machine intelligence*. Academic Press Professional, Inc., 1992.

[20] D. B. Kilfoyle and A. B. Baggeroer, "The state of the art in underwater acoustic telemetry," *IEEE Journal of Oceanic Engineering*, vol. 25, no. 1, pp. 4–27, 2000.

[21] T. H. Eggen, A. B. Baggeroer, and J. C. Preisig, "Communication over Doppler spread channels. Part I: Channel and receiver presentation," *IEEE Journal of Oceanic Engineering*, vol. 25, no. 1, pp. 62–71, 2000.

[22] W. A. Von Winkle and D. G. Browning, "Vertical noise directionality in the deep ocean: A review," DTIC Document, Tech. Rep., 1985.

[23] M. B. Porter, "The KRAKEN normal mode program," Naval Research Lab Washington DC, Tech. Rep., 1992.

[24] M. Porter, "The BELLHOP manual and user's guide: Preliminary draft," [Online]. Available: http://oalib.hlsresearch.com/Rays/HLS-2010-1.pdf, Tech. Rep., 2011.

[25] I. F. Akyildiz, D. Pompili, and T. Melodia, "Challenges for efficient communication in underwater acoustic sensor networks," *ACM Sigbed Review*, vol. 1, no. 2, pp. 3–8, 2004.

[26] F. Rashid-Farrokhi, K. R. Liu, and L. Tassiulas, "Transmit beamforming and power control for cellular wireless systems," *IEEE Journal on Selected Areas in Communications*, vol. 16, no. 8, pp. 1437–1450, 1998.

[27] J.-H. Cui, J. Kong, M. Gerla, and S. Zhou, "The challenges of building mobile underwater wireless networks for aquatic applications," *IEEE Network*, vol. 20, no. 3, pp. 12–18, 2006.

[28] W. Ye and J. Heidemann, "Medium access control in wireless sensor networks," in *Wireless Sensor Networks*. Springer, 2004, pp. 73–91.

[29] J. C. Liberti and T. S. Rappaport, *Smart antennas for wireless communications: IS-95 and third generation CDMA applications*. Prentice Hall PTR, 1999.

[30] R. Prasad, *CDMA for wireless personal communications*. Artech House, 1996.

[31] J. Litva and T. K. Lo, *Digital beamforming in wireless communications*. Artech House, 1996.

[32] M. Barrett and R. Arnott, "Adaptive antennas for mobile communisations," *Electronics & Communication Engineering Journal*, vol. 6, no. 4, pp. 203–214, 1994.

[33] A. F. Naguib, A. Paulraj, and T. Kailath, "Capacity improvement with base-station antenna arrays in cellular CDMA," *IEEE Transactions on Vehicular Technology*, vol. 43, no. 3, pp. 691–698, 1994.

[34] C. Farsakh and J. A. Nossek, "Spatial covariance based downlink beamforming in an SDMA mobile radio system," *IEEE Transactions on Communications*, vol. 46, no. 11, pp. 1497–1506, 1998.

[35] M. Rim, "Multi-user downlink beamforming with multiple transmit and receive antennas," *Electronics Letters*, vol. 38, no. 25, pp. 1725–1726, 2002.

[36] J. G. Proakis, E. M. Sozer, J. A. Rice, and M. Stojanovic, "Shallow water acoustic networks," *IEEE Communications Magazine*, vol. 39, no. 11, pp. 114–119, 2001.

[37] G. Lord and T. Plemons, "Characterization and simulation of underwater acoustic signals reflected from the sea surface," *The Journal of the Acoustical Society of America*, vol. 63, no. 2, pp. 378–385, 1978.

[38] M. S. Longuet-Higgins, "On the statistical distributions of sea waves," *Journal of Marine Research*, vol. 11, no. 3, pp. 245–265, 1952.

[39] M. Longuet-Higgins, "On the joint distribution of the periods and amplitudes of sea waves," *Journal of Geophysical Research*, vol. 80, no. 18, pp. 2688–2694, 1975.

[40] M. Denny, *Biology and the mechanics of the wave-swept environment*. Princeton University Press, 2014.

[41] L. M. Brekhovskikh, Y. P. Lysanov, and J. P. Lysanov, *Fundamentals of ocean acoustics*. Springer Science & Business Media, 2003.

[42] R. J. Urick, "Ambient noise in the sea," DTIC Document, Tech. Rep., 1984.

[43] G. M. Wenz, "Acoustic ambient noise in the ocean: spectra and sources," *The Journal of the Acoustical Society of America*, vol. 34, no. 12, pp. 1936–1956, 1962.

[44] M. Stojanovic, "On the relationship between capacity and distance in an underwater acoustic communication channel," *ACM SIGMOBILE Mobile Computing and Communications Review*, vol. 11, no. 4, pp. 34–43, 2007.

[45] R. H. Mellen, "The thermal-noise limit in the detection of underwater acoustic signals," *The Journal of the Acoustical Society of America*, vol. 24, no. 5, pp. 478–480, 1952.

[46] E. Axelrod, B. Schoomer, and W. Von Winkle, "Vertical directionality of ambient noise in the deep ocean at a site near bermuda," *The Journal of the Acoustical Society of America*, vol. 37, no. 1, pp. 77–83, 1965.

[47] W. Von Winkle, "Background noise in underwater acoustic listening systems," DTIC Document, Tech. Rep., 1979.

[48] G. R. Fox, "Ambient-noise directivity measurements," *The Journal of the Acoustical Society of America*, vol. 36, no. 8, pp. 1537–1540, 1964.

[49] R. J. Talham, "Ambient-sea-noise model," *The Journal of the Acoustical Society of America*, vol. 36, no. 8, pp. 1541–1544, 1964.

[50] V. C. Anderson, "Variation of the vertical directionality of noise with depth in the north pacific," *The Journal of the Acoustical Society of America*, vol. 66, no. 5, pp. 1446–1452, 1979.

[51] H. Beisner, "Numerical calculation of normal modes for underwater sound propagation," *IBM Journal of Research and Development*, vol. 18, no. 1, pp. 53–58, 1974.

[52] D. Stickler, "Normal-mode program with both the discrete and branch line contributions," *The Journal of the Acoustical Society of America*, vol. 57, no. 4, pp. 856–861, 1975.

[53] M. D. Collins, "User's guide for RAM versions 1.0 and 1.0 p," *Naval Research Lab, Washington, DC*, vol. 20375, 1995.

[54] M. B. Porter and H. P. Bucker, "Gaussian beam tracing for computing ocean acoustic fields," *The Journal of the Acoustical Society of America*, vol. 82, no. 4, pp. 1349–1359, 1987.

[55] M. Siderius and M. B. Porter, "Modeling broadband ocean acoustic transmissions with time-varying sea surfaces," *The Journal of the Acoustical Society of America*, vol. 124, no. 1, pp. 137–150, 2008.

[56] J. C. Peterson and M. B. Porter, "Ray/beam tracing for modeling the effects of ocean and platform dynamics," *IEEE Journal of Oceanic Engineering*, vol. 38, no. 4, pp. 655–665, 2013.

[57] M. B. Porter and Y.-C. Liu, "Finite-element ray tracing," *Theoretical and Computational Acoustics*, vol. 2, pp. 947–956, 1994.

[58] C. Liu, Y. V. Zakharov, and T. Chen, "Doubly selective underwater acoustic channel model for a moving transmitter/receiver," *IEEE Transactions on Vehicular Technology*, vol. 61, no. 3, pp. 938–950, 2012.

[59] I. F. Akyildiz, D. Pompili, and T. Melodia, "Underwater acoustic sensor networks: research challenges," *Ad Hoc Networks*, vol. 3, no. 3, pp. 257–279, 2005.

[60] E. Felemban, F. K. Shaikh, U. M. Qureshi, A. A. Sheikh, and S. B. Qaisar, "Underwater sensor network applications: A comprehensive survey," *International Journal of Distributed Sensor Networks*, vol. 11, no. 11, p. 896832, 2015.

[61] J. C. Kinsey and L. L. Whitcomb, "Preliminary field experience with the DVLNAV integrated navigation system for oceanographic submersibles," *Control Engineering Practice*, vol. 12, no. 12, pp. 1541–1549, 2004.

[62] J. C. Kinsey, R. M. Eustice, and L. L. Whitcomb, "A survey of underwater vehicle navigation: Recent advances and new challenges," in *IFAC Conference of Manoeuvering and Control of Marine Craft*, vol. 88, Lisbon, Portugal, Sep. 2006, pp. 1–12.

[63] R. Spindel, R. Porter, W. Marquet, and J. Durham, "A high-resolution pulse-Doppler underwater acoustic navigation system," *IEEE Journal of Oceanic Engineering*, vol. 1, no. 1, pp. 6–13, 1976.

[64] R. McEwen, H. Thomas, D. Weber, and F. Psota, "Performance of an AUV navigation system at Arctic latitudes," *IEEE Journal of Oceanic Engineering*, vol. 30, no. 2, pp. 443–454, 2005.

[65] G. Marani, S. K. Choi, and J. Yuh, "Underwater autonomous manipulation for intervention missions AUVs," *Ocean Engineering*, vol. 36, no. 1, pp. 15–23, 2009.

[66] C. Tyren, "Magnetic terrain navigation," in *IEEE Proceedings of the 1987 5th International Symposium on Unmanned Untethered Submersible Technology*, vol. 5, 1987, pp. 245–256.

[67] L. Whitcomb, D. Yoerger, and H. Singh, "Advances in Doppler-based navigation of underwater robotic vehicles," in *IEEE International Conference on Robotics and Automation*, vol. 1, Detroit, MI, USA, May 1999, pp. 399–406.

[68] S. E. Webster, R. M. Eustice, H. Singh, and L. L. Whitcomb, "Preliminary deep water results in single-beacon one-way-travel-time acoustic navigation for underwater vehicles," in *IEEE/RSJ International Conference on Intelligent Robots and Systems*, 2009, pp. 2053–2060.

[69] M. V. Jakuba, C. N. Roman, H. Singh, C. Murphy, C. Kunz, C. Willis, T. Sato, and R. A. Sohn, "Long-baseline acoustic navigation for under-ice autonomous underwater vehicle operations," *Journal of Field Robotics*, vol. 25, no. 11-12, pp. 861–879, 2008.

[70] M. M. Hunt, W. M. Marquet, D. A. Moller, K. R. Peal, W. K. Smith, and R. C. Spindel, "An acoustic navigation system," Woods Hole Oceanographic Institution, Tech. Rep., 1974.

[71] J. Bellingham, C. Goudey, T. Consi, J. Bales, D. Atwood, J. Leonard, and C. Chryssostomidis, "A second generation survey AUV," in *IEEE Symposium on Autonomous Underwater Vehicle Technology.*, Cambridge, MA, USA, July 1994, pp. 148–155.

[72] R. M. Eustice, L. L. Whitcomb, H. Singh, and M. Grund, "Experimental results in synchronous-clock one-way-travel-time acoustic navigation for autonomous underwater vehicles," in *IEEE International Conference on Robotics and Automation*, 2007, pp. 4257–4264.

[73] D. Titterton, J. L. Weston, and J. Weston, *Strapdown inertial navigation technology*. The Institution of Engineering and Technology, 2004, vol. 17.

[74] C. C. Eriksen, T. J. Osse, R. D. Light, T. Wen, T. W. Lehman, P. L. Sabin, J. W. Ballard, and A. M. Chiodi, "Seaglider: A long-range autonomous underwater vehicle for oceanographic research," *IEEE Journal of oceanic Engineering*, vol. 26, no. 4, pp. 424–436, 2001.

[75] I. A. Getting, "Perspective/navigation-the global positioning system," *IEEE spectrum*, vol. 30, no. 12, pp. 36–38, 1993.

[76] R. A. Monzingo and T. W. Miller, *Introduction to adaptive arrays*. Scitech publishing, 1980.

[77] D. Gerlach and A. Paulraj, "Adaptive transmitting antenna arrays with feedback," *IEEE Signal Processing Letters*, vol. 1, no. 10, pp. 150–152, 1994.

[78] D. J. Love, R. W. Heath, and T. Strohmer, "Grassmannian beamforming for multiple-input multiple-output wireless systems," *IEEE transactions on information theory*, vol. 49, no. 10, pp. 2735–2747, 2003.

[79] T. Curtis and R. Ward, "Digital beam forming for sonar systems," in *IEE Communications, Radar and Signal Processing*, vol. 127, no. 4, 1980, pp. 257–265.

[80] P. Barton, "Digital beam forming for radar," in *IEE Communications, Radar and Signal Processing*, vol. 127, no. 4, 1980, pp. 266–277.

[81] G. Caire and S. Shamai, "On the achievable throughput of a multiantenna Gaussian broadcast channel," *IEEE Transactions on Information Theory*, vol. 49, no. 7, pp. 1691–1706, 2003.

[82] A. Wiesel, Y. C. Eldar, and S. Shamai, "Linear precoding via conic optimization for fixed MIMO receivers," *IEEE Transactions on Signal Processing*, vol. 54, no. 1, pp. 161–176, 2006.

[83] M. Stojnic, H. Vikalo, and B. Hassibi, "Rate maximization in multi-antenna broadcast channels with linear preprocessing," *IEEE Transactions on Wireless Communications*, vol. 5, no. 9, pp. 2338–2342, 2006.

[84] M. Joham, W. Utschick, and J. A. Nossek, "Linear transmit processing in MIMO communications systems," *IEEE Transactions on Signal Processing*, vol. 53, no. 8, pp. 2700–2712, 2005.

[85] S. Shi, M. Schubert, and H. Boche, "Downlink MMSE transceiver optimization for multiuser MIMO systems: Duality and sum-MSE minimization," *IEEE Transactions on Signal Processing*, vol. 55, no. 11, pp. 5436–5446, 2007.

[86] Q. H. Spencer, A. L. Swindlehurst, and M. Haardt, "Zero-forcing methods for downlink spatial multiplexing in multiuser MIMO channels," *IEEE Transactions on Signal Processing*, vol. 52, no. 2, pp. 461–471, 2004.

[87] Z. Shen, R. Chen, J. G. Andrews, R. W. Heath, and B. L. Evans, "Low complexity user selection algorithms for multiuser MIMO systems with block diagonalization," *IEEE Transactions on Signal Processing*, vol. 54, no. 9, pp. 3658–3663, 2006.

[88] L.-U. Choi and R. D. Murch, "A transmit preprocessing technique for multiuser MIMO systems using a decomposition approach," *IEEE Transactions on Wireless Communications*, vol. 3, no. 1, pp. 20–24, 2004.

[89] K.-K. Wong, "Maximizing the sum-rate and minimizing the sum-power of a broadcast 2-user 2-input multiple-output antenna system using a generalized zeroforcing approach," *IEEE Transactions on Wireless Communications*, vol. 5, no. 12, 2006.

[90] Z. Pan, K.-K. Wong, and T.-S. Ng, "Generalized multiuser orthogonal space-division multiplexing," *IEEE Transactions on Wireless Communications*, vol. 3, no. 6, pp. 1969–1973, 2004.

[91] P. S. Udupa and J. S. Lehnert, "Optimizing zero-forcing precoders for MIMO broadcast systems," *IEEE Transactions on Communications*, vol. 55, no. 8, pp. 1516–1524, 2007.

[92] A. Wiesel, Y. C. Eldar, and S. Shamai, "Zero-forcing precoding and generalized inverses," *IEEE Transactions on Signal Processing*, vol. 56, no. 9, pp. 4409–4418, 2008.

[93] M. Stojanovic, "Low complexity OFDM detector for underwater acoustic channels," in *IEEE OCEANS 2006*, Boston, MA, USA, Sept. 2006, pp. 1–6.

[94] B. Li, S. Zhou, M. Stojanovic, L. Freitag, and P. Willett, "Multicarrier communication over underwater acoustic channels with nonuniform Doppler shifts," *IEEE Journal of Oceanic Engineering*, vol. 33, no. 2, pp. 198–209, 2008.

[95] C. R. Berger, S. Zhou, J. C. Preisig, and P. Willett, "Sparse channel estimation for multicarrier underwater acoustic communication: From subspace methods to compressed sensing," *IEEE Transactions on Signal Processing*, vol. 58, no. 3, pp. 1708–1721, 2010.

[96] Y. V. Zakharov and V. Kodanev, "Multipath-Doppler diversity of OFDM signals in an underwater acoustic channel," in *IEEE International Conference on Acoustics, Speech, and Signal Processing. ICASSP'00.*, vol. 5, Istanbul, Turkey, June 2000, pp. 2941–2944.

[97] S. Roy, T. M. Duman, V. McDonald, and J. G. Proakis, "High-rate communication for underwater acoustic channels using multiple transmitters and space–time coding: Receiver structures and experimental results," *IEEE Journal of Oceanic Engineering*, vol. 32, no. 3, pp. 663–688, 2007.

[98] H. Song, W. Hodgkiss, W. Kuperman, T. Akal, and M. Stevenson, "High-frequency acoustic communications achieving high bandwidth efficiency," *The Journal of the Acoustical Society of America*, vol. 126, no. 2, pp. 561–563, 2009.

[99] Z. Wang, S. Zhou, G. B. Giannakis, C. R. Berger, and J. Huang, "Frequency-domain oversampling for zero-padded OFDM in underwater acoustic communications," *IEEE Journal of Oceanic Engineering*, vol. 37, no. 1, pp. 14–24, 2012.

[100] X. Geng and A. Zielinski, "An eigenpath underwater acoustic communication channel model," in *MTS/IEEE Conference Proceedings OCEANS'95. Challenges of Our Changing Global Environment.*, vol. 2, San Diego, California, USA, Oct. 1995, pp. 1189–1196.

[101] R. Otnes, P. A. van Walree, and T. Jenserud, "Validation of replay-based underwater acoustic communication channel simulation," *IEEE Journal of Oceanic Engineering*, vol. 38, no. 4, pp. 689–700, 2013.

[102] W. H. Tranter, T. S. Rappaport, K. L. Kosbar, and K. S. Shanmugan, *Principles of communication systems simulation with wireless applications*. Prentice Hall New Jersey, 2004, vol. 1.

[103] M. Stojanovic, "Underwater acoustic communications: Design considerations on the physical layer," in *Fifth Annual IEEE Conference on Wireless on Demand Network Systems and Services*, Garmisch-Partenkirchen, Germany, January 2008, pp. 1–10.

[104] G. L. Stüber, *Principles of mobile communication*. Berlin, Germany: Springer Science & Business Media, 2011.

[105] N. O. Booth, A. T. Abawi, P. W. Schey, and W. S. Hodgkiss, "Detectability of low-level broad-band signals using adaptive matched-field processing with vertical aperture arrays," *IEEE Journal of Oceanic Engineering*, vol. 25, no. 3, pp. 296–313, 2000.

[106] J. Murray and D. Ensberg, "The Swellex-96 experiment," *URL: http://www. mpl. ucsd. edu/swellex96*, 1996.

[107] V. Chandrasekhar, W. K. Seah, Y. S. Choo, and H. V. Ee, "Localization in underwater sensor networks: survey and challenges," in *Proceedings of the 1st ACM international workshop on Underwater networks*, 2006, pp. 33–40.

[108] L. L. Whitcomb, "Underwater robotics: Out of the research laboratory and into the field," in *IEEE International Conference on Robotics and Automation. ICRA'00.*, vol. 1, San Francisco, CA, USA, April 2000, pp. 709–716.

[109] A. Alcocer, P. Oliveira, and A. Pascoal, "Underwater acoustic positioning systems based on buoys with GPS," in *Proceedings of the Eighth European Conference on Underwater Acoustics*, vol. 8, Carvoeiro, Portugal, June 2006, pp. 1–8.

[110] J. Curcio, J. Leonard, J. Vaganay, A. Patrikalakis, A. Bahr, D. Battle, H. Schmidt, and M. Grund, "Experiments in moving baseline navigation using autonomous surface craft," in *OCEANS Proceedings of MTS/IEEE*, Washington, DC, USA, Sept 2005, pp. 730–735.

[111] T. B. Curtin, J. G. Bellingham, J. Catipovic, and D. Webb, "Autonomous oceanographic sampling networks," *Oceanography*, vol. 6, no. 3, pp. 86–94, 1993.

[112] C. Clay, "Optimum time domain signal transmission and source location in a waveguide," *The Journal of the Acoustical Society of America*, vol. 81, no. 3, pp. 660–664, 1987.

[113] M. J. Hinich, "Maximum-likelihood signal processing for a vertical array," *The Journal of the Acoustical Society of America*, vol. 54, no. 2, pp. 499–503, 1973.

[114] G. C. Carter, "Variance bounds for passively locating an acoustic source with a symmetric line array," *The Journal of the Acoustical Society of America*, vol. 62, no. 4, pp. 922–926, 1977.

[115] H. P. Bucker, "Use of calculated sound fields and matched-field detection to locate sound sources in shallow water," *The Journal of the Acoustical Society of America*, vol. 59, no. 2, pp. 368–373, 1976.

[116] C. Soares, S. M. Jesus, and E. Coelho, "Environmental inversion using high-resolution matched-field processing," *The Journal of the Acoustical Society of America*, vol. 122, no. 6, pp. 3391–3404, 2007.

[117] A. Tolstoy, *Matched field processing for underwater acoustics*. World Scientific, 1993.

[118] A. B. Baggeroer, W. A. Kuperman, and P. N. Mikhalevsky, "An overview of matched field methods in ocean acoustics," *IEEE Journal of Oceanic Engineering*, vol. 18, no. 4, pp. 401–424, 1993.

[119] M. D. Collins and W. Kuperman, "Focalization: Environmental focusing and source localization," *The Journal of the Acoustical Society of America*, vol. 90, no. 3, pp. 1410–1422, 1991.

[120] C. Soares, M. Siderius, and S. M. Jesus, "Source localization in a time-varying ocean waveguide," *The Journal of the Acoustical Society of America*, vol. 112, no. 5, pp. 1879–1889, 2002.

[121] L. P. Maia, A. Silva, and S. M. Jesus, "Environmental model-based time-reversal underwater communications," *IEEE Access*, vol. 6, pp. 10 041–10 051, 2017.

[122] S. M. Kay, *Fundamentals of statistical signal processing*. Prentice Hall PTR, 1993.

[123] M. Erol-Kantarci, H. T. Mouftah, and S. Oktug, "A survey of architectures and localization techniques for underwater acoustic sensor networks," *IEEE Communications Surveys & Tutorials*, vol. 13, no. 3, pp. 487–502, 2011.

[124] R. Berry, K. Loebbaka, and E. Hall, "Sensors for mobile robots," in *Proceedings of the 3rd Conference on Robot Vision and Sensory Controls*, 1983, pp. 584–588.

[125] C. J. Cohen and F. V. Koss, "Comprehensive study of three-object triangulation," in *Mobile Robots VII*, vol. 1831. International Society for Optics and Photonics, 1993, pp. 95–107.

[126] M. Betke and L. Gurvits, "Mobile robot localization using landmarks," *IEEE transactions on robotics and automation*, vol. 13, no. 2, pp. 251–263, 1997.

[127] M. Erol, L. F. M. Vieira, and M. Gerla, "Auv-aided localization for underwater sensor networks," in *IEEE International Conference on Wireless Algorithms, Systems and Applications*, 2007, pp. 44–54.

[128] F. van Diggelen and P. Enge, "The worlds first gps mooc and worldwide laboratory using smartphones," in *Proceedings of the 28th International Technical Meeting of The Satellite Division of the Institute of Navigation*, 2015, pp. 361–369.

[129] Y. Zhang, M. A. Godin, J. G. Bellingham, and J. P. Ryan, "Using an autonomous underwater vehicle to track a coastal upwelling front," *IEEE Journal of Oceanic Engineering*, vol. 37, no. 3, pp. 338–347, 2012.

[130] S. B. Williams, O. R. Pizarro, M. V. Jakuba, C. R. Johnson, N. S. Barrett, R. C. Babcock, G. A. Kendrick, P. D. Steinberg, A. J. Heyward, P. J. Doherty *et al.*, "Monitoring of benthic reference sites: using an autonomous underwater vehicle," *IEEE Robotics & Automation Magazine*, vol. 19, no. 1, pp. 73–84, 2012.

[131] P. Rogowski, E. Terrill, M. Otero, L. Hazard, and W. Middleton, "Ocean outfall plume characterization using an autonomous underwater vehicle," *Water Science and Technology*, vol. 67, no. 4, pp. 925–933, 2013.

[132] A. Jenkins, P. Dutrieux, S. Jacobs, S. McPhail, J. Perrett, A. Webb, and D. White, "Autonomous underwater vehicle exploration of the ocean cavity beneath an antarctic ice shelf," *Oceanography*, vol. 25, no. 3, pp. 202–203, 2012.

[133] D. A. Smale, G. A. Kendrick, E. S. Harvey, T. J. Langlois, R. K. Hovey, K. P. Van Niel, K. I. Waddington, L. M. Bellchambers, M. B. Pember, R. C. Babcock *et al.*, "Regional-scale benthic monitoring for ecosystem-based fisheries management (EBFM) using an autonomous underwater vehicle (AUV)," *ICES Journal of Marine Science*, vol. 69, no. 6, pp. 1108–1118, 2012.

[134] C. M. Clark, C. Forney, E. Manii, D. Shinzaki, C. Gage, M. Farris, C. G. Lowe, and M. Moline, "Tracking and following a tagged leopard shark with an autonomous underwater vehicle," *Journal of Field Robotics*, vol. 30, no. 3, pp. 309–322, 2013.

[135] S. Smith and D. Kronen, "Experimental results of an inexpensive short baseline acoustic positioning system for AUV navigation," in *MTS/IEEE Conference Proceedings OCEANS'97.*, vol. 1, 1997, pp. 714–720.

[136] H.-H. Chen, "In-situ alignment calibration of attitude and ultra short baseline sensors for precision underwater positioning," *Ocean Engineering*, vol. 35, no. 14-15, pp. 1448–1462, 2008.

[137] B. W. Silverman, *Density estimation for statistics and data analysis*. CRC press, 1986, vol. 26.

[138] B. W. Silverman, "Some aspects of the spline smoothing approach to non-parametric regression curve fitting," *Journal of the Royal Statistical Society. Series B*, pp. 1–52, 1985.

[139] C. De Boor, C. De Boor, E.-U. Mathématicien, C. De Boor, and C. De Boor, *A practical guide to splines*. Springer-Verlag New York, 1978, vol. 27.

[140] P. Dierckx, *Curve and surface fitting with splines*. Oxford University Press, 1995.

[141] P. H. Eilers and B. D. Marx, "Flexible smoothing with B-splines and penalties," *Statistical Science*, pp. 89–102, 1996.

[142] F. O'sullivan, B. S. Yandell, and W. J. Raynor Jr, "Automatic smoothing of regression functions in generalized linear models," *Journal of the American Statistical Association*, vol. 81, no. 393, pp. 96–103, 1986.

[143] M. Wand and J. Ormerod, "On semiparametric regression with O'Sullivan penalized splines," *Australian & New Zealand Journal of Statistics*, vol. 50, no. 2, pp. 179–198, 2008.

[144] M. Rahmati and D. Pompili, "uwMIMO-HARQ: Hybrid ARQ for reliable underwater acoustic MIMO communications," in *ACM Proceedings of the 10th International Conference on Underwater Networks & Systems*, Arlington, VA, USA, October 2015, p. 12.

[145] J. Tao, Y. R. Zheng, C. Xiao, and T. Yang, "Robust MIMO underwater acoustic communications using turbo block decision-feedback equalization," *IEEE Journal of Oceanic Engineering*, vol. 35, no. 4, pp. 948–960, 2010.

[146] R. Hansen, "Preface: Special issue on active and adaptive antennas," *IEEE Transactions on Antennas and Propagation*, vol. 12, no. 2, pp. 140–141, 1964.

[147] J. Hudson, *Adaptive array principles*. IET, 1981, vol. 11.

[148] H.-P. Tan, R. Diamant, W. K. Seah, and M. Waldmeyer, "A survey of techniques and challenges in underwater localization," *Ocean Engineering*, vol. 38, no. 14-15, pp. 1663–1676, 2011.

[149] H. Cox, R. Zeskind, and M. Owen, "Robust adaptive beamforming," *IEEE Transactions on Acoustics, Speech, and Signal Processing*, vol. 35, no. 10, pp. 1365–1376, 1987.

[150] B. Chen, P. C. Hickey, and D. Pompili, "Trajectory-aware communication solution for underwater gliders using WHOI micro-modems," in *IEEE Communications Society Conference on Sensor Mesh and Ad Hoc Communications and Networks (SECON)*, Boston, MA, USA, June 2010, pp. 1–9.

[151] T. M. Kim, F. Sun, and A. J. Paulraj, "Low-complexity MMSE precoding for coordinated multipoint with per-antenna power constraint," *IEEE Signal Processing Letters*, vol. 20, no. 4, pp. 395–398, 2013.

[152] B. Bandemer, M. Haardt, and S. Visuri, "Linear MMSE multi-user MIMO downlink precoding for users with multiple antennas," in *IEEE International Symposium on Personal, Indoor and Mobile Radio Communications*, Helsinki, Finland, December 2006, pp. 1–5.

[153] X. Shao, J. Yuan, and Y. Shao, "Error performance analysis of linear zero forcing and MMSE precoders for MIMO broadcast channels," *IET Communications*, vol. 1, no. 5, pp. 1067–1074, 2007.

[154] J. G. Proakis, "Digital communications," *McGraw-Hill*, 1995.